PURDUE UNIVERSITY
GRADUATE SCHOOL
Thesis/Dissertation Acceptance

This is to certify that the thesis/dissertation prepared

By Joshua James Israel

Entitled Shape Optimization of Lightweight Structures under Blast Loading

For the degree of   Master of Science in Mechanical Engineering

Is approved by the final examining committee:

Andres Tovar
_____
Chair

Hazim El - Mounayri
_____

Tamer Wasfy
_____

To the best of my knowledge and as understood by the student in the *Research Integrity and Copyright Disclaimer (Graduate School Form 20)*, this thesis/dissertation adheres to the provisions of Purdue University's "Policy on Integrity in Research" and the use of copyrighted material.

Approved by Major Professor(s): __Andres Tovar_____

_____

Approved by: Alan Jones   04/22/2013
              Head of the Graduate Program   Date

SHAPE OPTIMIZATION OF LIGHTWEIGHT STRUCTURES

UNDER BLAST LOADING

A Thesis

Submitted to the Faculty

of

Purdue University

by

Joshua James Israel

In Partial Fulfillment of the

Requirements for the Degree

of

Master of Science in Mechanical Engineering

May 2013

Purdue University

Indianapolis, Indiana

ACKNOWLEDGMENTS

I would like to gratefully acknowledge my advisor, Andres Tovar, whose guidance and encouragement made this work possible. I consider it a privilege to have worked with you and I will always be grateful for the substantial part you have played in my education as an engineer. In addition, I would like to thank the members of my committee, Tamer Wasfy and Hazim El-Mounayri. Through your instruction, you have both provided me with an invaluable source of knowledge over the years.

I would like to take this opportunity to thank my fellow researchers: Satyajeet Sinde, Kunal Khadhe, Kai Liu, Anahita Emami, and Weigang An. It has been a pleasure to work with you all. Thank you for listening to my ideas and for your criticism. This research is much stronger having been exposed to your experience and encouragement. I would also like to thank the sources of financial support for this research. This material is based upon work supported by the U.S. Army TACOM Life Cycle Command, through a subcontract with Mississippi State University and the University of Notre Dame, and was performed for the Simulation Based Reliability and Safety (SimBRS) research program.

Most importantly, I would like to thank my family for their support and encouragement. The unfailing support of my parents, James Israel and Rebecca Cobb, made this work and all of my previous endeavors possible. The constant optimism and assistance from my brother, Ross Israel, was instrumental to the success of this research - he truly is a prince among men. Lastly, none of this work or any other would be possible without the daily love and support of my fiancée, Amber Clark. Thank you to you all.

CONTENTS

v

LIST OF TABLES

LIST OF FIGURES

LIST OF SYMBOLS

$\boldsymbol{d}$	Vector of design variables
M	Mass function
P_c	Cabin penetration function
$P_{c\,max}$	Maximum allowable penetration
S	Envelope constraint function
t	Time in seconds
$\boldsymbol{x}$	Vector of x-coordinate values for all nodes
$\boldsymbol{y}$	Vector of y-coordinate values for all nodes
$\boldsymbol{z}$	Vector of z-coordinate values for all nodes
c	Element thickness
h	Structure height
α	Gaussian spread variable
δ	Gaussian height variable
C_0, C_1, C_2, C_3	Polynomial function coefficients
R	Radius of surface of revolution
$a_1, a_{21}, a_{22}, f_1, f_2$	Trigonometric function coefficients
r	Radial coordinate of surface of revolution
y^*	Target deflection threshold
K_α, K_β	HCA control gains
N	Number of free nodes in the design space
ρ	Element density
$\dot{\varepsilon}$	Strain rate
$\boldsymbol{X}$	Vector of random input variables

μ_P mean of the protection performance

σ_P^2 variance of the protection performance

P_f^T Probability of failure target

F_C Cost function

μ_T Target nominal mean value

LIST OF ABBREVIATIONS

ALE   Arbitrary Lagrange-Eulerian

CDF   Cumulative Distribution Function

FORM   First Order Reliability Method

HCA   Hybrid Cellular Automaton

IED   Improvised Explosive Device

MPP   Most-Probable Point

PCE   Polynomial Chaos Expansion

PDF   Probability Density Function

PMI   Performance Moment Integration

QP   Quadratic Programming

RBDO   Reliability Based Design Optimization

RBF   Radial Basis Function

RBRDO   Reliability-Based Robust Design Optimization

RDO   Robust Design Optimization

SORM   Second Order Reliability Method

SQP   Sequential Quadratic Programming

UDR   Univariate Dimensional Reduction

UQ   Uncertainty Quantification

ABSTRACT

Israel, Joshua James. M.S.M.E., Purdue University, May 2013. Shape Optimization of Lightweight Structures under Blast Loading. Major Professor: Andres Tovar.

Structural optimization of vehicle components for blast mitigation seeks to counteract the damaging effects of an impulsive threat on occupants and critical components. The strong and urgent need for improved protection from blast events has made blast mitigating component design an active research subject. Standard up-armoring of ground vehicles can significantly increase the mass of the vehicle. Without concurrent modifications to the power train, suspension, braking and steering components, the up-armored vehicles suffer from degraded stability and mobility. For these reasons, there is a critical need for effective methods to generate lightweight components for blast mitigation.

The overall objective of this research is to make advances in structural design methods for the optimization of lightweight blast-mitigating systems. This thesis investigates the automated design process of isotropic plates to mitigate the effects of blast loading by addressing the design of blast-protective structures from a design optimization perspective. The general design problem is stated as finding the optimum shape of a protective shell of minimum mass satisfying deformation and envelops constraints.

This research was conducted in terms of three primary research projects. The first project was to investigate the design of lightweight structures under deterministic loading

conditions and subject to the same objective function and constraints, in order to compare feasible design methodologies through the expansion of the problem dimension in order to reach the limits of performance. The second research project involved the investigation of recently developed uncertainty quantification methods, the univariate dimensional reduction method and the performance moment integration method, to structures under stochastic loading conditions. The third research project involved application of these uncertainty quantification methods to problems of design optimization under uncertainty, in order to develop a methodology for the generation of lightweight reliable structures.

This research has resulted in the construction of a computational framework, incorporating uncertainty quantification methods and various optimization techniques, which can be used for the generation of lightweight structures for blast mitigation under uncertainty. Applied to practical structural design problems, the results demonstrate that the methodologies provide a practical tool to aid the design engineer in generating design concepts for blast-mitigating structures. These methods can be used to advance research into the generation of reliable structures under uncertain loading conditions inherent to blast events.

1. INTRODUCTION

1.1   Justification

The Unites States Armed Forces have been involved in multiple prolonged conflicts over the past decade. Chief among them are Operation Iraqi Freedom and Operation Enduring Freedom, commonly referred to as the wars in Iraq and Afghanistan. These military operations have brought the problem of blast protection systems for vehicles to the forefront of investigation, due to the large number of casualties reported as the result of attacks on light vehicles by improvised explosive devices (IED), or roadside bombs. Lt. Gen. Michael Barbero, testifying before a Senate subcommittee, stated that in 2012 there were nearly 1900 casualties reported resulting from IED explosions in Afghanistan alone [1]. Approximate totals from other news outlets put the number of casualties resulting from IED explosions in Iraq and Afghanistan combined at over 2400 [2] [3]. The strong need for improved protection from these blast events have made lightweight component design an active research subject.

Figure 1.1 A U.S. light vehicle after an IED attack in Iraq, 2007 [4]

Vehicle crew injuries are caused by a number of factors including: gross vehicle acceleration, overpressure within the vehicle cabin, and penetration of the material into

the cabin. From the evaluation of conventional up-armoring methods, Grujicic and Arakere have determined that an effective means of attenuating gross vehicle accelerations in a blast event is by increasing the mass of the vehicle with additional armor components [5]. The inverse relationship between impulse absorption and vehicle mass is generally well known. Dynamic vehicle responses to shallow buried detonations, as given in McAndrew's account of shock isolation mechanisms, exhibit this same relationship between vehicle mass and vertical acceleration [6]. The up-armoring of existing vehicles to better protect against blast events involves the addition of sacrificial components that can deflect and/or absorb the energy released by the blast. Light vehicles that were originally intended for use in logistical support roles have seen an increased number of attacks from IED in urban settings and seem particularly vulnerable [5].

Although it can lead to improved blast isolation characteristics, increasing the mass of a light ground vehicle has been shown to cause problems in other aspects of vehicle performance. Standard up-armoring of ground vehicles can add up to 2000 kg of additional mass to the vehicle. Without concurrent modifications to the power train, suspension, braking and steering components, the up-armored vehicles suffer from degraded stability and mobility. Such practices have contributed to increased instances of vehicle stability related accidents [5]. For these reasons, there is a critical need for effective methods to generate lightweight components for blast mitigation.

1.2   Literature Review

1.2.1   Plate Armor Design

This thesis investigates the automated design process of isotropic plates to mitigate the effects of blast loading. Methods of blast energy absorption have been evaluated through extensive design investigations of composite materials [7, 8], as well as numerical [9] and experimental [10] simulations of sacrificial structures. The goal of these efforts is

to develop an armor system which could absorb or deflect a significant portion of the blast energy, thereby protecting the underlying structure. Although there has been substantial work performed in this research area, the field is still primarily academic. No successful application of an energy absorbing armoring system has been implemented in the production of ground vehicles.

A common trend in armor design is multi-material armor, sometimes referred to as integral armor or sandwich structure armor [11, 12, 13]. The goal of a multiple material approach is to develop plate armor that can withstand a variety of attacks while maintaining a low weight and cost. Differences in material properties between the layers of the structure affect blast wave propagation, thus layer arrangement and selection of layer material is of the greatest importance in these endeavors [14, 15]. Examples of multiple material investigations include: aluminum-titanium laminates [16], ceramic inter-layers [17], and the use of sandwich structures of metal plating with an inner honeycomb patterned core [11]. As yet, there is no definite blast mitigation strategy involving the use of multiple material plate structures.
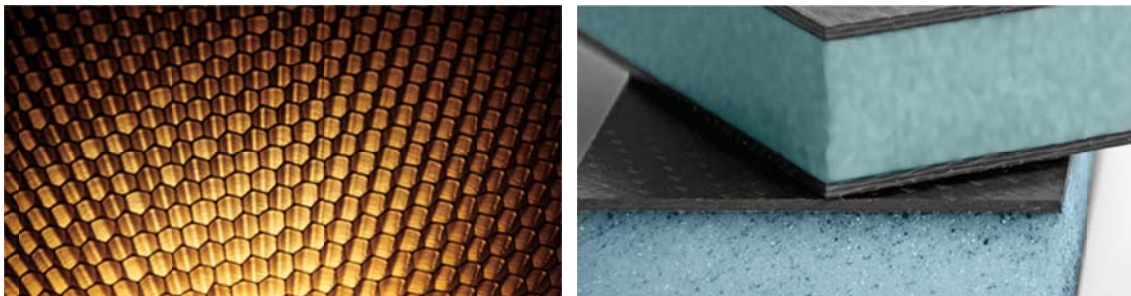
Figure 1.2 Honeycomb material used for the inner core of sandwich structures (left), and two examples of foam core composites (right) [18]

There has also been substantial work on analysis of the effects of blast loading on isotropic plate shell structures. As early as 1990, the work of Dharaneepathy and Sudhesh investigated the response of square plate structures under blast loading rendered as shell elements in finite element simulation [19]. Their work, rooted in the selection of stiffening patterns to reduce dynamic deflection of the structure, is an early example of investigations into blast mitigation strategies involving isotropic plates that utilized deflection as a key

performance metric. Argod and Belegunda have shown significant improvement of structure design of isotropic plates using velocity-field based optimization and have demonstrated what they refer to as the "double bulge" optimum shape, as well as the effects of different boundary conditions for plates of this kind [20]. Belegunda and Rajan have achieved similar results utilizing basis shapes and multiple-material sandwich plate structures [21] as shown in Figure 1.3.
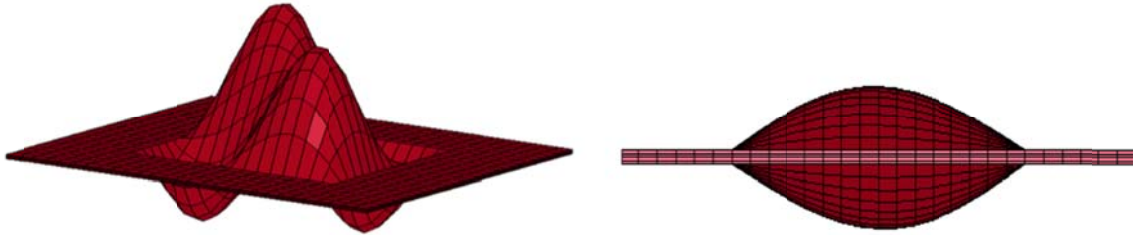
Figure 1.3 Example results of plate topography optimization from the work of Belegunda and Rajan, the "double-bulge" shape is shown to the right [21]

Often framed against the problem of blast protection systems design for vehicle applications, previous investigations of lightweight armor design have measured performance in terms of structural mass and dynamic deflection. The work of Tovar *et al.* has demonstrated a two-material topology optimization approach which utilizes peak plate displacement as a key metric [22]. Their work focuses on reducing dynamic displacement of the plate through shape optimization while keeping the mass constant. Subsequent investigations into topography optimization using mass constraints have also made use of deflection constraints as failure and optimization criteria [23]. Multiple additional studies have focused on reducing the dynamic deflection of armor plating [24, 16, 21].

1.2.2 Blast Events

Physical nonlinearities are abundant in the process of a blast event. In such events, the kinetic energy is transferred to the structure by means of a fluid structure interaction. The dynamics of the events and their interactions with solid structures is an area that has been extensively researched [25]. The governing equations of thermo-mechanics that characterize blast loading conditions require the conservation of mass and energy, balance

of linear and angular momentum, heat equations, stress/strain relations, and, in the case of blast pressure calculations and shrapnel penetration calculations, kinetic and caloric equations of state; Kinetic and caloric equations of state are required in solving the behavior of pressurized gases upon detonation, volumetric equations of state may be used to solve for the behavior of the target ceramic material. From this basic thought process, it appears that in order to solve for the behavior of the target material while accounting for all the thermo-mechanical interactions of the blast wave and projectile impacts, the solution of all sixteen equations are required. To reduce the total governing equations required, it may be necessary to simplify or dissect the phenomena of detonation into more manageable models.

Several experimental investigations have been conducted in the field of detonation events [26]. The CONWEP model developed by the Army Research Laboratory, and currently used in commercial finite element blast simulations, is considered adequate for use in engineering studies of vehicle response to the blast from land mines [25]. The CONWEP algorithm does not explicitly simulate the effects of the detonation reaction with air nor does it calculate the shock wave propagation and its reactions with the target structure. In continuum mechanics the Arbitrary Lagrange-Eulerian method is commonly applied in the finite element analysis of fluid structure interactions. The ALE method is popular in its application to large shear deformations where a traditional Lagrangian mesh breaks down due to geometric instabilities. Compared to a traditional Eulerian mesh such as those used in computational fluid dynamics analysis, the ALE method is better suited to tracking fluid boundaries and resolving flow details involving large volume changes [27]. Due to the importance of fluid structure interactions in many engineering applications, the ALE algorithm has been applied to commercial finite element solvers and is currently available in the LS-DYNA 971 release.

The length and time scales in blast analysis are very different from that of the traditional linear elastic quasi-static optimization problems. In such previously studied problems the material stress strain relations are assumed to follow linear elastic models for

quasi-static problems and linear plastic deformation relations are assumed for material yielding under dynamic simulations. Materials in the design domain are generally assumed to be isometric and the density of the material is assumed to be controllable and linearly proportional to the material properties. The blast optimization problem proposed involves pressure and mechanical loading conditions that cannot be properly modeled using the existing linear elastic material models. The time scale involved under blast loading conditions involves irreversible processes that require a more complete model of thermal mechanical reactions than that currently available. Of primary concern in the detonation and explosion interaction event as opposed to a crash event is the interaction of the blast shock wave with the target structure.

1.2.3   Uncertainty Quantification

Another important aspect of this work is the development of a methodology for design under uncertainty in blast mitigation. There is a significant need to apply existing and recently developed methods of design under uncertainty to the area of topography optimization for blast mitigation. Only recently have investigations into topography optimization employing stochastic methods emerged [23]. Of chief importance in the application of any design under uncertainty method is the quantification of uncertainties in performance as result of uncertain inputs. The quantification of how uncertainty propagates throughout the system is the general goal of such endeavors and is commonly referred to as uncertainty quantification (UQ) [28].

The recent work of Chen and Lee has set out to examine the various methods of UQ and investigate the relative merits of each with respect to engineering test problems [28]. Their work divides the methods for UP into five general categories. The first category is composed of simulation based methods such as the Monte Carlo simulation [29, 30], and the adaptive sampling method [31]. The second category is made up of local-expansion based methods such as Taylor-series based expansion methods [30]. The third category is the most-probable point (MPP) based methods [32]. First order and second order reliability

based method are two well know method that fall into that category. The fourth category is composed of functional expansion based methods. In the past two decades, methods in this category such as the polynomial chaos expansion method (PCE) [33, 34], have been growing in application to the areas of uncertainty representations and stochastic mechanics [28]. The last category as described by Chen is the numerical integration based methods. In these methods, the first and second statistical moments are first calculated using by numerical integration and then probability density is approximated using empirical distribution.

Due to the highly non-linear performance functions observed in blast loading optimization problems, some of these uncertainty propagation methods are ill-suited for application in this research. The Monte Carlo simulation method, as well as other simulation based methods, involves large amounts of function evaluations to achieve acceptable accuracy. When the method for function evaluation is rooted in finite element analysis as it is in blast mitigation optimization, those methods are overly computationally expensive. Local expansion based methods, such as the Taylor-series expansion method, are extremely sensitive to nonlinearity of the structural response, thus making them a poor choice of application [35]. While there have been applications of the PCE method recently to aleatory uncertainties, which are irreducible variabilities found in nature [33], this method has not been proven for the quantification of epistemic uncertainness which stem for a direct lack of data, as are studied in this research.

The investigations in this thesis are focused on the application of two methods that full into the numerical integration based category. The univariate dimensional reduction method (UDR) is based in the decomposition of a multi-dimensional function into sum of several one-dimensional functions [36, 37]. This method is well-suited for the problems at hand as it is fairly computationally efficient for problems involving few random inputs [38]. The second method under investigation here is the performance moment integration method (PMI) as proposed by Choi *et al.* for robust design optimization [35]. Similar to

UDR, this method is also a numerical integration technique, but the integration is performed on the output domain as opposed to the input domain.

<div align="center">1.3   Objectives</div>

The fundamental optimization problem to be analyzed in the design of a structure for blast mitigation is that of minimizing the kinetic energy transfer from the blast wave to the solid body. The goal of such efforts is to develop a system that could absorb a significant amount of the energy released in a blast event such that the underlying structure may be preserved. This thesis will focus on various design techniques for isotropic plate structures within the same design space, building on the efforts in topography optimization mentioned previously which aim to minimize the mass of the structure compliant to dynamic deflection constraints [23, 20, 21]. The first objective of this work is to investigate the design of lightweight structures under deterministic loading conditions and subject to the same objective function and constraints. The purpose of is to compare feasible design methodologies through the expansion of the problem dimension in order to reach the limits of performance. To this end, seven profiles are evaluated, each under the same loading and boundary conditions.

The second objective of this research involves the application of uncertainty quantification methods recently proposed by Choi *et al.*, Xu and Rahman [35, 36] to the design of lightweight structures under stochastic loading conditions. The methods under investigation are the univariate dimensional reduction method (UDR) and the performance moment integration method (PMI), both of which will be evaluated with a test problem and applied to the performance of plate structures under blast loading. This investigation will provide a basis for design under uncertainty methods which have previously been little applied to the design of lightweight structures for blast mitigation. The application of these uncertainty quantification methods to problems of design optimization under uncertainty is the final objective of this research.

A summary of the objectives is as follows:

• Development of a substantially-realized system for shape optimization of plate structures under deterministic blast loading conditions. This objective will involve the following tasks:

- Generation of an integrated system of LS-DYNA finite element software and the Matlab optimization toolbox to solve blast mitigation optimization problems for the automated generation of lightweight structures.

- Development of seven separate, progressively more complex design methods to investigate the effects an increase in design variables has on the performance results :

  ▪ Flat Plate design

  ▪ Pyramid profile design

  ▪ Gaussian function design

  ▪ Polynomial function design

  ▪ Trigonometric function design

  ▪ HCA topography design

  ▪ Inverted profile design

• Investigation and evaluation of recently proposed methods for uncertainty quantification for application in design under uncertainty problems for plates under blast loading

  - Mean-based univariate dimensional reduction (UDR) – evaluation of the method through experimentation with non-linear test problem and application to blast loading problem.

  - Performance moment integration (PMI) – evaluation of the method through experimentation with non-linear test problem and application to blast loading problem.

• Through the application of uncertainty quantification methods described above, development and evaluation of design under uncertainty methodology for blast-

resistant component design under stochastic loading conditions. This objective will involve the generation of methods and development of automated design software for the following design under uncertainty methods:

- Reliability Based Design Optimization (RBDO)
- Robust Design Optimization (RBO)
- Reliability-Based Robust Design Optimization (RBRDO)

1.4 Organization

This thesis illustrates the methods and results utilized in the generation of lightweight structures for blast mitigation under uncertainty. As was stated previously, the overall objective of this research is to make advances in structural design methods for the optimization of lightweight blast-mitigating systems, and the research is carried out incrementally in terms of primary research projects.

The main body of this thesis is composed of five chapters, each of which provides the details of those research projects and any and all conclusions from the work. Chapter 1 consists of the social and technical justification for the work, as well as the literature review and description of the primary objectives. Chapter 2 contains all information related to the methods used to carry out the deterministic design project: the general optimization problem, the algorithms used, FEA details, etc. Correspondingly, Chapter 3 contains all methods utilized for the design under uncertainty portion of the research. Chapter 4, Numerical Models and Applications, contains results of the application of methodologies as well as discussion of the results and salient conclusions. The conclusion of the work, Chapter 5, contains all primary and secondary contributions of the research and recommendations for future endeavors. In addition, a brief appendix contains samples of the computer code that composes the computational framework generated by the research.

2. DETERMINISTIC DESIGN METHODOLOGY

2.1 Optimization Problem Definition

In blast protection system design for vehicle applications, there are two primary performance measures of critical relevance: weight and cabin penetration. Weight is privileged as a key performance measure stemming from the need for lightweight, compact structures that can be fitted to existing vehicle designs without extensive re-design of the frame or other vehicle systems. The goal is to design light structures that do not adversely affect vehicle performance. Large deflections of the plate structure due to a blast event can cause penetration into the passenger cabin of the vehicle and result in occupant injury. In this way, cabin penetration can be seen as a means of quantifying the degree to which the blast energy has been mitigated; if the deflection of the plate structure post-blast exceeds a certain amount, the design is unsuccessful. In consideration of these performance measures, the objective function is formulated as the mass of the plate structure and is minimized subject to displacement constraints (cabin penetration) and design space limitations. The general optimization problem for deterministic cases addressed in this paper is

$$
\begin{aligned}
&\text{find} &&\boldsymbol{d}\\
&\text{minimize} &&M(\boldsymbol{d})\\
&\text{subject to} &&P_c(\boldsymbol{d}) - P_{c\,max} \leq 0\\
& &&S(\boldsymbol{x}, \boldsymbol{y}, \boldsymbol{z}, \boldsymbol{d}) = 0\\
& &&\boldsymbol{d}^L \leq \boldsymbol{d} \leq \boldsymbol{d}^U
\end{aligned}
\tag{2.1}
$$

where $\boldsymbol{d} \in \mathbb{R}^n$ is the set of all design variables characterizing the shape and thickness of the plate, $M(\boldsymbol{d})$ is the plate's mass, $P_c(\boldsymbol{d})$ is the penetration after the blast event with respect to datum plane, $P_{c\,max}$ is the maximum allowable value for penetration. The envelope constraint $S(\boldsymbol{x}, \boldsymbol{y}, \boldsymbol{z}, \boldsymbol{d})$ is a function of the nodal coordinates $\mathbf{x}$, $\boldsymbol{y}$, and $\boldsymbol{z}$. The
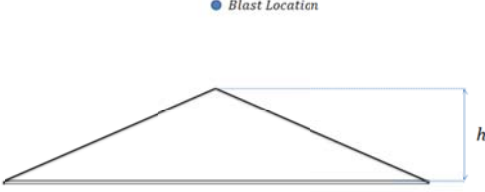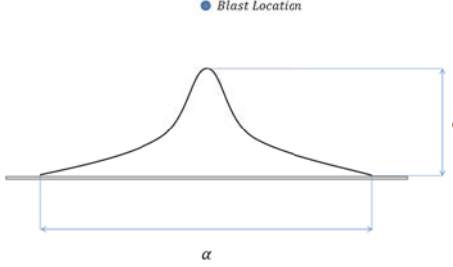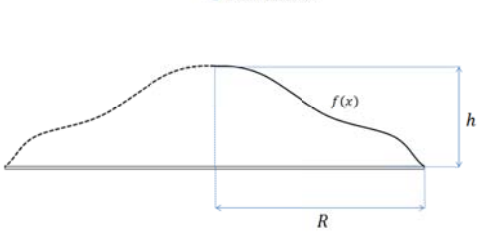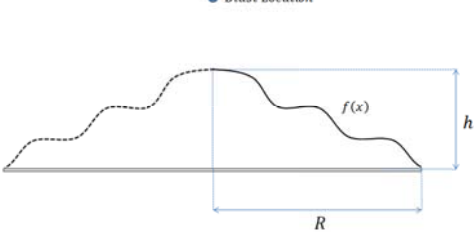
box constraint $\boldsymbol{d}^L$ and $\boldsymbol{d}^U$ are the lower and upper bounds for the design variables, respectively. The envelope constraint S is progressively relaxed so the design space is expanded to contain more design variables. This allows increasing the performance design problem at expenses of more complex topographies.

2.2 Geometrically Constrained Designs

This work is framed in the context of vehicle protection from blast events. Five envelope constraints are considered in this work, as given by Table 2.1 (next page). These envelope constraints define geometrically constrained designs whose shape is can be characterized through only a few design variables. A description of each geometrically constrained design along with a brief motivation for each is given here:

- **Flat Plate Design.** This topography for flat plane is defined by the condition in which the all the $z-$coordinate values for every node is the same. This design is regarded as the baseline for comparison with each progressive candidate design.

- **Pyramid Profile Design.** Methods of blast mitigating structure design have been evaluated extensively through experimental efforts in the development of lightweight V-shaped hulls, and have demonstrated that V-shaped designs can mitigate the effects of blast events [39]. The pyramid profile design is an improvement of the V-shape design used in concept designs, due to the fact that it is constrained on four sides.

- **Gaussian Function Design.** In the interest of creating more complex curves through minimal expansion of the design domain, a plate structure that takes on the shape of a Gaussian function of two variables is generated. Previous explorations of this shape demonstrated promising, yet inconclusive results [40].

- **Polynomial Function Design**. And **Trigonometric Function Design**. Two additional design methodologies are examined which relax the problem further. In both the polynomial function and trigonometric function cases, a function of several variables is used to generate a complex curve. The plate design is achieved as a surface of revolution by rotating the curve about the $z-$axis.

Table 2.1 Envelope constraints and corresponding number of design variables

Envelope Constraint	Schematic	Num. of design variables
Flat Plate		1
Pyramid Profile Pyramid		2
Gaussian		3
Polynomial		5
Trigonometric		6

2.3 Free Shape Designs

As the number of design variables increases, so does the complexity of the analytical description of each design. A large increase in the number of design variables makes the problem intractable in that an analytical solution for sensitivity has not been derived. In short, for traditional sensitivity-based design optimization, the cost of sensitivity limits the number of design variables. In order to overcome those limitations, two alternative methods are examined which utilize a large design domain and rely on user input to avoid intractability. These free shape designs deal with the most relaxed problem, as there is no underlying analytical description of the shape:

- **Inverted Profile Design**. There has been some interest in creating a plate that takes on an inversion of the topography of a flat plate after a blast event - largely inspired by the mathematical idea of the catenary curve, the idealized shape that a chain assumes under its own weight. The reasoning being that the complex blast pressure distribution would then determine the shape of the plate and influence the z-coordinate at each node proportional to the magnitude of the loading. This approach has been utilized in the design of bridges as well as in the world of architectural design [41] [42].

- **HCA Topography Design**. The Hybrid cellular automata method, or HCA, is an approach that allows us to handle many design variables. In this approach, the field variable, in this case the nodal z-coordinate, is driven toward a pre-determined set point. HCA methods have been used in the past by Goetz and Tovar to develop two-material topologies for blast mitigation [22] , but there is a need to demonstrate the uses of HCA for topography optimization.

2.4   Finite Element Analysis

2.4.1   Explicit FEA using LS-DYNA

Consider the system of 2nd order differential equations that govern a discretized structure

$$M\ddot{x}(t) + C\dot{x}(t) + Kx(t) = F(t) \tag{2.2}$$

where M is the mass matrix, C is the damping matrix, K is the stiffness matrix and $\ddot{x}(t)$, $\dot{x}(t)$, $x(t)$ are the vectors of acceleration, velocity, and displacement (respectively) for the nodal locations at any given time t. $F(t)$ is the vector of external forces applied to the structure. Solving for acceleration, equation (2.2) becomes

$$\ddot{x}(t) = M^{-1}\left(F(t) + F_s(t)\right) \tag{2.3}$$

where $F_s(t)$ is the vector of internal structural forces. In blast simulations, which concern highly nonlinear dynamic analysis, quasi-static assumptions for inertia effects are not fulfilled due to the fact that the dynamic problem involves loads and responses that vary with time and the duration of loads are small [43]. One method for solving such highly non-linear problems is to use an explicit finite element method.

The terms implicit and explicit refer to time integration algorithms. An Explicit FEA analysis utilizes an incremental procedure to solve for nodal dynamics. At the end of each increment, it updates the stiffness matrix based on geometry changes (if applicable) and material changes (if applicable).   Then a new stiffness matrix is constructed and the next increment of load (or displacement) is applied to the system. The purpose for this explicit approach is that if the increments are small enough, then the results will be accurate. One problem with this method is that the time increment must be very small for a high level of accuracy and thus the simulation can be extremely computationally expensive. If the time increment is too large, the solution tends to drift from the correct solution. In blast simulations, the load conditions are dynamic and the total duration of the simulation is often very small, approximately 0.005 seconds, so an explicit solver is a sound choice.

This research uses the LS-DYNA explicit solver for all nonlinear finite element analysis. For solving systems of differential equations such as (2.2), LS-DYNA utilizes a modification of the central difference method for time integration as an explicit method [44]. For nonlinear dynamic problems the initial conditions for position and velocity must be known. Once the initial conditions are defined, LS-DYNA obtains the nodal velocities and accelerations at the next time increment from the following equations:

$$\dot{x}(t) = \frac{1}{2\Delta t} \left(x(t+1) - x(t-1) \right) \tag{2.4}$$

$$\ddot{x}(t) = \frac{1}{(\Delta t)^2} \left(x(t+1) - 2x(t) + x(t-1) \right) \tag{2.5}$$

where Δt is the time increment. The accelerations are integrated over time using the central difference rule. Subsequently, the velocities are integrated through time and added to the initial displacement to generate new displacement values. Dynamic equilibrium is then satisfied at the beginning of the time increment and the accelerations for the next increment are known. In order to initialize the time integration, LS-DYNA uses the following equation to update displacement

$$x(t-1) = x_0 - \Delta t \dot{x}_0 + \frac{\Delta t^2}{2} \ddot{x}_0 \tag{2.6}$$

where x_0 and $\dot{x}_0$ are the initial conditions at time $t = 0$ [45].

Stability requires that the time increment be smaller than the highest frequency of the system [44]. LS-DYNA determines the time increment based on the smallest element in the structure excluding any rigid elements that do not deform. The time increment can be roughly estimated by

$$\Delta t = 0.9 \frac{l}{c} \tag{2.7}$$

where l is the smallest element dimension and c is the speed of sound in the material [44]. In this research, the time increment varies due to the use of different mesh discretization, but in general the time increment used by the explicit solver is on the order of 0.5×10^{-6} seconds.

<div style="text-align:center">2.4.2 Material Modeling</div>

An LS-DYNA input deck consists of a series of cards which contain user-defined model information. The material properties and behavior is contained in the *MAT card. A commonly used [46] [21] material model assigned to metal materials in LS-DYNA is the material model 024-PIECEWISE_LINEAR_PLACTICITY. This model is an elasto-plastic material where an arbitrary stress versus strain curve and an arbitrary strain rate dependency can be defined [44]. The input card for this material is shown in Figure 2.1. Complete material property definitions can be found in Chapter 4 of this thesis, which deals with the numerical models.

Figure 2.1 Input card for MAT_ PIECEWISE_LINEAR_PLACTICITY in LS-PrePost

It is possible to define a set of points of effective plastic strain values and corresponding values of yield stress. However, a simplified bilinear stress strain curve was used for this study through the definition of values for stress value and tangent modulus. The tangent modulus is used as the slope of the stress strain curve after the proportional limit governed by Young's modulus is exceeded, as shown in Figure 2.2. The strain rate is accounted for by the Cowper and Symonds model [47] which scales the yield stress with the relation

$$\frac{\sigma_d}{\sigma_s} = 1 + \left(\frac{\dot{\varepsilon}}{C}\right)^{\frac{1}{P}} \tag{2.8}$$

where σ_d is the dynamic yield stress, σ_s is the static yield stress, $\dot{\varepsilon}$ is the strain rate, and C and P are the Cowper-Symonds constants.
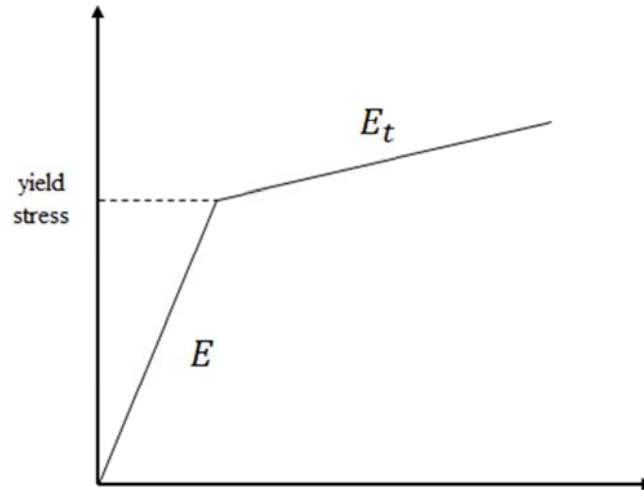
Figure 2.2 Bilinear stress-strain curve demonstrating transition from Young's modulus to tangent modulus

It should be noted that elemental strain values are not included in the analysis, and subsequently, failure of elements is not considered in the optimization routine. This research operates under the assumption that there is no fracture of the material, therefore the default failure stress value of 10^{21} Pa is used in all FEA simulations.

2.4.3   Blast Loading

The blast loading applied to the structure is calculated in LS-DYNA by using a set of empirical loading functions implemented in the ConWep code.   The ConWep equations were developed by Kingery and Bulmash [48] and implemented in LS-DYNA by Randers-McPherson and Bannister [25] as a means of simulating blast loading conditions in a finite element environment. The equations are a means to apply distributed pressure on a surface based on the location and magnitude of the initial charge. A number of investigations have been published concerning the validation of these empirical models, including extensive work by DRDC Valcartier [49, 50]. The pressure distribution modeled by the ConWep equations applied to a square plate such as the ones examined in this research is shown in Figure 2.3.
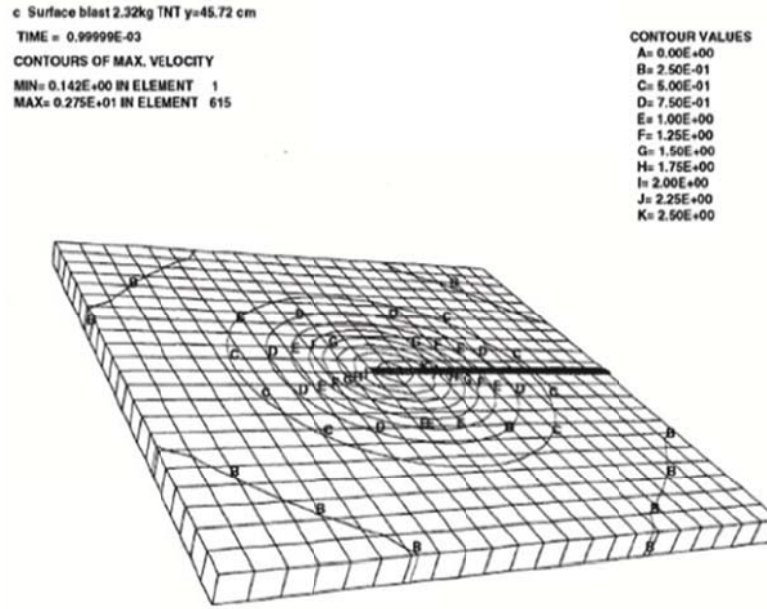
Figure 2.3 Contours of pressure loading from ConWep on a simple square plate [50]

The implementation of the ConWep code in LS-DYNA is achieved by the population of the *LOAD_BLAST_ENHANCED card, shown in Figure 2.4. This input card allows the designer to define the location (in Cartesian coordinates) and magnitude (in units of kg TNT) of the blast, as well as the time of detonation and the type of blast (air or surface).

Figure 2.4 Input card for LOAD_BLAST_ENHANCED in LS-PrePost

The blast functions in LOAD_BLAST_ENHANCED can be used for two cases, the air detonation of a spherical charge or the surface detonation of a hemispherical charge.

The surface charge is intended to approach the conditions associated with the blast produced by a mine or other road-side improvised explosive device; however, there are limitations to this model. There are a number of factors which can have a significant effect on the energy released by the explosion which are not taken into account by the CONWEP blast model. These factors include: burial depth, surface material (soil, sand, etc.), and atmospheric moisture conditions [49]. Thus, the accuracy of the hemispherical charge, without the modeling of the immediate environment and without accounting for fluid-structure interaction is in question. In addition, there has been shape optimization work on isotropic plate structures conducted using air blast loading as the preferred loading case [21] [19]. For these reasons, the air blast option is chosen for this research and is used consistently for all cases throughout. Future research will include full fluid modeling and hemispherical charges that can account for reflected waves and other ground effects.

2.5   Optimization Algorithm

There are two primary algorithms used throughout this research for the purpose of solving the optimization problems. The first and most extensively used here is sequential quadratic programming (SQP), specifically the active-set based quadratic programming algorithm. The second optimization algorithm used here is the hybrid cellular automata method, developed for application to continuum structures [51]. The development of this optimization method was inspired by the biological process of bone remodeling.

2.5.1   Constrained Optimization

Consider the following expression for a standard constrained optimization problem:

$$
\begin{aligned}
&\text{find} &&\boldsymbol{x} \\
&\min &&f(\boldsymbol{x}) \\
&\text{s.t.} &&G_i(\boldsymbol{x}) = 0 \\
& &&G_j(\boldsymbol{x}) \leq 0
\end{aligned}
\tag{2.9}
$$

where $f(x)$ is the objective function[1] and $G_i(x)$ is the set of equality constraints and $G_j(x)$ is the set of inequality constraints. In constrained optimization, the general aim is to transform the problem into an easier sub-problem that can then be solved and used as the basis of an iterative process. Current methods for solving this type of problem have focused on the solution of the Karush-Kuhn-Tucker (KKT) equations [52]. The KKT equations are necessary conditions for optimality for a constrained optimization problem. If the problem is a so-called convex programming problem, that is, $f(x)$, and $G_i(x)$, and $G_j(x)$ are convex functions, then the KKT equations are both necessary and sufficient for a global solution point.

Given the problem description in (2.9) the principal idea behind the KKT equations is rooted in the Lagrangian function

$$L(x, \lambda, \mu) = f(x) + \sum_{i=1}^{m} \lambda_i \cdot G_i(x) + \sum_{j=1}^{n} \mu_j \cdot G_j(x) \tag{2.10}$$

where λ_i are the Lagrange multipliers associated with the equality constraints and μ_j are the Lagrange multipliers associated with the inequality constraints. If we assume that x^* is a regular point, then x^* is a minimum of $f(x)$ only if the conditions given by the following equations are satisfied:

$$\nabla L(x^*, \lambda, \mu) = 0 \tag{2.11}$$

$$\lambda_i \cdot G_i(x^*) = 0 \tag{2.12}$$

$$\lambda_i \geq 0 \tag{2.13}$$

$$G_i(x^*) \leq 0 \tag{2.14}$$

---

[1] Note: for the remainder of section 2.5, the symbol x refers only to a generic vector of variables used to demonstrate the method of constrained optimization. It does not refer to the vector of nodal x-coordinates as in previous sections.

$$G_j(\boldsymbol{x}^*) = 0 \,. \tag{2.15}$$

Note that only the Lagrange multipliers λ_i associated with the inequality constraints are restricted in sign; The Lagrange multipliers associated with the equality constraints can be positive or negative [53].

The solution of the KKT equations forms the basis to many nonlinear programming algorithms. These algorithms attempt to compute the Lagrange multipliers directly. Constrained quasi-Newton methods, such as the Davison-Fletcher-Powell method or the Broyden-Fletcher-Goldfarb-Shanno (BFGS) method, guarantee super-linear convergence by accumulating second-order information regarding the KKT equations using a quasi-Newton updating procedure. These methods are commonly referred to as Sequential Quadratic Programming (SQP) methods, since a Quadratic Programming (QP) sub-problem is solved at each major iteration.

2.5.2   Sequential Quadratic Programming (SQP)

SQP methods represent the state of the art in nonlinear programming methods. Based largely on the contributions of Biggs [54], Han [55], and Powell [56, 57], the method allows you to closely mimic Newton's method for constrained optimization just as is done for unconstrained optimization. At the execution of each global iteration, an approximation is made of the Hessian of the Lagrangian function using the quasi-Newton BFGS updating method. This is then used to generate a QP sub-problem whose solution is used to form a search direction for a line search procedure. An overview of the general SQP method is stated here.

Step 1: Approximation of Hessian Matrix - At each global iteration a positive definite quasi-Newton approximation of the Hessian of the Lagrangian function, *H*, is calculated using the BFGS method.

Step 2: Quadratic Programming Solution - Given the problem description in (2.9) the principal idea is the formulation of a QP sub-problem based on a quadratic approximation of the Lagrangian function given by equation (2.10). The quadratic programming sub-problem can be obtained through the linearization of the constraints, expressed as

$$\begin{aligned} \min \quad & \frac{1}{2}\boldsymbol{r}^T \boldsymbol{H}_k \boldsymbol{r} + \nabla f(\boldsymbol{x}_k)^T \boldsymbol{r} \\ \text{s.t.} \quad & \nabla G_i(\boldsymbol{x}_k)^T \boldsymbol{r} + G_i(\boldsymbol{x}_k) = 0 \\ & \nabla G_j(\boldsymbol{x}_k)^T \boldsymbol{r} + G_j(\boldsymbol{x}_k) \leq 0 \end{aligned}$$

(2.16)

where the matrix $\boldsymbol{H}_k$ is a positive definite approximation of the Hessian matrix of the Lagrangian function, and $\boldsymbol{r}$ is the search direction. This sub-problem can be solved using any QP algorithm. The solution is used to form a new iterate

$$\boldsymbol{x}_{k+1} = \boldsymbol{x}_k + \alpha_k \boldsymbol{r}_k$$

(2.17)

The step length parameter α_k is determined by an appropriate line search procedure so that a sufficient decrease in a merit function is obtained.

2.5.3   Active-set Search Algorithm

As is stated above, at each global iteration of the SQP method, a QP problem is solved. The method for solving this QP problem is commonly the differentiating factor between SQP algorithms. This research uses an active-set algorithm to solve QP problems, which involves a restatement of equation (2.16) in the following form,

$$\begin{aligned} \min \quad & \frac{1}{2}\boldsymbol{r}^T \boldsymbol{H}_k \boldsymbol{r} + \nabla f(\boldsymbol{x}_k)^T \boldsymbol{r} \\ \text{s.t.} \quad & A_i \boldsymbol{r} = b_i \\ & A_j \boldsymbol{r} \leq b_j \end{aligned}$$

(2.18)

where A_i refers to the ith row of the matrix A. The solution procedure involves two phases. The first phase involves the calculation of a feasible point. If a feasible point exists, the second phase involves the generation of a local iterative sequence of feasible points that converge to the solution. In this method, an active set, A_k, is maintained that is an estimate of the active constraints at the solution point, or those that are on the

constraint boundaries. A_k is updated at each iteration k, and this is used to form a basis for a search direction $\boldsymbol{r}_k$. Equality constraints always remain in the active set A_k. The notation for the local variable $\boldsymbol{r}_k$ is used here to distinguish it from $\boldsymbol{r}$ in the global iterations of the SQP method. The search direction $\boldsymbol{r}_k$ is calculated and minimizes the objective function while remaining on any active constraint boundaries. The feasible subspace for $\boldsymbol{r}_k$ is formed from a basis Z_k whose columns are orthogonal to the estimate of the active set A_k of the form

$$A_k Z_k = 0 . \tag{2.19}$$

Thus a search direction, which is formed from a linear summation of any combination of the columns of Z_k, is guaranteed to remain on the boundaries of the active constraints.

This SQP active set algorithm can be implemented using Matlab's optimization toolbox and the *fmincon* function. This function can be fully customized in terms of objective function, equality and inequality constraints, and optimization algorithm. Although the default algorithm used by the *fmincon* function is a trust-region algorithm, this method requires a numerical formulation of the gradient, which is not feasible for the highly non-linear performance functions experienced in blast loading. Thus the active-set algorithm is chosen as a solution procedure [52].

2.5.4 Hybrid Cellular Automata

The hybrid cellular automaton (HCA) algorithm is a structural design methodology inspired by the biological process of bone adaptation [58, 59]. This methodology assumes that cellular automata (CAs) form a structure or design domain, and sensors and actuators within the CAs activate local formation and resorption of material. With a proper control strategy, this process drives the overall structure to an optimal topography by updating the nodal locations. Using distributed controlled rules, the problem optimization problem can be stated as

$$
\begin{aligned}
&\text{find} && t_i, \mu \\
&\text{minimize} && \left| \widehat{MPE_\iota}(\boldsymbol{t}) - MPE^*(\boldsymbol{t}, \mu) \right| \\
&\text{subject to} && M = \sum_{i=1}^{n} \rho A_i t_i \leq M_{max} \\
& && t_{min} \leq t_i \leq t_{max} \\
& && \boldsymbol{R} = \boldsymbol{0}
\end{aligned}
\tag{2.20}
$$

where μ is the Lagrange multiplier associated with the mass constraint. In (2.20) MPE^* is the target value to be achieved by every element in the structure. This target is a function of the thickness distribution $\boldsymbol{t}$ and μ. In order to preserve a consistent topology design that is independent of the number of cells, an effective element mutual potential energy $\widehat{MPE_\iota}$ defined as a function of the cell's neighborhood size,

$$
\widehat{MPE_\iota} = \frac{\sum_{j \in N_i} MPE_i}{|N_i|}
\tag{2.21}
$$

where N_i is the neighborhood of the i-th cell defined by

$$
N_i = \{ j : d(i,j) \leq r \}
\tag{2.22}
$$

and $d(i,j)$ denotes the distance between the i-th and the j-th cells. The neighborhood layout depends on the distance r referred to as the range of the neighborhood. Figure 2.5 shows the CA neighborhood layouts for different ranges.

Empty   von Neumann   Moore   Radial
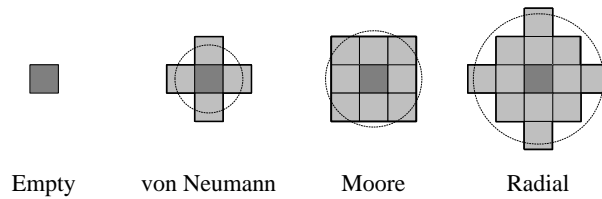
Figure 2.5 CA neighborhood layouts for different ranges

The iterative approach may be achieved using a control-based algorithm [60, 61] or a ratio approach [62]. The specific application of this algorithm to the plate structure topography problem and the control rules used to govern its execution are addressed in Chapter 4 of this thesis.

2.5.5   Metamodelling

Metamodelling involves the generation of one (or possible more) levels of abstraction from an existing analytical model; Just as a model is an abstraction from some phenomena or object in the real world, a metamodel is an abstract representation of the existing model [63]. This research explores the implementation of radial basis function networks as a metamodelling technique. It is the intention that the radial basis function network tools can be used to approximate the response of the system normally calculated be means of FEA simulation, and therefor improve computational efficiency.

Radial basis function networks are a type of artificial neural network. An artificial neural network, inspired by the neurobiological workings of the brain, is composed of an interconnected group of artificial neurons. The network processes information as a relation of connections between these neurons, often referred to as the connectionist approach to computation [64]. A radial basis function (RBF) is simply a function whose value is based on the distance from the origin. In turn, a radial basis network is a neural network that uses RBF functions as the method of neural approximations [65].

A radial basis function network, as shown in Figure 2.6, has three layers: an input layer, a hidden layer containing RBF functions, and an output layer. The input layer can be modeled as vector of real numbers $\boldsymbol{i} \in \mathbb{R}^n$ and the output is a scalar function of the input vector $\varphi : \mathbb{R}^n \rightarrow \mathbb{R}$. The hidden layer, which contains the RBF functions, is used to approximate the output function expressed as

$$\varphi\,(\boldsymbol{ni}) = \sum_{i-1}^{N} a_i \rho\,(\|\boldsymbol{i} - c_i\|) \tag{2.23}$$

where N is the number of neurons, c_i is the center vector for neuron i, and a_i is the weight of neuron i in the linear output neuron [65]. The values for c_i and a_i are chosen such that $\varphi\,(\boldsymbol{x})$ best fits the data.

Weights

Linear Weights

Input
Design Variables d

Radial Basis Functions

System Response
Mass M
Protection C_p
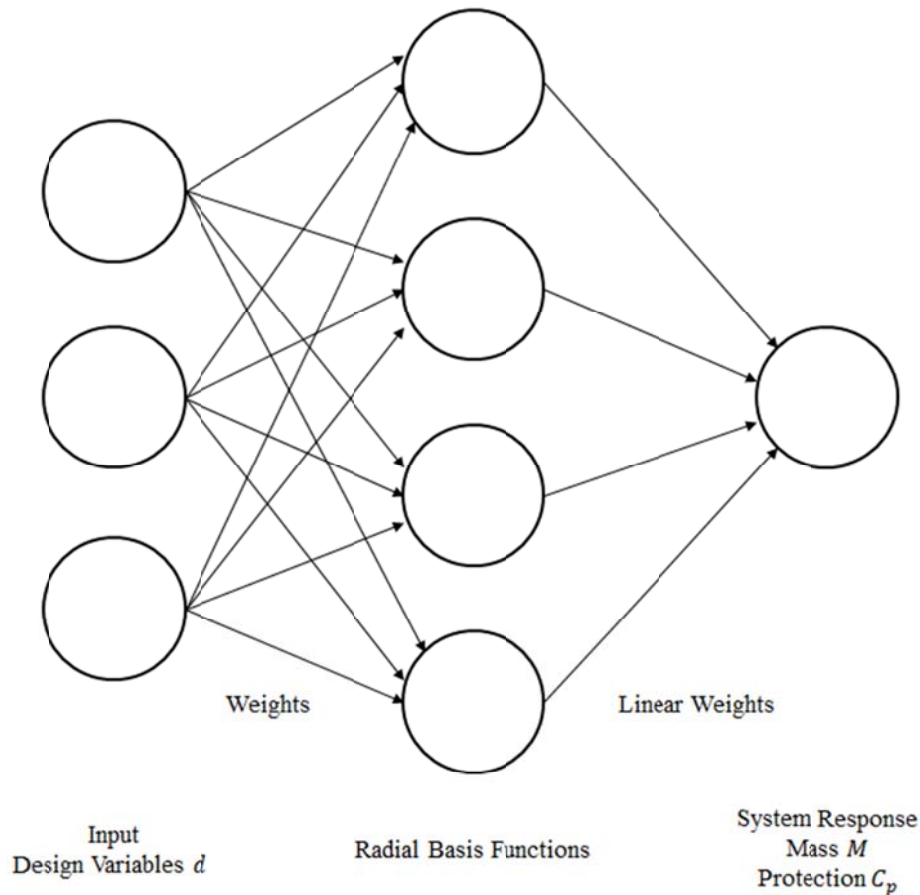
Figure 2.6 Radial basis function architecture

Due to the best-fit scheme for the weights, it is necessary to train the neural network with several sets of input data to achieve the desired level of accuracy. As is shown in Figure 2.6, the RBF network takes the set of design variables d as inputs and approximates a value for the system response of interest. LS-DYNA finite element simulations are used to train the network initially through a factorial of the input variables. The optimization problem is then solved and the output is compared to an additional FEA simulation for evaluation of network accuracy. The optimization routine is illustrated in Figure 2.7. The RBF network implemented here is the function "newrbe" which exists as part of the Matlab neural toolbox plug-in.

The flowchart contains the following elements:

- Begin optimization
- Create network — Create initial network with 2^n FEA function calls
- Solve optimization problem — Sequential quadratic programming algorithm with RBF network
- Update network
- Evaluate — Solution is approximately equal to single additional FEA function call
  - No → Update network
  - Yes → Converged
- Converged

Figure 2.7: Radial basis function network optimization process flow.

3. DESIGN UNDER UNCERTAINTY METHODOLOGY

3.1 Introduction

Design under uncertainty refers to the broad field of design methods that take into account the stochastic nature of the design variables and other input parameters. In deterministic design methods such as those described in Chapter 2, the loading, material properties, and environmental conditions of the design process are considered to have singular, deterministic values. In design under uncertainty, some or perhaps all of those parameters are assumed to have random behavior, and can be analyzed using probability theory.

We can characterize all of the design problems discussed herein as black box type problems, that is they can be defined in terms of their inputs and outputs without knowledge of their internal workings, as in Figure 3.1. All of the input and output parameters can be classified into one of four general categories: Signal factors, which act as targets for the design, Control factors, which represent design variables over which the designer has control, Noise factors, which are uncontrollable factors associated with instability in the design environment, and Response, which represents the output of the design.
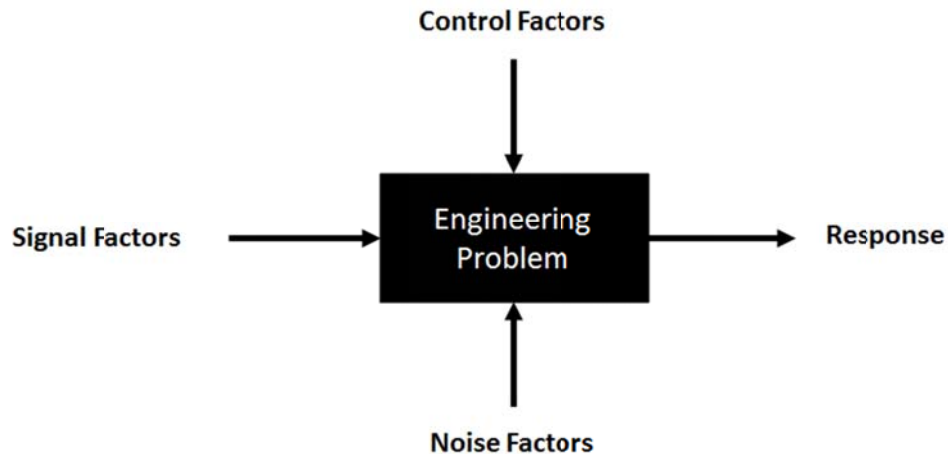
Figure 3.1 Black box description of design problem

In deterministic cases, all of these inputs and have single deterministic values, and singular inputs yield singular responses. In cases of design under uncertainty, the randomness of the inputs yields randomness in the response. For plate structure design as discussed in this work, the control factors (such as the height or thickness of the structure) are fully under control, stemming from the fact that only computer models are used for investigation and there are no manufacturing processes that could introduce error. Instead, the randomness is introduced by variations in noise factors, specifically the dynamic loading conditions to which the plate is subject. The classification of the design parameters for the plate structure design problem is as follows, as shown in Figure 3.2. There are two signal factors: mass, which is targeted as the lower the better, and protection, which is characterized as the having a small post-blast plate deflection that is within defined tolerance (i.e. cabin penetration is equal to zero). There are two control factors: The thickness of the plate and the topography of the plate, although the topography factor may contain many sub-variables to fully describe the shape.
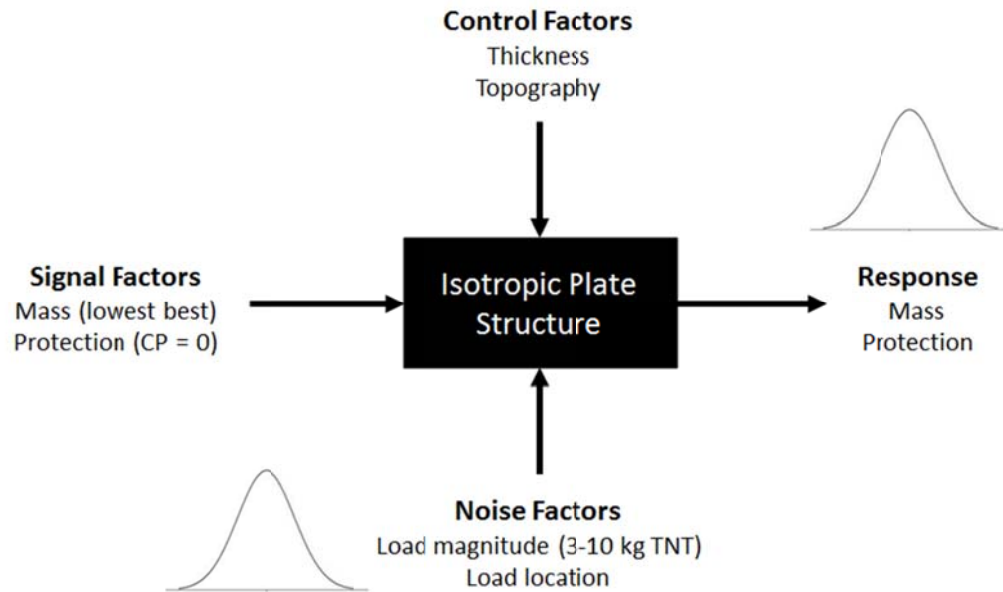
Figure 3.2 Classification of parameters for plate design problem

The noise factors, which are the source of random input to the design problem, are the magnitude of the load and the location of the load. The variation of these two loading conditions causes a corresponding variation in the performance of the design. The response, or output of the design problem, is characterized by the parameters mass and protection, which correspond to the target inputs or signal factors. Black box formulations such as this are common in design optimization practice, and have been used to classify the parameters for problems in design under uncertainty with similar noise factor stochastic behavior by Chen and Mistree [66].

Due to the probabilistic nature of the response of these types of problems, all methods of design under uncertainty rely on some kind of uncertainty quantification method to characterize the variation of the response with respect to the uncertainty introduced by the variation of the random input variables. The propagation of this uncertainty from input to output becomes the chief interest for design under uncertainty problems, with specific interest in the approximation of the low-order statistical moments of the response, namely the mean and variance of the response resulting from the

introduction of random inputs. The potentially endless possibilities of engineering problems which can exist inside a black box have resulted in the formulation of many different methods for uncertainty quantification. The appropriate method can be chosen based on a number of factors including the level of accuracy required, the computational cost, and the degree on non-linearity of the design problem [67]. Some examples of common uncertainty propagation methods are simulation based methods such as the Monte Carlo simulation [68], most-probable point methods such as FORM and SORM [69], and numerical integration based methods [36, 35].

Due to the highly non-linear problems associated with the response to blast loading, the two methods for uncertainty quantification used here fall under the numerical integration based category. Numerical integration based methods first approximate the statistical moments of the response and then the probability density function can be approximated using empirical distribution systems [67]. The univariate dimensional reduction method (UDR) as proposed by Rahman and Xu [36, 37] decomposes the performance function into the sum of several univariate functions, which can become costly when the number of random variables is large. The performance moment integration (PMI) method [35] makes use of numerical integration on the output space of the performance function and therefor requires few quadrature points to approximate the statistical moments regardless of the number of random variables, but it does require the solution of addition inverse reliability problems to determine the terms for integration [38].

The end result of both uncertainty quantification methods is the approximation of the first two ordinary statistical moments of the system response, mean and variance, which can be used to characterize the probability distribution of system performance. This probabilistic information can be used to develop new designs that incorporate uncertainty and in turn increase confidence in product performance. Robust design optimization (RDO) refers to a category of design under uncertainty methods whose goal is to reduce the sensitivity of the product with respect to variation of the random or

otherwise uncontrollable input factors [70]. Reliability-based design optimization (RBDO) refers to a class of methods which aim to increase the confidence in a design with respect to user-defined failure criteria [71, 72]. Both of the above mentioned methodologies use probabilistic information about the system response to generate higher performance designs, and have been integrated into an additional methodology; Reliability-based robust design optimization (RBRDO) is a hybridization which combines RDO and RBDO to achieve multiple goals simultaneously [38, 35].

3.2 Univariate Dimensional Reduction (UDR)

The univariate dimensional reduction method is based in the decomposition of a multi-dimensional function into sum of several one-dimensional functions. Consider the decomposition of the performance function $g(\boldsymbol{X})$ as shown:

$$g(\boldsymbol{X}) \cong \hat{g}(\boldsymbol{X}) = \sum_{i=1}^{N} g(\mu_1, \dots, X_i, \dots \mu_N) - (N-1) * g(\mu_1, \dots \mu_N) \qquad (3.1)$$

where μ_i is the mean value of the random variable X_i, $g(\mu_1, \dots, X_i, \dots \mu_N)$ is a random response that depends on the ith random variable, and N is the total number of random variables. It can be demonstrated that a Taylor series expansion of the approximation function $\hat{g}(\boldsymbol{X})$ contains all of the single variable terms of the Taylor series of $g(\boldsymbol{X})$, which means that the approximation error is due only to the terms with two or more variables. A demonstration of the Taylor series expansion of the univariate approximation, complete with determination of the residual error can be found in Xu and Rahman [36].

This univariate decomposition can be applied to the multi-dimensional integral for moment calculation given as

$$E\left[\left(g(\boldsymbol{X})\right)^k\right] = \int_{-\infty}^{\infty} \dots \int_{-\infty}^{\infty} \left(g(\boldsymbol{X})\right)^k f_x(\boldsymbol{X}) d\boldsymbol{X} \qquad (3.2)$$

where $f_x(X)$ is the joint probability density function of X, and E is the expectation operator. According to the moment based integration rule [36], which is similar to Gaussian quadrature techniques for numerical integration, the statistical moments of a function can be obtained through the numerical approximation of (3.2) expressed by the following:

$$E\left[\left(g(X)\right)^k\right] = \sum_{i=1}^{n} w_i g^k(x_i) \tag{3.3}$$

where w_i are the weights associated with the quadrature and x_i are the quadrature points. If the probability density function (PDF) of the random input variables are known, for example standard normal distribution, then the weights and quadrature points can be found via the moment based quadrature rule (MBIR) [73]. Similar to Gaussian quadrature, the degree of precision is $2n - 1$. Therefor for highly nonlinear functions, more quadrature points will result in a higher accuracy of approximation.

Through the combination of Equations (3.1), (3.2) , and (3.3) the mean and variance of the performance function can be expressed as

$$\mu_G = E[g(X)]$$
$$\cong \sum_{j=1}^{n}\sum_{i=1}^{N} w_{ji}\left[g(\mu_1,\dots,\mu_{i-1},X_{ji},\mu_{i+1},\dots,\mu_N) - (N-1)g(\mu_1,\ \dots,\mu_N)\right] \tag{3.4}$$

and

$$\sigma_G^2 = E[g^2(X)]\ - (E[g(X)])^2$$
$$\cong \sum_{j=1}^{n}\sum_{i=1}^{N} w_{ji}\left[g^2(\mu_1,\dots,\mu_{i-1},X_{ji},\mu_{i+1},\dots,\mu_N) - (N-1)g^2(\mu_1,\ \dots,\mu_N)\right] - \mu_G^2 \tag{3.5}$$

where n is the number of quadrature points and N is the number of random variables. It can be understood from the above equations that the UDR method involves a double approximation to calculate the statistical moments: the first approximation which

decomposes the function into the sum of several univariate functions, and a second to approximate the multi-dimensional integral for moment calculation. Due to highly nonlinear performance functions observed in the investigation of blast loading of plates, five quadrature points are used for all approximations as shown in Table 3.1.

Table 3.1 MBIR Quadrature Points and Weights

MBIR Quadrature Points, x_i	Weights, w_i
± 2.856970	0.011257
± 1.355626	0.222076
0.0	0.533333

The computational efficiency of this method is dependent on the number of random variables and the number of quadrature points used in the approximation. Generally speaking, assuming symmetric distribution of the random variables, the number of function evaluations of $g(X)$ necessary for the approximation of the first two statistical moments is

$$\text{No. of function evaluations} = nN + 1 \qquad (3.6)$$

where n is the number of quadrature points and N is the number of random variables.

3.3 Performance Moment Integration (PMI)

An additional method for calculating the statistical moments of the performance function $g(X)$ called performance moment integration (PMI) has been developed recently to handle functions with a relatively large number of random variables [35]. Similar to UDR, this method is also a numerical integration technique, but the integration is performed on the output domain as opposed to the input domain. This requires a transformation from the original X-space of the function $g(X)$ to standard normal U-space. By Rosenblatt transformation [74], if we consider a vector of random variables X, where the cumulative distribution function (CDF) is denoted as $F_x(X)$, we can define a transformation from X-space to U-space as:

$$T = \begin{cases} u_1 = \Phi^{-1}[\,F_{x1}(X_1)] \\ u_1 = \Phi^{-1}[\,F_{x2}(X_2|X_1)] \\ \quad\vdots \\ u_1 = \Phi^{-1}[\,F_{xN}(X_N|\,X_1, X_2, \dots, X_{N-1})] \end{cases} \tag{3.7}$$

where N is the dimension of the vector or random variables and $F_{xN}(X_N|\,X_1, X_2, \dots, X_{N-1})$ is the conditional CDF stated as

$$F_{xN}(X_N|\,X_1, X_2, \dots, X_{N-1}) = \frac{\int_{-\infty}^{x_i} f_{x_1 x_2 \dots x_N}(x_1, \dots, x_{N-1}, \xi)d\xi}{f_{x_1 x_2 \dots x_N}(x_1, \dots, x_{N-1})} \tag{3.8}$$

and $\Phi(\cdot)$ is the standard normal operator stated as

$$\Phi(u) = \frac{1}{\sqrt{2\pi}} \int_{-\infty}^{u} \exp\left(-\frac{1}{2}\,\xi^2\right)d\xi\,. \tag{3.9}$$

An inverse transformation can be obtained from (3.7) as well. When the random vector **X** is independent such that the joint PDF is given as the product of marginal PDFs as

$$f_x(\boldsymbol{X}) = \prod_{i=1}^{N} f_{xi}(x_i) \tag{3.10}$$

then the Rosenblatt transformation and its inverse can be simplified as

$$u_i = \Phi^{-1}[\,F_x(x_i)] \tag{3.11}$$

and

$$x_i = F_x^{-1}[\Phi(u)] \tag{3.12}$$

where $F_x(x_i)$ are the marginal CDFs. For random variables which are normally distributed the transformation is

$$X = \mu + \sigma U \tag{3.13}$$

where μ is the mean and σ is the standard deviation.

By means of this transformation we can map a function into independent normal U-space as shown in Figure 3.3, and perform the numerical integration in the output domain. The figure shows a function of two random variables both having the characteristics of being normal, i.e. $\boldsymbol{X} \in N[5,1]$, displayed in X-space and then mapped to U-space. In normal U-space, the origin is the location where both random variables are at their mean values. The concentric rings in the U-space representation indicate loci of points where the probability of the function value occurring is equal.
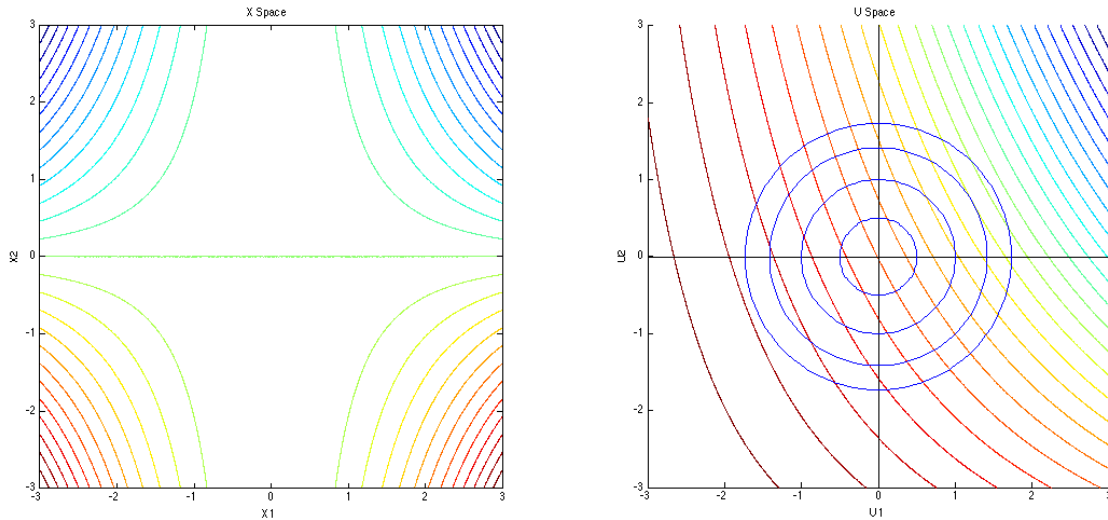
Figure 3.3 A function of two variables in standard X-space (left) mapped to normal U-space (right)

Using this transformation, the multi-dimensional integral for moment calculation can be re-written as

$$
\begin{aligned}
E\left[(g(\boldsymbol{X}))^k\right] &= \int_{-\infty}^{\infty} \cdots \int_{-\infty}^{\infty} (g(\boldsymbol{X}))^k f_x(\boldsymbol{X}) d\boldsymbol{X} \\
&= \int_{-\infty}^{\infty} \cdots \int_{-\infty}^{\infty} (g(\boldsymbol{X}(\boldsymbol{u})))^k \phi_U(\boldsymbol{u}) d\boldsymbol{u}
\end{aligned}
\tag{3.14}
$$

which is then rewritten in terms of its output distribution

$$
E\left[(g(\boldsymbol{X}))^k\right] = \int_{-\infty}^{\infty} \cdots \int_{-\infty}^{\infty} (g(\boldsymbol{X}(\boldsymbol{u})))^k \phi_U(\boldsymbol{u}) d\boldsymbol{u} = \int_{-\infty}^{\infty} g\, f_G(g) dg
\tag{3.15}
$$

where $f_G(g)$ is the PDF of the output performance function $g(X)$. The CDF of the performance function can then be expressed in terms of the standard normal CDF using the transformation as provided by Lee [75]:

$$F_G(g) = \Phi(t) \tag{3.16}$$

where t is the distance from the origin in U-space to the point of interest, as shown in Figure 3.4.
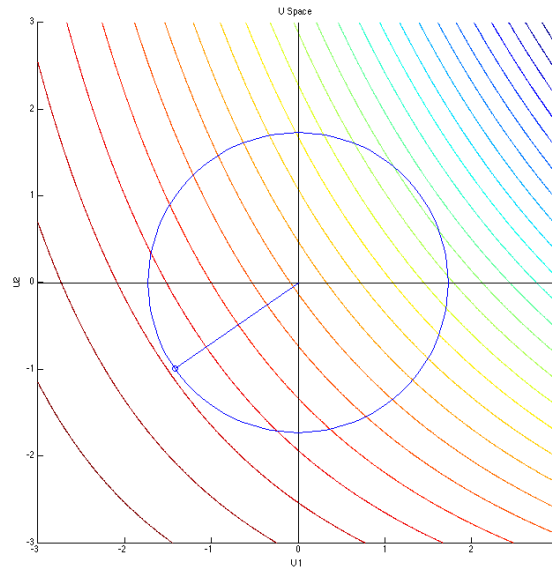
Figure 3.4 U-space representation displaying the vector t

Combining (3.15) and (3.16), we can reduce the multivariable integration to single variable integration of the following form

$$E\left[(g(X))^k\right] = \int_{-\infty}^{\infty} g(t)\phi(t)dt. \tag{3.17}$$

Applying the same quadrature-type approximation to the above equation as was stated in equation (3.3), we can obtain three-point integration. Three points is considered the minimum needed to maintain good accuracy in integrating the first two statistical moments [76]. Since the distribution in U-space is normal we can use values of $x = \{g_{\beta=-\sqrt{3}}, g(\mu),\ g_{\beta=+\sqrt{3}}\}$ and $w = \left\{\frac{1}{6}, \frac{4}{6}, \frac{1}{6}\right\}$ for the quadrature points and the weights respectively, and the formulations for the mean and variance become

$$\mu_G = E[g(\boldsymbol{X})]$$

$$\cong \frac{1}{6}g_{\beta=-\sqrt{3}} + \frac{4}{6}\,g(\mu_x) + \frac{1}{6}g_{\beta=+\sqrt{3}}$$

(3.18)

and

$$\sigma_G^2 = E[g^2(\boldsymbol{X})]$$

$$\cong \frac{1}{6}\left(g_{\beta=-\sqrt{3}}\right)^2 + \frac{4}{6}\,g^2(\mu_x) + \frac{1}{6}\left(g_{\beta=+\sqrt{3}}\right)^2 - \mu_G^2$$

(3.19)

The numerical value for $g(\mu_x)$ is simply the value of the performance function evaluated at the mean values of all random variables. The values of the points $g_{\mathrm{B}=-\sqrt{3}}$ and $g_{\mathrm{B}=+\sqrt{3}}$ must be obtained via inverse reliability analysis of the function in U-space [76] by solving the optimization problem

$$\begin{aligned} &\text{find} && u^* \\ &\text{min} && g(\boldsymbol{u}) \\ &\text{s.t.} && \|\boldsymbol{u}\| = \sqrt{3} \end{aligned}.$$

(3.20)

The optimum result of this problem is the value for $g_{\beta=-\sqrt{3}}$. Similarly, the value for $g_{\beta=+\sqrt{3}}$ can be found by maximizing $g(\boldsymbol{u})$ in equation (3.20). Unlike the UDR method, the number of quadrature points for PMI does not increase with the number of random variables, but instead stays constant since the integration is performed in the output space. The cost of the PMI method comes from the number of function evaluations necessary to solve the optimization problem stated in equation (3.20) to find the values for $g_{\beta=-\sqrt{3}}$ and $g_{\beta=+\sqrt{3}}$.

Due to the highly nonlinear performance functions involved in this research, it would be far too computationally expensive to solve equation (3.20) by sequential quadratic programming methods that rely solely on finite element simulation. This approach would in effect create a double-loop that would negate any computational savings gained through the use of the PMI method. Alternatively, this research utilizes

the RBF network metamodelling method as described in Chapter 2 to solve equation (3.20) for the quadrature values.

3.4   Robust Design Optimization (RDO)

As was stated in Chapter 2, this research considers two performance metrics for the design of lightweight structures: structure mass and dynamic structural deflection. Dynamic deflection in the deterministic case investigations is defined in terms of cabin penetration: a maximum allowable amount of deflection is utilized as an inequality constraint in the optimization problem. The fundamental goal of all robust design optimization is to minimize variations in performance caused by variations in random inputs without eliminating the causes themselves [77]. In order to implement a basic robust design method, this research makes use of the protection response (penetration) and employs a simple robust design optimization problem expressed as

$$
\begin{aligned}
&\text{find} && \boldsymbol{d} \\
&\text{minimize} && \sigma_P^2(\boldsymbol{d}, \boldsymbol{X}) \\
&\text{subject to} && P_c(\boldsymbol{d}) - P_{c\,max} \leq 0
\end{aligned}
\tag{3.21}
$$

where $\boldsymbol{d} \in \mathbb{R}^n$ is the set of all design variables characterizing the shape and thickness of the plate, $\boldsymbol{X}$ is the set of all random variables which could be of several distributions (normal, uniform, Gumbel, etc.), $P_c(\boldsymbol{d})$ is the penetration after the blast event with respect to datum plane, $P_{c\,max}$ is the maximum allowable value for penetration. The term $\sigma_P^2(\boldsymbol{d}, \boldsymbol{X})$ is the variance of the protection performance (maximum plate deflection) and is a function of both the design variables and the random variables.

This problem can be optimized by means of the SQP active-set optimization method as described in Chapter 2. To carry out the optimization procedure, the statistical moments μ_P and σ_P^2 must be calculated at each iteration of the process. In addition, the sensitivities of the statistical moments with respect to the vector of design variables, $\boldsymbol{d}$, must also be calculated, but second-order information about the statistical moments with

respect to the random inputs, **X,** is not necessary. A process flow for the optimization routine is shown in Figure 3.5.

Figure 3.5 Robust design optimization process flow diagram

3.5   Reliability-Based Design Optimization (RBDO)

Reliability-based design optimization is characterized by the calculation of probability of failure for some performance function [30]. This probability of failure can be generally stated as the integral

$$P_f \equiv P[g(X) > 0] = \int f_x(X)dx \qquad (3.22)$$

where **X** is the set of all random variables and $f_x(X)$ is a joint probability density function of the random variables. The exact value this integral can be extremely difficult to obtain

due to the fact the fact that $f_x(\boldsymbol{X})$ is often highly non-linear in practical engineering examples. One solution to this problem in the past has been to employ a first order reliability method (FORM) or a second order reliability method (SORM) [78]. These methods are most-probable point (MPP) methods which have been developed extensively over the past thirty years [32]. To approximate the integral by these methods, the MPP is utilized to generate the cumulative distribution function (CDF) of a system output by evaluating probability estimates at various states across the range of output performance [72].

In contrast, this research calculates the integral through approximation of the statistical moments of the performance function followed by direct integration. First, the low-order moments of the protection performance function, μ_P and σ_P^2, are approximated via the uncertainty quantification methods described above. Assuming the distribution of the protection performance to be normal, we can then approximate the probability of failure against the failure criterion $P_{c\,max}$ as

$$P[P_c(\boldsymbol{d},\boldsymbol{X}) > P_{c\,max}] \cong \int_{-\infty}^{P_{c\,max}} \frac{1}{\sqrt{2\pi\sigma_P^2}} \exp\left(-\frac{(\xi - \mu_P)^2}{2\sigma_P^2}\right) d\xi \qquad (3.23)$$

by replacing the joint probability distribution function in (3.22) with the normal continuous probability distribution.

If some standard for probability of failure P_f^T is introduced, for example if the designer chooses that only a 5% probability of failure is acceptable, then the equation for probability of failure can be applied to the general optimization problem as an inequality constraint

$$
\begin{aligned}
&\text{find} &&\boldsymbol{d}\\
&\text{minimize} &&M(\boldsymbol{d})\\
&\text{subject to} &&P[P_c(\boldsymbol{d},\boldsymbol{X}) > P_{c\,max}] \leq P_f^T
\end{aligned}
\qquad (3.24)
$$

where $\boldsymbol{d} \in \mathbb{R}^n$ is the set of all design variables, $M(d)$ is the mass of the structure and $P[P_c(\boldsymbol{d},\boldsymbol{X}) > P_{c\,max}]$ is the probability that the deflection of the plate will exceed the

maximum allowable value $P_{c\,max}$ as defined by (3.23). The ultimate result of this type of optimization is the generation of structures for which the uncertainty in the performance response is above a certain design threshold. In other words, the mean of the response is shifted and the variance reduced such that the probability of the performance being below a target value is small, as illustrated in Figure 3.6.
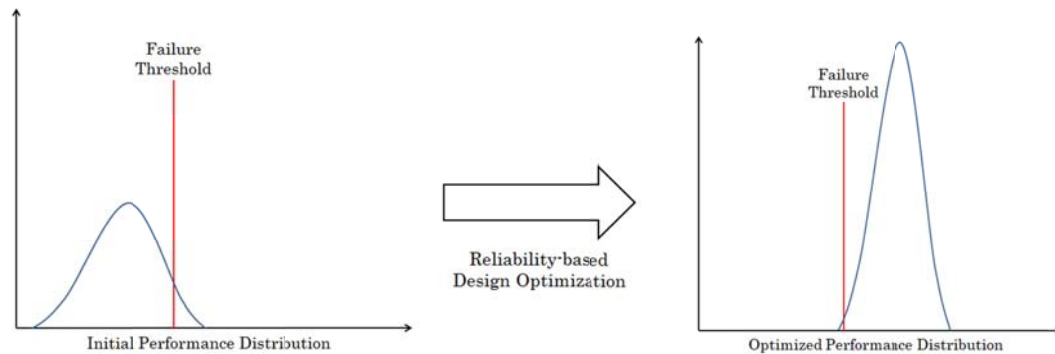
Figure 3.6 Illustration of intended results of reliability-based design optimization

Similar to the procedure for RDO, this problem can be optimized by means of the SQP active-set optimization method as described in Chapter 2. To carry out the optimization procedure, the statistical moments μ_P and σ_P^2 must be calculated at each iteration of the process. The sensitivity of the mass with respect to the design variables must be calculated as part of the optimization routine, but the mass of the plate is independent of the random variables. In addition, the sensitivities of the probability of failure with respect to the vector of design variables, $\boldsymbol{d}$, must also be calculated, but second-order information about the statistical moments with respect to the random inputs, $\boldsymbol{X}$, is not necessary. A process flow for the optimization routine is shown in Figure 3.7 .
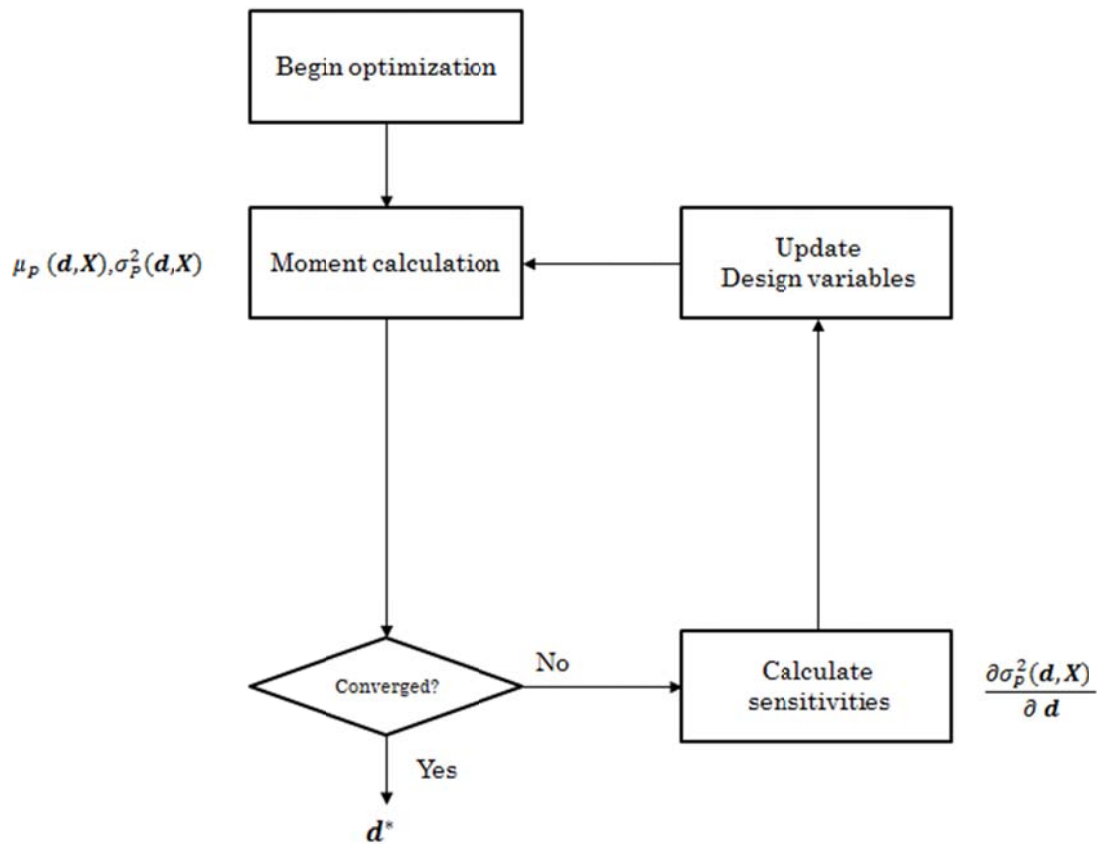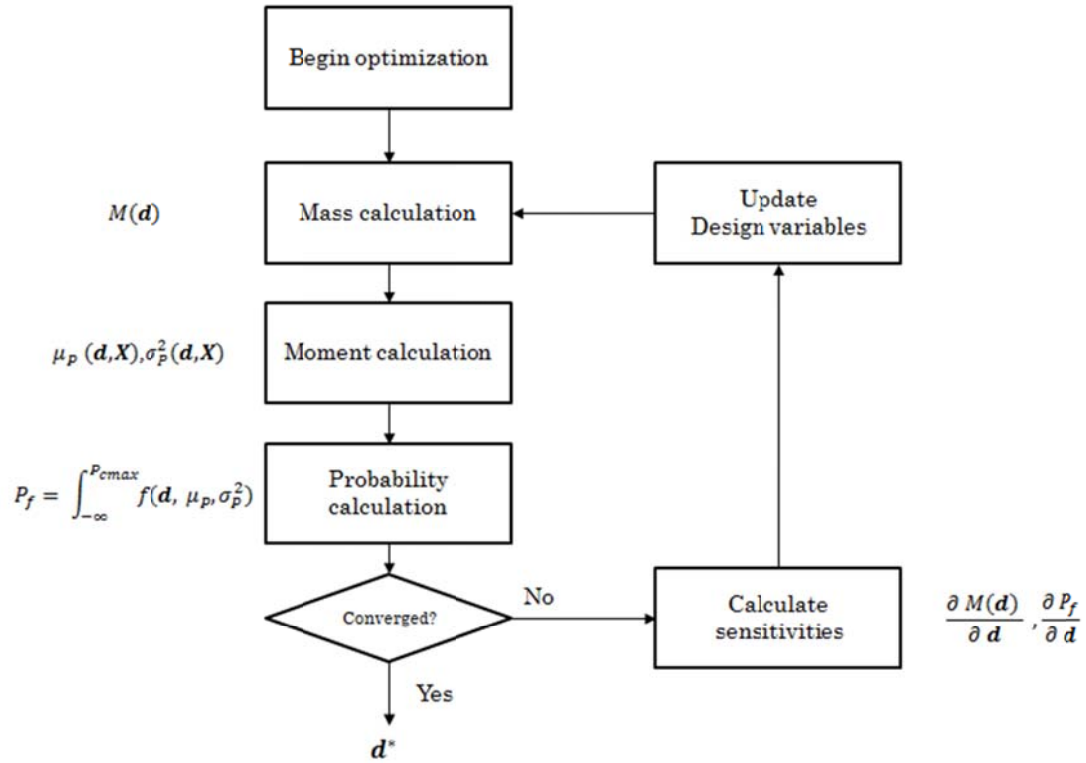
Figure 3.7 Reliability-based design optimization process flow diagram

3.6 Reliability-based Robust Design Optimization (RBRDO)

Reliability-based robust design optimization (RBRDO) is a hybridization which combines RDO and RBDO to achieve multiple goals simultaneously [38, 35]. This class of optimization combines the variance reduction goal of RDO with the probability constraint based optimization of RBDO into a new optimization problem expressed as

$$
\begin{aligned}
&\text{find} && \boldsymbol{d} \\
&\text{minimize} && F_C(\boldsymbol{d}, \mu_P, \sigma_P^2) \\
&\text{subject to} && P[P_c(\boldsymbol{d}, \boldsymbol{X}) > P_{c\,max}] \le P_f^T
\end{aligned}
\tag{3.25}
$$

where $\boldsymbol{d} \in \mathbb{R}^n$ is the set of all design variables, $F_C(\boldsymbol{d}, \mu_P, \sigma_P^2)$ is the cost function, and $P[P_c(\boldsymbol{d}, \boldsymbol{X}) > P_{c\,max}]$ is the probability that the deflection of the plate will exceed the maximum allowable value $P_{c\,max}$ constrained to be less than the target probability P_f^T. This hybridization allows the designer to minimize the variance of the design with

respect to random inputs as in robust design optimization, while including the failure constraints that are the hallmark of reliability-based design.

Characterization of the cost function $F_C(\boldsymbol{d}, \mu_P, \sigma_P^2)$ has a substantial impact on the outcome of the optimization, and there various ways that the cost function may be formulated [35]. In the context of design of lightweight structures for blast mitigation, two different cost function formulations are investigated. The first formulation is based on the "nominal-the-best" type as proposed by Chandra and found in the works of Choi and Lee [79] [75]:

$$F_C(\boldsymbol{d}, \mu_P, \sigma_P^2) = w_1 \left(\frac{\mu_P - \mu_T}{\mu_{P0} - \mu_T} \right)^2 + w_2 \left(\frac{\sigma_P}{\sigma_{P0}} \right)^2 \qquad (3.26)$$

where μ_T is the target nominal value for the mean of the performance function, and w_1 and w_2 are the weights to be chosen by the designer. To reduce the dimensionality problem of the two terms, each is divided by an initial value μ_{P0} and σ_{P0}. The value of the cost function is dependent on terms associated with both the mean μ_P and variance σ_P of the performance function, thus it is a bi-objective problem. The optimum value of this bi-objective problem is heavily dependent on the weights of each term; Variation of the weight values is investigated in the numerical applications section of this thesis. The second cost function investigated is based on a formulation used for optimum design for crashworthiness by Lee *et al.* [38] given as

$$F_C(\boldsymbol{d}, \mu_P, \sigma_P^2) = w_1 \left(\frac{M(\boldsymbol{d})}{M_0(\boldsymbol{d}_0)} \right) + w_2 \left(\frac{\sigma_P}{\sigma_{P0}} \right)^2 \qquad (3.27)$$

where $M(\boldsymbol{d})$ is the mass of the structure and $M_0(\boldsymbol{d}_0)$ is the mass of the structure calculated as a function of the initial design variable values.

To carry out the optimization procedure, the statistical moments μ_P and σ_P^2 must be calculated at each iteration of the process. The sensitivity of the cost function with respect to the design variables must be calculated as part of the optimization routine, but

the mass of the plate is independent of the random variables. In addition, the sensitivities of the probability of failure with respect to the vector of design variables, **d,** must also be calculated, in a similar manner to the RBDO procedure. An additional similarity is that second-order information about the statistical moments with respect to the random inputs, **X,** is not necessary. A process flow for the optimization routine is shown in Figure 3.8.
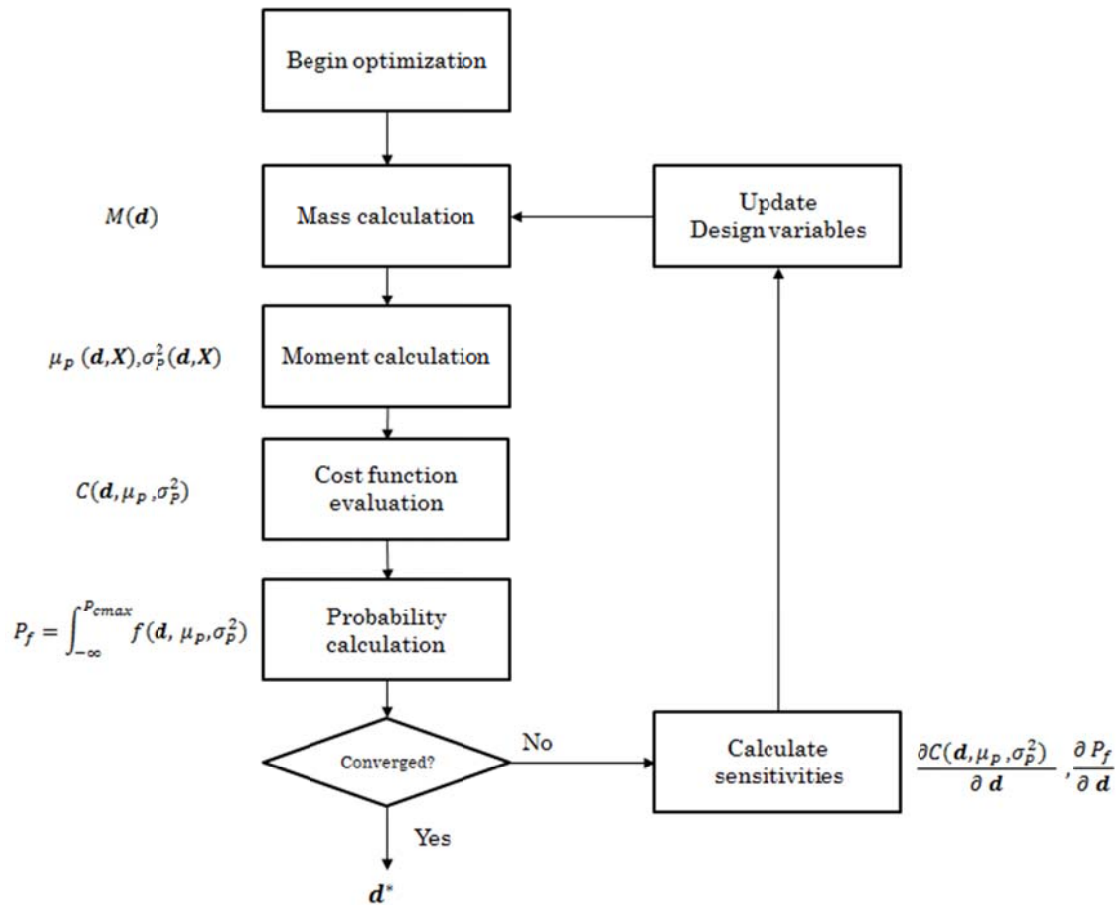
Figure 3.8: Reliability-based robust design optimization process flow diagram.

4   NUMERICAL MODELS AND APPLICATIONS

4.1   Numerical Models

4.1.1   Design Domain

The design domain, which defines the envelope constraints and boundary conditions for the problem, is chosen is such a way as to simulate under-vehicle conditions. Consider the vehicle model shown in Figure 4.1.
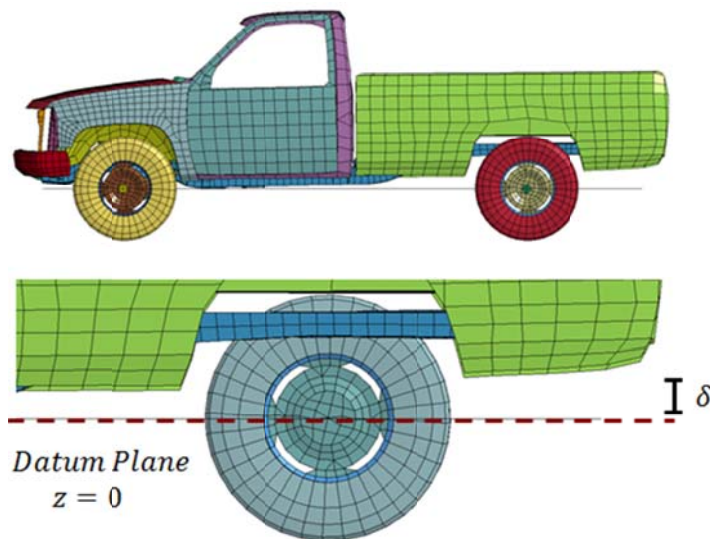
Figure 4.1 Truck model for design space development (top) and detail of under-vehicle showing datum plane (bottom)

The design domain is chosen as a three dimensional space of the same dimensional order as the vehicle model shown in the figure, where the datum plane (shown as the dotted line) is an arbitrary distance $\delta = 0.03\ m$ from the upper plane of the design space to account for the distance between an under-vehicle plate structure and the

passenger cabin. This distance allows for some penetration below the datum plane without penetrating the cabin.

In order to privilege the display of the optimized plate designs, the full design domain has been modeled from beneath or "upside down" orientation, resulting in a 1 m by 1 m by 0.15 m three-dimensional space with the datum plane distance δ from the bottom plane as shown in Figure 4.2. For this orientation, a node is considered to penetrate the cabin if its nodal z −coordinate is less than -0.03 m.
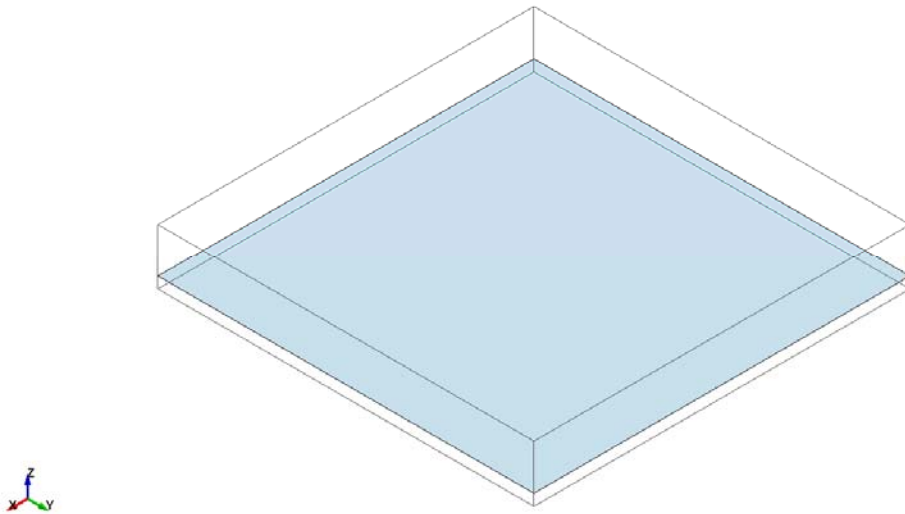
Figure 4.2 Full design domain representation with datum plane (z = 0) shown

The penetration it is taken as the z-displacement relative to the initial position. The thickness of the plate, c, is computed as the sum of the distance between the through-integration points for the shell elements. For all models, shell elements with five through thickness integration points are used. In some design candidate cases, the nodal locations are determined as a function of additional design parameters. Additional design parameters are shown on a case-by-case basis below.

While the majority of the design methods examined here make use of the full design domain, there are two exceptions. The design methods that are based in the generation of a surface of revolution, i.e. the polynomial function design and the trigonometric function design, make use of only the center portion of the full domain.

Labeled the radial domain, this domain has its origins at the center of the plate and extends radially as shown in Figure 4.3. For comparability of results, these designs are considered a separate class of design methodology and their results are compared accordingly.
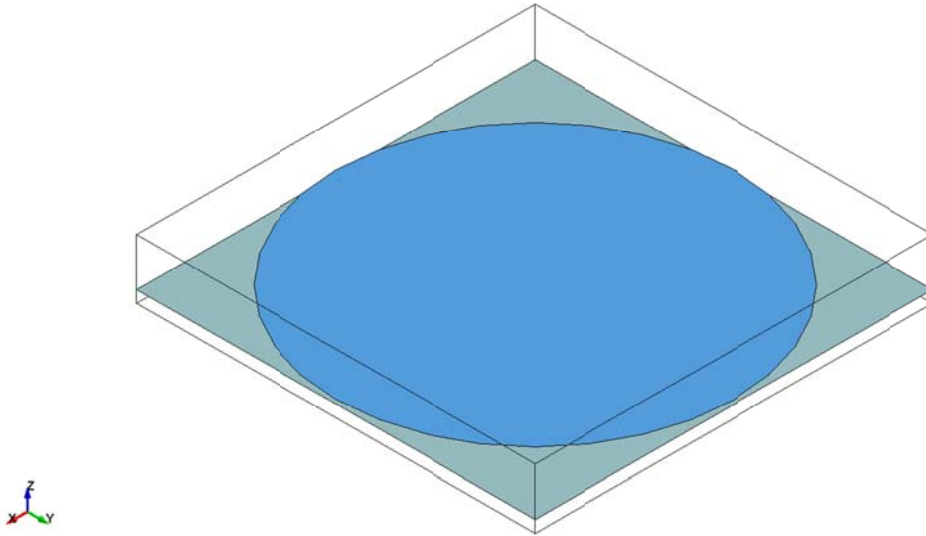
Figure 4.3 Radial design domain representation with datum plane (z = 0) shown

4.1.2   Baseline Design and Mesh Refinement

The baseline design, which serves a starting shape for the optimization methods, is a flat, isotropic steel plate with the following characteristics:

- Uniform thickness: each element has the same through thickness based on the distance between integration points.
- Fixed on all sides: all degrees of freedom are constrained for all nodes at the sides of the plate. These boundary conditions have been demonstrated to have quantitatively the same $z-$displacement response over time as a free plate with a stiffener support around the edge [20].   This is meant to simulate a plate capable of maintaining rigidity at the edges and approximate conditions in vehicle design.

The plate is modeled using four node shell elements with five through thickness integration points. Mesh density studies showed that the $z-$displacement was relatively

insensitive to mesh refinement. In order to preserve computational efficiency, the plate was modeled with a coarse mesh grid of 26 by 26 nodes, for a total of 625 elements, as shown in Figure 4.4. In the case of the trigonometric function design method, the topography of the plate takes on very complex and small curvature, which requires a finer mesh discretization. For that design methodology, a similar plate with plate was modeled with a mesh grid of 201 by 201 nodes, for a total of 40,000 elements.
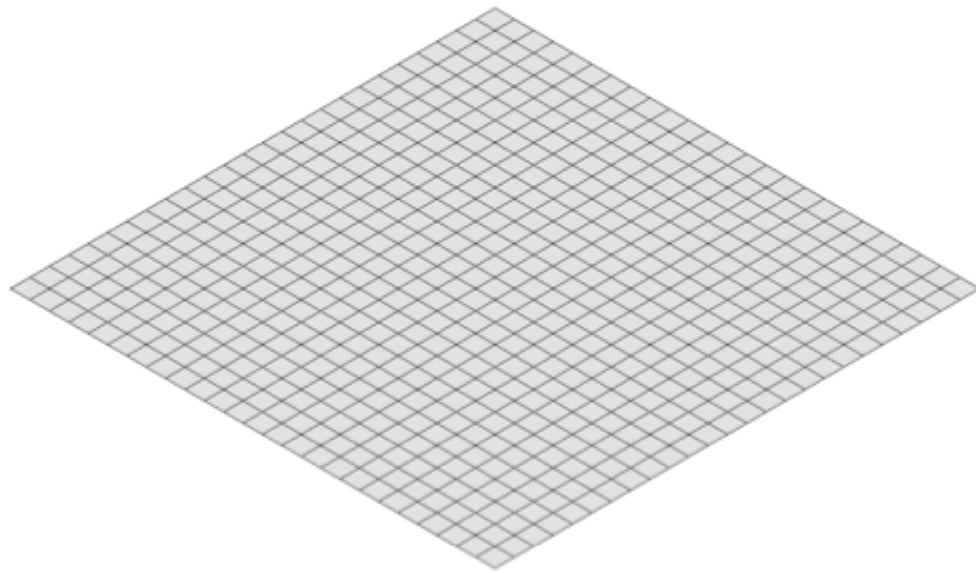
Figure 4.4 Baseline design 26 x 26 node plate

The plate is modeled as A36 type structural steel with linear elastic-plastic behavior – LS-DYNA input card *MAT_PIECEWISE_LINEAR_PLACTICITY. The following material properties are used in each design case: mass density 7800 kg/m^3, Young's modulus 200 GPa, Poisson's ratio 0.3, yield stress 220 MPa, tangent modulus 2 GPa.

4.1.3   Loading Conditions and Time Considerations

The loading conditions were applied using the ConWep BLAST_ENHANCED engineering model of an air blast, with the same set of parameters used consistently for

deterministic cases throughout to ensure continuity for comparative purposes: charge magnitude = 5 kg TNT, charge location = 40 cm above the center of the plate (0, 0, 0.4), type of blast source = spherical free-air burst (LS-DYNA keyword input – BLAST=2). The peak pressure loading P_0, as shown in Figure 4.5, occurs very quickly after the initial detonation time and the maximum z-displacement occurs as a result of this pressure [80]. Thus, a very small simulation time ($t \leq 0.0055$ s) was chosen. Exact simulation time for each design was chosen on a case-by-case basis.
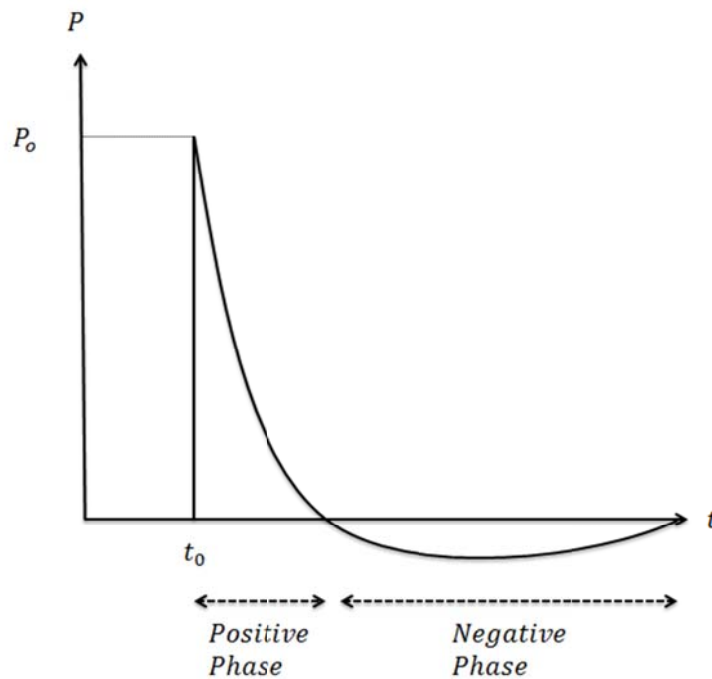
Figure 4.5 Blast pressure time history

4.1.4 Adaptation of Optimization Problem

Each candidate design is considered individually and adapted to the existing optimization problem as the number of design variables in $\boldsymbol{d}$ increases. In each case the objective function and the bounds on $\boldsymbol{d}$ are different, but the penetration constraints and envelope are the same case in each:

- Penetration constraint: $P_c(\boldsymbol{d}, t) - P_{c\,max} \leq 0$

$P_{c\,max} = 0.03$ is chosen to ensure that the optimized topography results in a design where the lowest z −coordinate after the blast event is -0.03 m, i.e., there is no cabin penetration.

- Design domain constraint: $\mathbf{z}^L \leq \mathbf{z} \leq \mathbf{z}^U$

$\mathbf{z}^L = -0.03$ m and $\mathbf{z}^U = 0.12$ m are chosen to ensure that the design does not violate the domain constraints.

4.1.5   Approximation of Surface Area – Parallelogram Method

For a given surface of two variables, the area can be determined analytically according to the following equation:

$$\iint \sqrt{1 + \left(\frac{\partial}{\partial x}\, f(x,y)\right)^2 + \left(\frac{\partial}{\partial y}\, f(x,y)\right)^2}\ dx\ dy\,. \tag{4.1}$$

For complicated surface geometry whose functions involve non-linear equations of several variables as the ones examined here, analytical methods of determining the surface area of the plate become problematic. Instead, the surface area of the plate is approximated based on nodal locations. If we consider a single element as shown below in Figure 4.6, we can define vectors that begin and end on the nodes associated with each element.
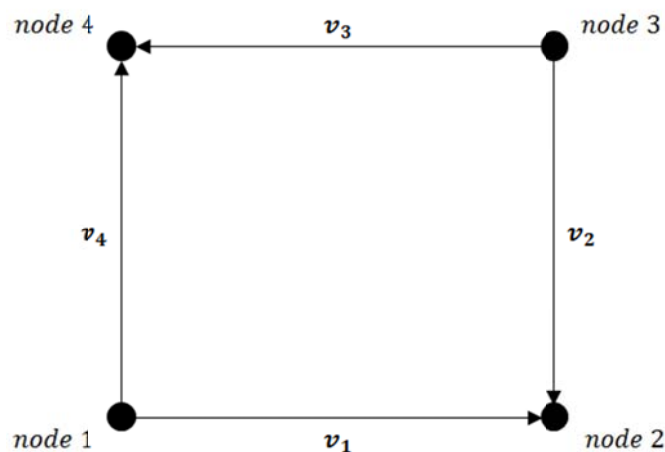
Figure 4.6 Vector numbering to determine element area

For a given surface divided into N parallelogram elements, the surface area can be described as in (4.2) where a new set of vectors is generated for each element (k) based on nodal coordinate information.

$$A \cong \sum_{k=1}^{N} \frac{1}{2} \| v_1^k \times v_2^k \| + \frac{1}{2} \| v_3^k \times v_4^k \| \tag{4.2}$$

Mass calculations based on this method of approximating surface area were compared to the mass results generated by the LS-DYNA internal method and were found to be within $\pm 1\%$ in nearly all cases.

4.2   Deterministic Designs – Full Design Domain

Including the baseline design, five design candidates which utilize the full design domain are generated. These five methods are developed using the optimization problem as described in the proceeding sections, except the HCA topography design methodology which makes use of a controls-based algorithm to find the optimum shape. All other benchmark candidate optimization problems are solved using an active set algorithm. The non-linear programming algorithm is described by Powell [56] and incorporated in Matlab. Regardless of the optimization technique, all of the design methods in this section make use of the full design domain as shown in Figure 4.7.
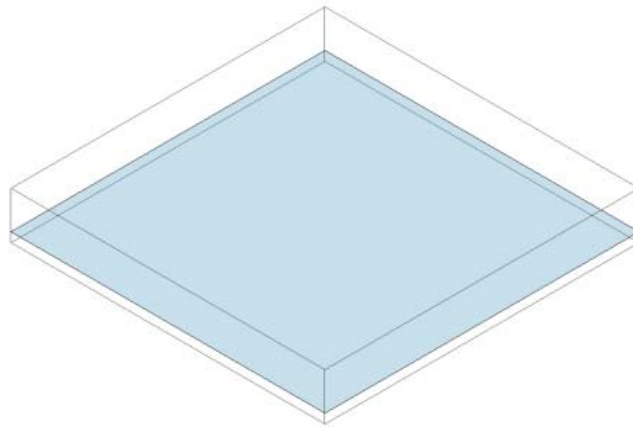
Figure 4.7 Full design domain

The full design domain methods are presented here in order of the number of design variables each uses to generate complete plate topography. In other words, the method are presented in order of dimension of the vector of design variable, **d**. As the number of design variables increases, so does the complexity of the analytical description of each design. A large increase in the number of design variables makes the problem intractable in that an analytical solution for sensitivity has not been derived. In short, for traditional sensitivity-based design optimization, the cost of sensitivity limits the number of design variables. In order to overcome those limitations, two alternative methods are examined which utilize a large design domain and rely on user input to avoid intractability. These free shape designs deal with the most relaxed problem, as there is no underlying analytical description of the shape.

4.2.1 Flat Plate Design

The baseline for all candidate design comparisons is a plate in which all nodal locations are initially zero. The objective function is a single variable function in which only the thickness c of the plate is varied until the constraints are satisfied. The optimization problem for the flat plate candidate design is:

$$
\begin{aligned}
&\text{find} && c \\
&\text{minimize} && M(c) = \rho \, A \, c \\
&\text{subject to} && P_c(c) - P_{c\,max} \leq 0 \\
& && \mathbf{z} = \mathbf{0} \\
& && 7.5 \text{ mm} \leq c \leq 50 \text{ mm}
\end{aligned}
\tag{4.3}
$$

The thickness of the plate is computed as constant at every node. Initial z-coordinate values are uniform for the initial surface, i.e., all pre-blast nodal locations $\mathbf{z} = \mathbf{0}$. The $P_{c\,max}$ value allows the plate to deflect a small amount while still satisfying the constraints, but the optimized design exhibits a relatively large increase in mass in order to absorb the blast wave while ensuring that the deflection constraint is satisfied. This result illustrates the problem associated with the up-armoring of vehicles using only thick, flat plate structures: the large increase in vehicle mass associated with ensuring an appropriate level of protection is often enough to cause other vehicle-performance issues.

The mass characteristics of all proceeding designs are compared to this result as a measure of design performance. The results of the active set method optimization are thickness $c = 29.2$ mm with a corresponding mass $M = 226.4$ kg.

4.2.2 Pyramid Profile Design

There are well-documented studies that demonstrate the ability of v-shaped plate structures to deflect/absorb the energy from a blast event. This candidate design is meant to emulate that V-shaped profile in rendering a symmetric pyramidal design for optimization. As the base of the pyramid is fixed at all constrained nodes, the analytical description for the plate structure is a function of the height of the structure. The number of design variables for this method is increased to two: the height of the structure and the thickness of the plate are optimized. After the profile generation procedure, the plate takes on a pyramid profile where the height h and thickness c of the plate are allowed to vary and is optimized with the objective function as a two variable function as

$$
\begin{aligned}
&\text{find} && c, h \\
&\text{minimize} && M(c, h) = 2\,\rho\,c\,\sqrt{h + {}^{1}\!/_{4}} \\
&\text{subject to} && P_c(c, h) - P_{c\,max} \leq 0 \\
& && z - \frac{h}{0.5}\,x + h = 0 \\
& && 7.5\,\text{mm} \leq c \leq 50\,\text{mm} \\
& && 0\,\text{mm} \leq h \leq 120\,\text{mm}
\end{aligned}
\tag{4.4}
$$

Preliminary results demonstrated that the pyramid tends toward the maximum allowable height; therefore, the maximum height of the design was chosen as 120 mm for the optimization in order to ensure that the envelope constraints were not violated. Convergent results demonstrate an increase in height to the boundary of the design domain while exhibiting a thickness less than half of that of the baseline design, resulting in a structure of significantly smaller mass. As can be seen Figure 4.8, the blast deforms the structure in such a way that the pyramid structure is nearly flattened, but the deflection of the plate in the z-direction is within the allowable tolerance.

Figure 4.8: Finite Element model showing the optimized pyramid profile design before (side view, top left and isometric view, top right) and after a blast event (side view, bottom left and isometric view, bottom right). Convergent numerical results: thickness = 12.4 mm, height = 120 mm, and mass = 99.1 kg.

4.2.3   Gaussian Function Design

Continued investigation of designs with more complex curvature led to the development of a plate structure with topography that conforms to the surface described by a Gaussian function of two variables. The common single variable equation for a Gaussian function is given as

$$f(x) = a \exp\left[-\frac{(x-b)^2}{2\,c^2}\right] \tag{4.5}$$

where a , b, and c are all constants. In three-dimensional space, given a mesh grid of x and y values, we can define a surface that is described by the equation

$$f(x,y) = \delta \exp\left[-\left(\frac{(x-x_0)^2}{\alpha} + \frac{(y-y_0)^2}{\alpha}\right)\right] \qquad (4.6)$$

where δ is the height of the surface, α is a constant related to the spread of the bulge in the center. The curve is centered as point (x_0, y_0). This allows us to optimize a plate structure that can take on complex curvatures, while allowing the use of the common optimization problem used throughout and only increasing the dimensional order of the design problem by one.

After the profile generation procedure, the plate takes on a Gaussian profile where α and δ and thickness of the plate are allowed to vary and is the design is optimized with the objective function as a function of the three variables c, α, and δ to as

$$
\begin{aligned}
&\text{find} && c, \alpha, \delta \\
&\text{minimize} && M(c, \alpha, \delta) = \rho \, c \, A(\alpha, \delta) \\
&\text{subject to} && P_c(c, \alpha, \delta) - P_{c\,max} \leq 0 \\
&&& z - \delta \exp\left[-\left(\frac{(x-x_0)^2}{\alpha} + \frac{(y-y_0)^2}{\alpha}\right)\right] = 0 \qquad (4.7) \\
&&& 7.5\text{ mm} \leq c \leq 50\text{ mm} \\
&&& 0 \leq \alpha \leq 1 \\
&&& 0 \leq \delta \leq 0.12
\end{aligned}
$$

The optimized shape before and after blast events is shown in Figure 4.9, The design exhibits deformational characteristics similar to the pyramid profile design in that is nearly flattened by the blast pressure while deflecting/absorbing enough of the energy to allow only a small amount of deflection in the negative $z-$direction.

Figure 4.9: FE model showing the optimized Gaussian profile design before (side view, top left and isometric view, top right) and after a blast event (side view, bottom left and isometric view, bottom right). Convergent numerical results: thickness = 11.8 mm, $\alpha =$ 0.099, $\delta = 0.12$, mass = 94.3 kg.

The mass of the convergent design is significantly lower than that of the baseline design (-58.4 %) and improves upon the mass reduction exhibited by the pyramid profile design by a small margin (-4.84 %). In this case, an increase in the number of design variables resulting in a more complex shape also yielded a more successful design.

4.2.4   Inverted Profile Design

There has been some interest in creating a plate that takes on an inversion of the topography of a flat plate after a blast event. The reasoning being that the complex blast pressure distribution would then determine the shape of the plate and increase the z-coordinate at each proportional to the magnitude of the loading. The basic procedure used to generate the topography for this plate is as follows:

- Expose a flat plate of some thickness c to a blast event of time $t = t_c$ in order to capture the maximum deflection caused by the blast.
- Invert the shape about the xy-plane ($\mathbf{z} = -\mathbf{z}$ for all nodal locations)
- Scale all $\mathbf{z}$ values to remain within the design space (if necessary)

Through the execution of this procedure, the topography of the plate is determined without the application of any rigorous analytical description. This inversion procedure allows the designer to create complex shapes proportional to the loading condition without the need for complicated analytical descriptions that would not be feasibly solvable by traditional gradient-based optimization methods. After the inversion procedure, the topography of the plate is fully specified, and the design is optimized via the active-set algorithm used to find the convergent results as in the previous sections. The objective function is a single variable function where only the thickness of the plate structure is allowed to vary:

$$
\begin{aligned}
&\text{find} && c \\
&\text{minimize} && M(c) = \rho\,A\,c \\
&\text{subject to} && P_c(c) - P_{c\,max} \leq 0 \\
&&& 7.5\text{ mm} \leq c \leq 50\text{ mm}
\end{aligned}
\tag{4.8}
$$

The optimized design, shown in Figure 4.10, exhibits a performance increase over the baseline design in terms of mass reduction very similar to the geometrically constrained designs but with an optimization problem of order one, whose solution can be found with much less computation. In addition, it utilizes the entire square area of the design domain and could easily be applied to irregularly shaped design domains with little difficulty.
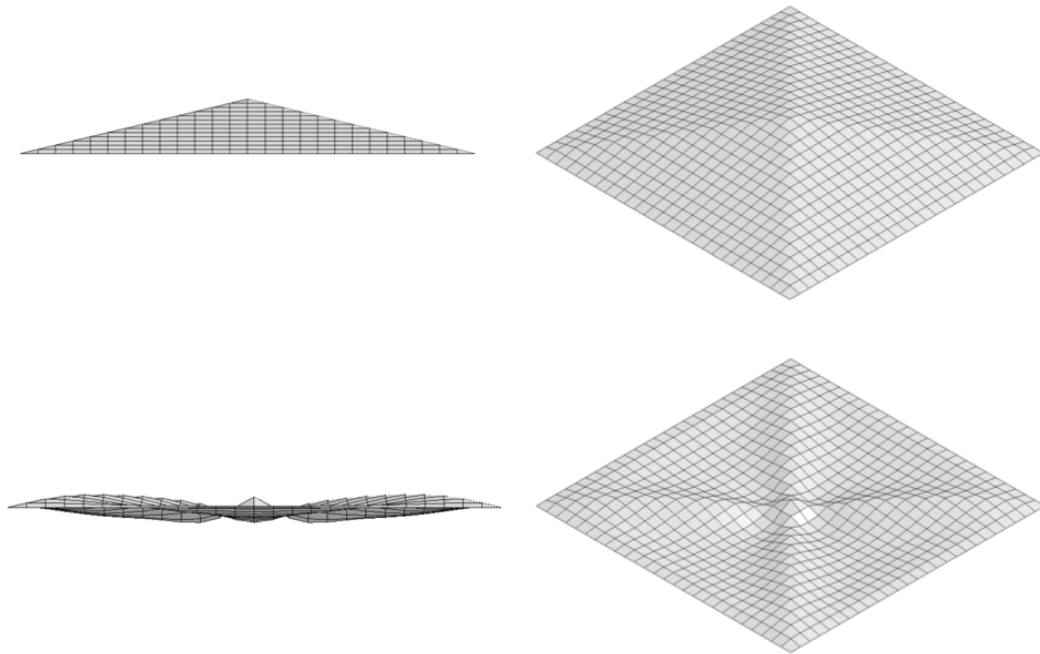
60
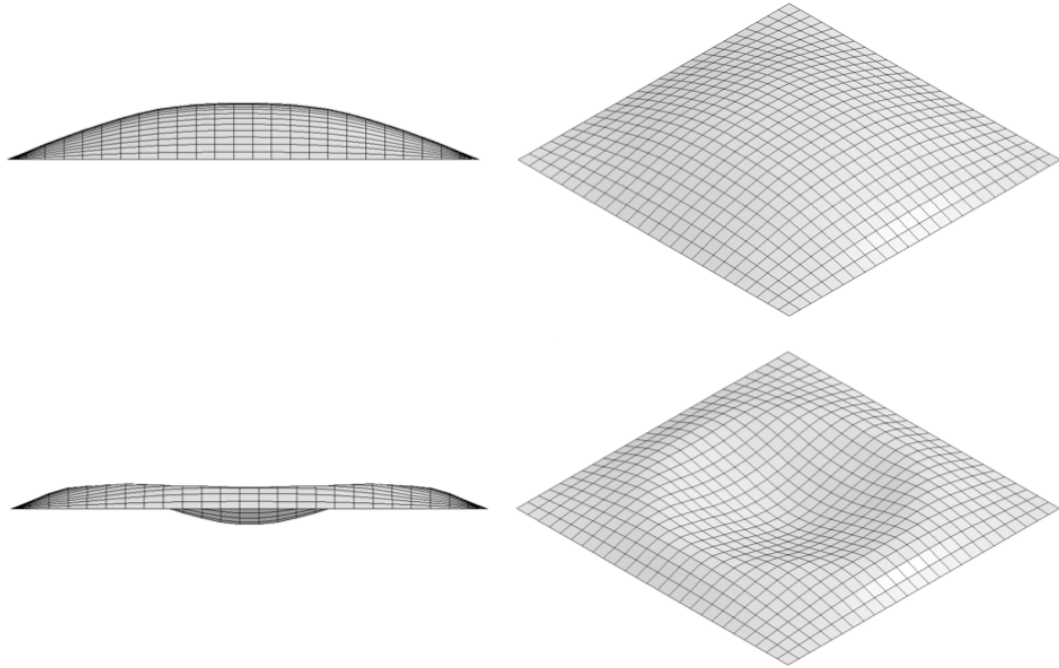
Figure 4.10 Finite Element model showing the optimized inverted profile design before (side view, top left and isometric view, top right) and after a blast event (side view, bottom left and isometric view, bottom right). Convergent numerical results: thickness = 13.6 mm, mass = 105.8 kg.

4.2.5   HCA Topography Design

The HCA topography design is an alternative free shape design method, which allows for the generation of complex curved structures without the need for complex analytical description.   The HCA algorithm considers the nodal z-coordinates of all unconstrained nodes in the design domain at every iteration. Thus, the objective function is of dimension N, where N is the total number of free nodes in the design domain. The convergence behavior is such that the shape depth is increased incrementally at each iteration of the control-based HCA algorithm until the penetration constraint is satisfied. The thickness of the plate is fixed, and the objective function M, is purely a function of the plate geometry. The optimizer does not evaluate the mass at every iteration, but simply iterates until the constraints are met. Given an initially flat surface (all nodal locations $\tilde{z} = 0$) and a fixed elemental thickness ($c = c_i$), the HCA algorithm is applied

to the design domain iteratively until convergence criteria as fixed by the designer are met.

After preliminary analysis, a thickness of $c_i = 12.2$ mm was chosen in order to keep the structure as lightweight as possible while utilizing the entire design domain without violating deflection constraints. The final design obtained from the nodal HCA algorithm is given in Figure 4.11 below, with the resulting parameter information given.

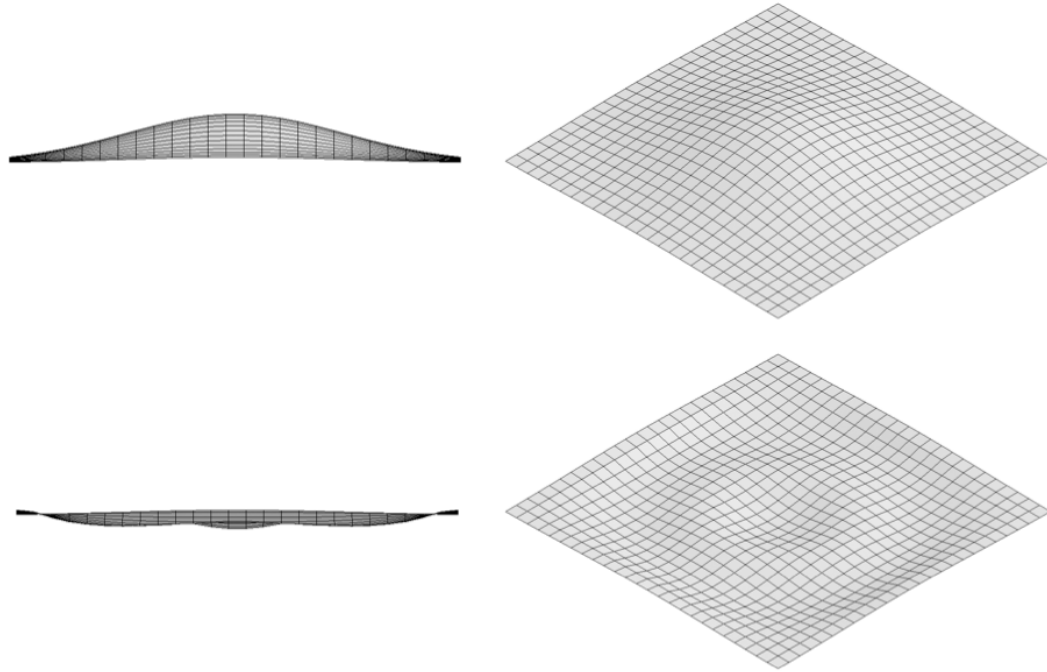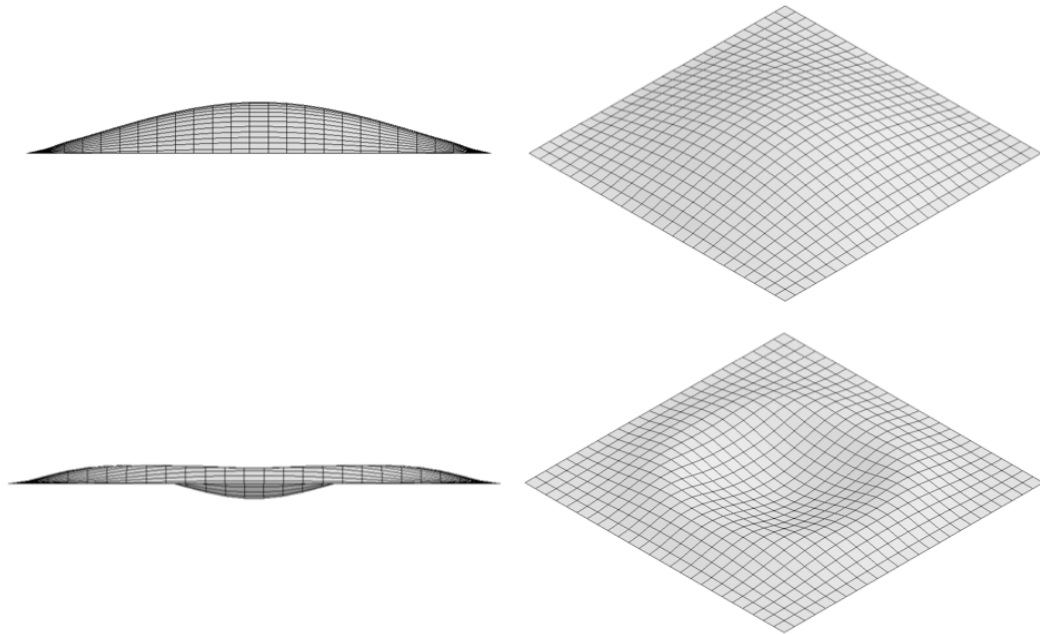Figure 4.11 Finite Element model showing the optimized HCA profile design before (side view, top left and isometric view, top right) and after a blast event (side view, bottom left and isometric view, bottom right). Numerical results: thickness = 12.2 mm, structure height = 11.9 mm, mass = 97.8 kg.

To demonstrate the dependence of the converged solution on user inputs, a second design is generated using an initial starting thickness of $c_i = 0.015$ m. This second structure satisfies the same penetration constraint with a lower height, while exhibiting an increase in mass. In other words, the plate is designed to be thicker and have more mass with the trade-off that it takes up less space in the vertical direction, demonstrating the high-level of control the designer can maintain in the customization of the structure. Table 2 shows the comparative results.

Table 4.1 Numerical comparison of HCA profile designs 1 and 2.

Trial	Thickness (mm)	Height of Structure (mm)	Mass (kg)
HCA Design 1	12.2	11.9	97.8
HCA Design 2	15.0	8.61	118.7

While the geometrically constrained candidate designs can be optimized with gradient-based methods, this approach is not feasible for the HCA objective function due to the large dimensional order of the optimization problem. Convergence criteria must instead be chosen by the designer based on specific performance goals and the application of the structure. In addition, the design rules are extremely problem dependent and are determined through algorithmic testing. Despite the problems of demonstrating convergence and the heuristic nature of the design, the HCA method exhibits some key advantages over geometrically constrained designs: computational efficiency and a broad potential for application to irregular design domains.

Design algorithm

The hybrid cellular automaton (HCA) method combines the basis of the cellular automaton (CA) paradigm, introduced by Stanislaw Ulam and John von Neumann in 1950s [81], and the theory of finite element-based structural optimization, introduced by Lucien Schmit in 1960s [82]. The HCA method presented by Tovar, et al. [83] incorporates local updating schemes such as control rules (i.e., on-off, proportional, integral and derivative controllers and ratio techniques). These local rules drive a defined field variable to an optimum state or set point. The expression for the field variable and the value of the set point are derived from the optimality conditions of the structural design problem [58]. A proof of the global convergence of the HCA technique, under certain circumstances, to an optimal design has been derived [22].
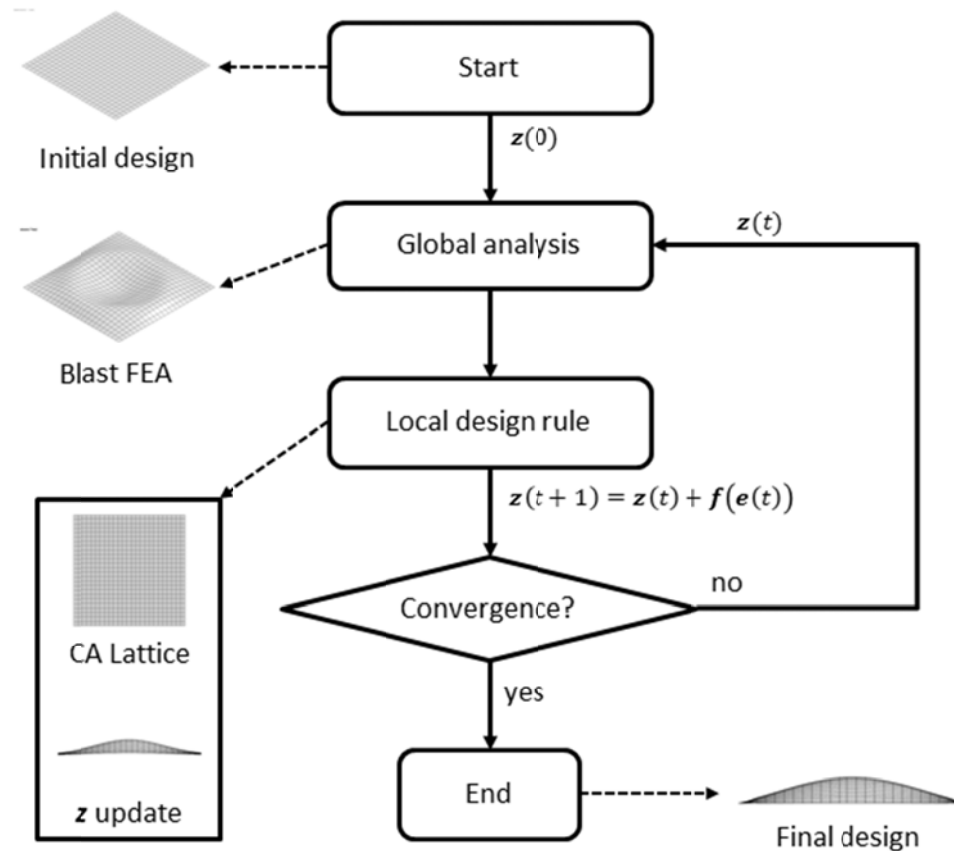
Figure 4.12 HCA algorithm process flow diagram showing plate structure application.

The HCA algorithm as applied to the plate topography problem is illustrated in Figure 4.12 above. This methodology assumes that cellular automata (CAs) form a structure or design domain, and sensors and actuators within the CAs activate local formation and resorption of material. With a proper control strategy, this process drives the overall structure to an optimal topography by updating the nodal locations. Using distributed controlled rules, the optimization problem can be stated as

$$
\begin{aligned}
&\text{find} && \mathbf{z} \\
&\text{minimize} && |q^* - q_{min}| \\
&\text{subject to} && |q_{min}| - P_{c\,max} \le 0 \\
&&& \mathbf{z}^L \le \mathbf{z} \le \mathbf{z}^U
\end{aligned}
\tag{4.9}
$$

where $\mathbf{z}$ is the set of all nodal coordinate values associated the plate topography. In (2.20) q^* is the target deflection threshold value to be achieved by every element in the structure.

The iterative approach may be achieved using a control-based algorithm or a ratio approach. A control-based approach is implemented to perform topography optimization as shown in Figure 4.13. Multiple gains (K_α and K_β) allow the designer control over the rate at which the topography of the structure is updated.
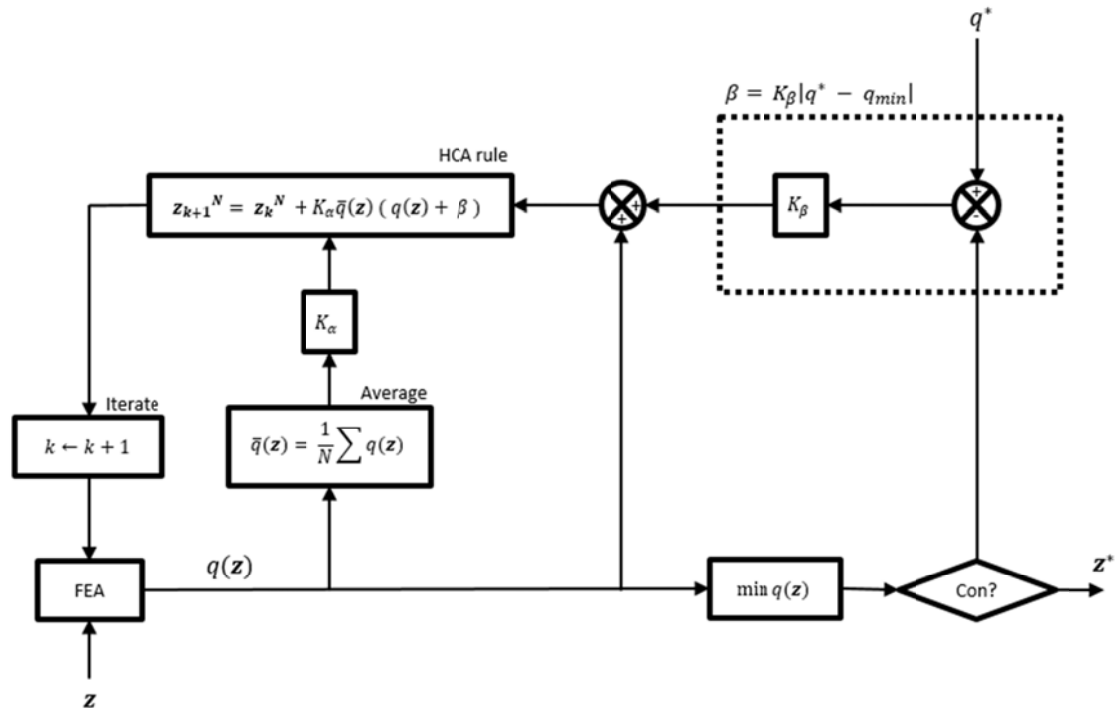
Figure 4.13 Control-based strategy for updating nodal locations to optimize topography.

Computational efficiency and convergence considerations

The computational efficiency of the HCA topography design is rooted in two key characteristics of the design method. The first is the relative insensitivity to mesh refinement. Due to the nature of the shape produced by HCA topography a fairly coarse mesh can be used to generate structures, as opposed to some of the more complex geometrically constrained design methodologies, which require a higher level of mesh refinement for modeling accuracy. A mesh convergence study performed on the HCA method demonstrated nearly identical results for models containing 625 elements and 40000 elements in terms of mass and deflection.

Table 4.2 HCA mesh convergence study results.

Grid size	Number of elements	Mass of converged design (kg)
25 x 25	625	97.8
100 x 100	10000	98.1
200 x 200	40000	98.1

In addition to the relatively low mesh requirements, the HCA method is in general more computationally efficient in that it only requires one function call per iteration, independent of the number of design variables. Gradient-based optimization methods can require many function calls, in some cases hundreds per iteration to determine the gradient and hessian matrices for higher-dimension optimization problems. In the case of structure design, these multiple function calls to FEA simulation can be very computationally expensive. This benefit is augmented by the controls-based optimization routine, which allows the designer to control the rate of convergence through gain adjustments in the control rule.

Application to irregular design domains

The other primary advantage of the HCA topography has over the geometrically constrained designs is its potential for much broader application to irregular design domains. While some of the geometrically constrained designs are dependent on symmetric bounds (e.g. the pyramid profile design) and others fail to take advantage of the entire design domain due to their inherently circular footprint (e.g. the polynomial and trigonometric function designs), the HCA can be applied without difficulty to a wide range of design domains under vastly different loading and support conditions. Figure 4.14 below demonstrates the adaptation of the HCA method to an irregular design space meant to simulate the under-armoring of a vehicle.
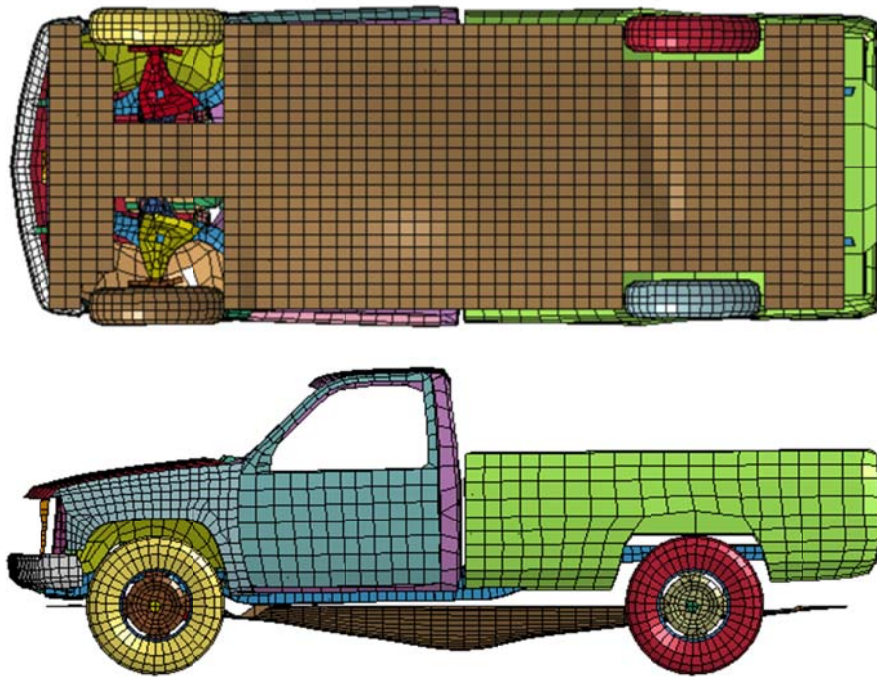
Figure 4.14 HCA topography design in application to under-vehicle design domain. The domain is shown from the bottom of the vehicle (above) and the convergent design is shown in application from the right (below).

4.3   Deterministic Designs – Radial Design Domain

The baseline design can be considered a baseline for the full design domain methods as well as the radial design domain cases, since it conforms to both design domains. In addition to the baseline design, two design candidates which utilize the radial design domain are generated. These two methods are developed using the optimization problem as described in the proceeding sections. Regardless of the optimization technique, all of the design methods in this section make use of the radial design domain as shown in Figure 4.15.
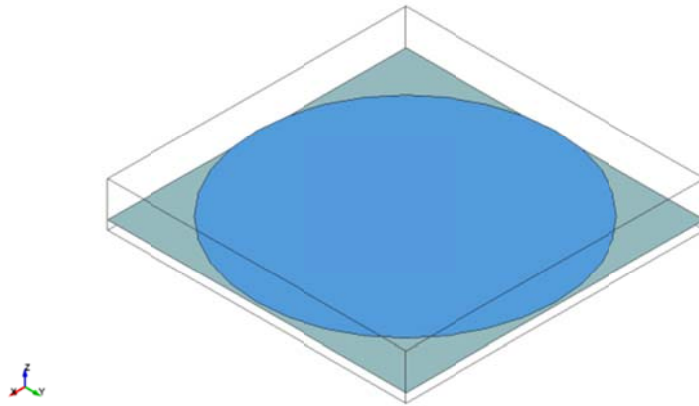
Figure 4.15 Radial design domain.

4.3.1   Polynomial Function Design

In the interest of creating more complex curved surfaces that could be controlled through the variation of only a few variables and increase the dimension of the problem further, a method for generating plate structures that take on a 3rd order polynomial curve was developed. Given the design space as stated above, a 3rd order polynomial curve is assumed to begin at some height (h) at the center of the plate and end at a height of zero at some distance (R) from the center. The polynomial function can then be used to generate a surface by rotating the curve about the z-axis. It should be noted that this method does not make use of the entire square design domain of the plate but instead utilizes a radial design domain extending from the center of the plate.

Staring with the equation for a third order polynomial

$$f(x) = C_0 + C_1x + C_2x^2 + C_3x^3 \tag{4.10}$$

boundary conditions are applied as stated above as equality constraints in the optimization problem, which results in a plate design method as a function of five variables: the four polynomial coefficients and the thickness of the plate. This in turn increases the dimension of the problem to five and the plate takes on a polynomial profile, which can be optimized as a function of five variables:

$$
\begin{aligned}
&\text{find} && c, C_0, C_1, C_2, C_3 \\
&\text{minimize} && M(c, C_0, C_1, C_2, C_3) = \rho\, A(C_0, C_1, C_2, C_3)\, c \\
&\text{subject to} && P_c(c, C_0, C_1, C_2, C_3) - P_{c\,max} \leq 0 \\
& && x_i^2 + y_i^2 = r_i^2 \\
& && z - C_0 + C_1 r + C_2 r^2 + C_3 r^3 = 0 \\
& && h = 120\ mm \\
& && 7.5\ \text{mm} \leq c \leq 50\ \text{mm} \\
& && C_0 - h \leq 0 \\
& && C_0 + RC_1 + R^2 C_2 + R^3 C_3 = 0
\end{aligned}
\tag{4.11}
$$

The optimized shape before and after blast events is shown in Figure 4.16 and similarly to the previous candidate designs, the plate structure exhibits deformation characteristics in which the structure is nearly flattened by the blast, while allowing only a small amount of deflection in the z-direction below the datum plane, within the tolerance of the penetration constraint. The optimized design is an improvement over the baseline design in terms of mass reduction, but demonstrates an increase in comparison to the pyramid profile and Gaussian profile designs due to an increase in thickness in the converged results. It is thought that this increase in thickness is in compensation for a feature of this design nit present in the previous two design methods mentioned here. Due to the fact that the design is generated as a surface of revolution, which is inherently circular, while the shape of the plate as described by the domain is square; the whole design domain is not used on the generation of the plate profile. In turn, this creates an inherent weakness in the plate structure in the portion of the plate beyond the area described by the surface of revolution – i.e. the flat portions of the plate outside of the bulging center portion.

Figure 4.16 Finite Element model showing the optimized polynomial function surface design before (side view, top left and isometric view, top right) and after a blast event (side view, bottom left and isometric view, bottom right). Convergent numerical results: thickness = 14.1 mm, C_0 = 0.112, C_1 = -0.332, C_2 = 0.642, C_3 = -0.859, mass = 113.1 kg.

4.3.2 Trigonometric Function Design

The trigonometric function design was developed in an effort to explore a design whose surface exhibits a more complex curvature than a 3rd order polynomial without substantially raising the dimension of the design problem. Although the polynomial design did not demonstrate an increase in performance correlated to an increase in problem dimension, this design allows a dramatic increase in curvature complexity with only a marginal increase in the problem dimension. While the shape generation process is very similar to the one used in the polynomial function design, the surface of revolution is based on the sum of a set of oscillating functions, namely *cos* and *sin*. Through the definition of a few coefficients, this function allows for curvature that could only be represented by a very high-order polynomial function. Similar to the polynomial design method described above, this method does not make use of the entire square

design domain of the plate but instead utilizes a radial design domain extending from the center of the plate.

Given the design space as stated above, a curve is assumed to begin at some height (h) at the center of the plate and end at a height of zero at some distance (R) from the center. We define $f(x)$ as the sum of a cos and sin function with coefficients to allow customization of the curve within the design domain:

$$f(x) = C_0 \cos C_1 x + C_2 \sin C_3 x \tag{4.12}$$

After some development, the coefficients are chosen to allow the designer to control overall height and width of the structure and allow for some amplitude and frequency modulation of the second term to generate a wave shape. This would allow for the creation of plate structures of much greater complexity than a 3rd order polynomial. The coefficients in the equation above become the design variables and the trigonometric function for design generation is:

$$f(x) = a_1 \cos \pi x + \left[\frac{(a_{21} - a_{22})}{R} x + a_{21} \right] \sin \left[\left(\frac{(f_2 - f_1)}{R} x + f_2 \right) 2\pi x \right] \tag{4.13}$$

This method exhibits an increase in problem dimension to six and the plate takes on a trigonometric function profile, which can be optimized via gradient based methods as a function of six variables:

$$
\begin{aligned}
&\text{find} && c, a_1, a_{21}, a_{22}, f_1, f_2 \\
&\text{minimize} && M(c, a_1, a_{21}, a_{22}, f_1, f_2) = \rho \, A(c, a_1, a_{21}, a_{22}, f_1, f_2) \, c \\
&\text{subject to} && P_c(c, a_1, a_{21}, a_{22}, f_1, f_2) - P_{c\,max} \leq 0 \\
&&& x_i^2 + y_i^2 = r_i^2 \\
&&& z - a_1 \cos \pi r + \left[\frac{(a_{21} - a_{22})}{R} r + a_{21} \right] \sin \left[\left(\frac{(f_2 - f_1)}{R} r + f_2 \right) 2\pi r \right. \\
&&& 7.5 \text{ mm} \leq c \leq 50 \text{ mm} \\
&&& h = 120 \text{ mm} \\
&&& 0 \leq a_1 \leq h - a_{21} \\
&&& 0 \text{ mm} \leq a_{21} \leq 20 \text{ mm} \\
&&& 0 \text{ mm} \leq a_{22} \leq 5 \text{ mm} \\
&&& 0 \leq f_1 \leq 50 \\
&&& 0 \leq f_2 \leq 50
\end{aligned}
$$

(4.14)

The complex curvature of the surfaces generated by the trigonometric function design were not able to be rendered with accuracy in the standard 26 x 26 plate used throughout this study. The design can exhibit many small rippling curvatures which cannot be captured by a course mesh. As shown in Figure 4.17, an increase in the level of mesh refinement is necessary to obtain valid experimental results.
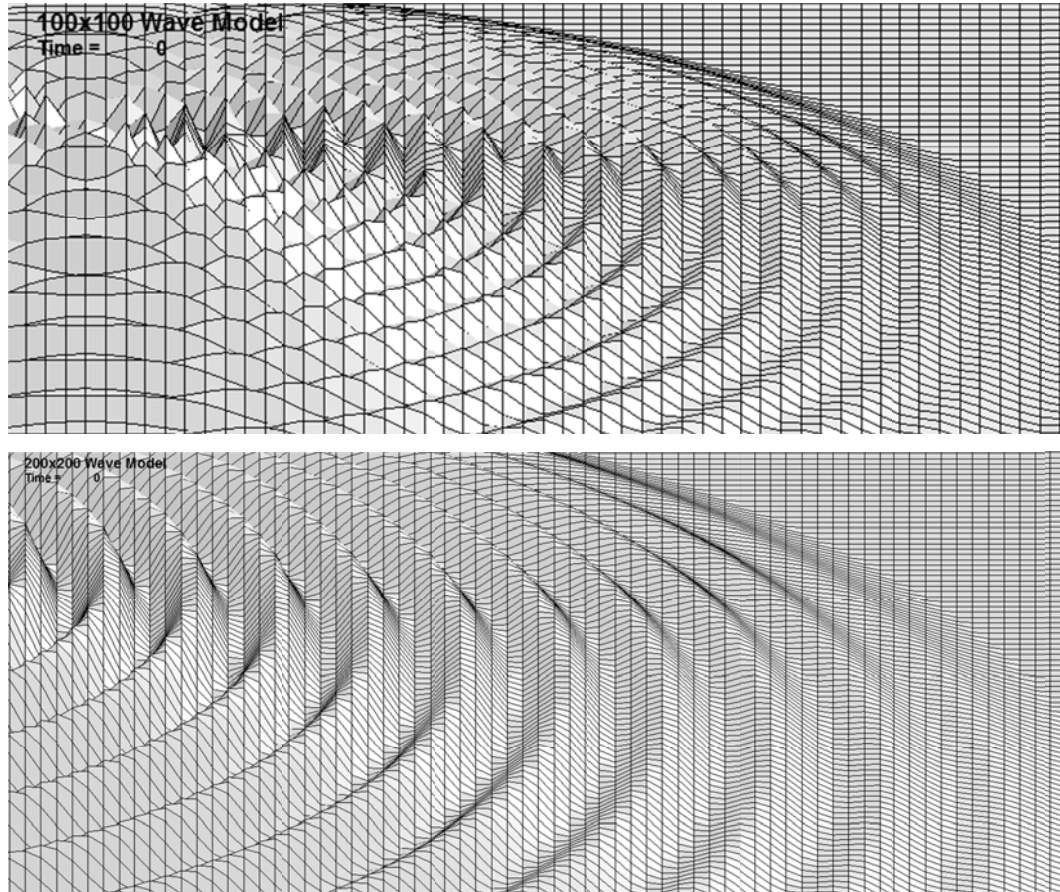
Figure 4.17 Detail of plate showing mesh refinement to capture detailed curvature of trigonometric function design method. 100x100 element mesh refinement (top) and 200x200 element mesh refinement (bottom) are shown.

Through a mesh convergence study it was found that a 200 x 200 mesh discretization of the design domain was adequate to achieve accurate results. This mesh refinement comes at the cost of dramatically increased computational time however, as the number of elements increases from 625 to 40000. This increase correlates to an increase in FEA simulation time from approximately 5 seconds to over 10 minutes in some cases. When the bounds on the design variables are large, the number of function

calls necessary to find the gradient for optimization can be high, resulting in a convergence time for this optimization problem that is unreasonably high. In order to overcome this problem, the optimization is carried out in two stages of fidelity. A model in which the design domain is discretized into 100 x 100 elements, considered a low-fidelity model with a relatively large error, is used to narrow the bounds to within reasonable spans. After the span of bounds has been reduced, a high-fidelity, accurate model is used to find the convergent design. This process resulted in an accurate, convergent design at a fraction of the computational cost.

The convergent design, shown in Figure 4.18, exhibits some amplitude and frequency modulation of the second trigonometric term, and the plate takes on the appearance of raised concentric ripples emanating from the center of the structure.
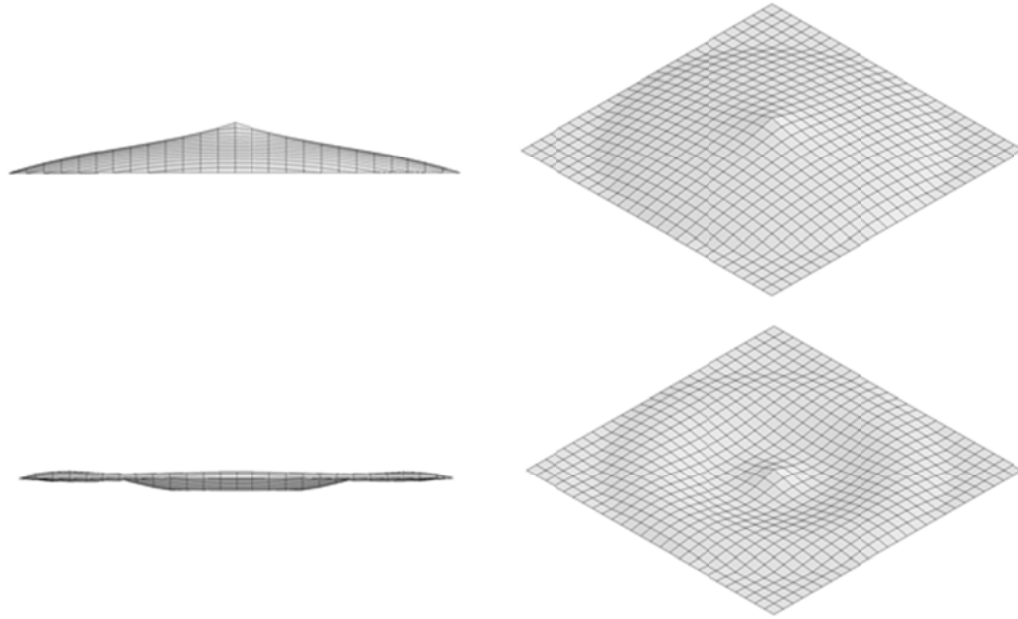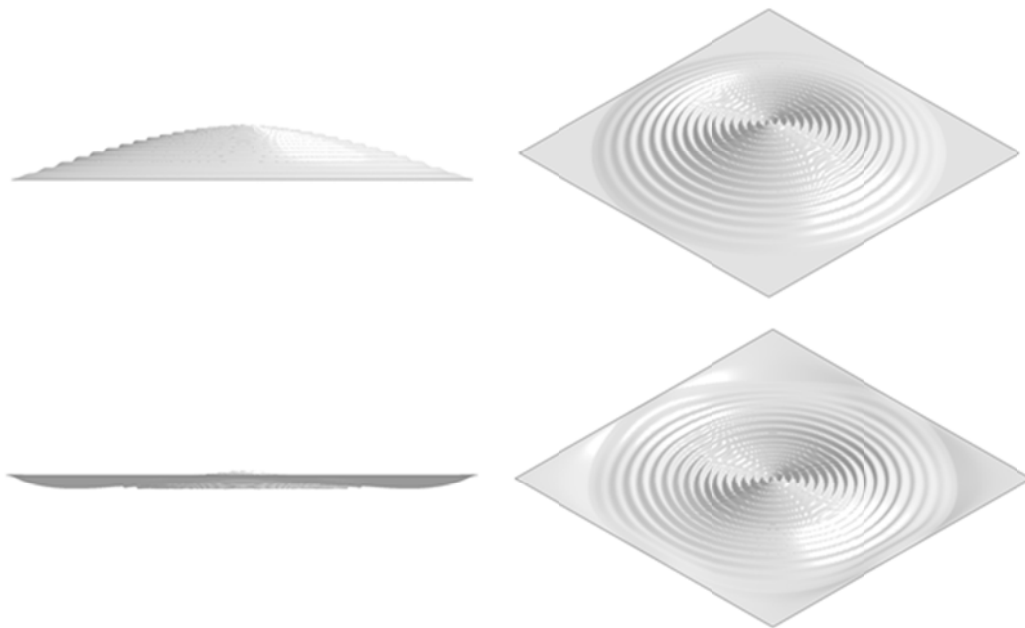

Figure 4.18 Finite Element model showing the optimized trigonometric function surface design before (side view, top left and isometric view, top right) and after a blast event (side view, bottom left and isometric view, bottom right). Convergent numerical results: thickness = 8.31 mm, $a_1 = 0.1045$, $a_{21} = 0.01549$, $a_{22} = 0.0000$, $f_1 = 44.794$, $f_2 = 34.000$, mass = 81.2 kg.

This design method yields the greatest reduction in mass over baseline (-64.1 %) and a substantial reduction in mass over the Gaussian design, the next best performing method (-14.0 %). Despite the increase in the complexity of the curvature, the reduction in mass is due to a thinner structure than was found in previous results. In this case, an increase in the order of the optimization problem allowed for a more pronounced relaxation of the design, and resulted in a higher performance, more complex structure.

4.4   Comparison of Deterministic Results

The numerical results of the convergent designs are divided into two tables in order to compare only designs operating within the same design domain. Table 4.3 contains performance values for the full design domain methods. The results are presented as to demonstrate the increase in performance associated with an increase in design variables. As the number of design variables increases from one to three, i.e. from the flat plate design to the Gaussian function design, there is a decrease in mass of the converged structure.

Table 4.3 Comparative numerical results: full design domain

Method	No. of design variables	No. of iterations	No. of function calls	Mass of converged design (kg)	Mass reduction from baseline (%)
Flat Plate Design	1	18	71	226.4	0.0
Pyramid Profile Design	2	17	121	99.1	-56.2
Gaussian Function Design	3	9	82	94.3	-58.4
Inverted Profile Design	n/a	16*	68*	105.8	-53.3
HCA Topography	N**	112	112	97.8	-56.8

* The procedure of inverting the shape does not apply to the computational efficiency of the design method
** N is equal to the number of free nodes in the design domain

Note the division line between the geometrically constrained designs and the free shape designs, i.e. the inverted profile and HCA topography design methods. This research represents a straight comparison of these heuristic techniques with other deterministic design methods, and the number of design variables in these cases needs

further explanation. In the inverted profile design method, first the shape is produced through the inversion procedure described in Section 4.2.4, and then the thickness is optimized via SQP methods. For this reason, the number of design variables is technically one, although the shape is produced heuristically without any formal optimization procedure, thus this design method should not be considered as part of the trend of increased design variables.

Along a similar line of thought, the HCA concept technically has N number of design variables, where N is the number of free nodes in the design domain. However, this dramatic increase in design variables did not result in a continuation of the trend of increased performance. Comparisons between these geometrically constrained methods and free shape methods are tenuous, however, and this method should not be considered as part of the procession of increased design variables, but instead simply compared in terms of performance for methods existing within equal design domains.

As was stated previously, the validation of HCA concept designs can be extremely problematic, but an attempt is made here to accomplished validation through direct comparison to benchmark results. The summary of numerical results as an improvement of the baseline design is given in Table 4.3. In every case, the penetration for the converged design is zero. The comparative numerical results for the HCA method demonstrate a substantial performance improvement over the baseline design in terms of mass reduction and performance approximately equal to or better than all converged candidate designs, with the exceptions of the Gaussian function design and the trigonometric function design method. These results demonstrate the success of the HCA topography design in generating structures of equal and in some cases superior to geometrically constrained designs while using fewer computational resources and allowing the designer a higher degree of control. In general, more development is required of the HCA heuristic approach in order for it to compare favorably with other deterministic design methods.

Table 4.4 contains performance values for the radial design domain methods. In both design domain cases, radial and full, there is a trend of increased performance in terms of mass reduction as the number of design variables increases. The trigonometric function design exceeds the performance of all other design by far, demonstrating a reduction in mass over baseline by -64.1%, with the trade-off of a vast increase in computational cost. Despite the large computational cost, this design method shows potential for further consideration.

Table 4.4: Comparative numerical results: radial design domain

Method	No. of design variables	No. of iterations	No. of function calls	Mass of converged design (kg)	Mass reduction from baseline (%)
Flat Plate Design	1	18	71	226.4	0.0
Polynomial Function Design	5	173	1398	113.1	-50.0
Trigonometric Function Design	6	272*	1723*	81.2	-64.1

* These totals are a sum of the iterations necessary for the high and low fidelity models to converge

4.5   Uncertainty Quantification Examples

This section demonstrates the application of the uncertainty quantification methods outlined in Chapter 3, namely the univariate dimensional reduction method (UDR) and the performance moment integration method (PMI). For this research, the success of each method is measured in terms of accuracy and computational efficiency. The investigation is divided into two sections. In Section 4.5.1, three numerical test problems are used as sample performance functions and the UDR and PMI methods are applied to approximate the low-order statistical moments. In Section 4.5.2, the methods are applied to the plate design problems and are used to approximate the performance of deterministic plate designs under uncertain loading conditions.

4.5.1   Test Problem Applications

In the following numerical examples, test functions are used as sample performance functions to investigate the accuracy of the uncertainty quantification methods. In each case, the test function $h(X)$ is a function of two variables. The vector of random variables X is composed of two normally distributed variables with a mean of 5 and a variance of 1: $X \sim N[5,1]$. To check the accuracy of the methods, the results of the UDR and PMI are compared with the results of a Monte Carlo simulation of 10000 samples. In each test problem case, UDR method is applied using five quadrature points. Therefore, the number of function evaluations necessary for moment approximation is eleven, according to the formula

$$\text{No. of function evaluations} = nN + 1 \qquad (4.15)$$

where n is the number of random variables and N is the number of quadrature points. However, due to the normal distribution of the random variables, that number can be reduced since the value for the quadrature point when the weight is equal to 0.53333, i.e. the value when both random variables are at their respective mean values, is known. Taking advantage of this, equation (4.15) becomes

$$\text{No. of function evaluations} = n(N - 1) + 1 \qquad (4.16)$$

and the total number of function evaluations necessary for moment approximation is reduced to nine.

As was stated in Chapter 3, the PMI method requires a transformation from X-space to standard normal U-space and the numerical integration is performed in the output space. This can be done without the need for any function evaluations; the cost of the PMI method stems from the need to solve inverse reliability problems in order to determine the quadrature points $g_{B=-\sqrt{3}}$ and $g_{B=+\sqrt{3}}$. For these numerical test problem examples, the sequential quadratic programming methods described in Chapter 2 are applied to solve the inverse reliability optimization problem. In order to investigate the results if increasing the number of quadrature points, both 3-point and 5-point quadrature schemes for the PMI are employed. The values for the quadrature points are weights for all methods are given in Chapter 3.

4.5.1.1   Linear Test Function

A simple linear function

$$h(\boldsymbol{X}) = 2X_1 + X_2 + 100 \tag{4.17}$$

is used as a trial performance function to investigate the accuracy of the uncertainty quantification methods. Figure 4.19 shows a contour of the function in standard X-space and the transformation to standard U-space for random variables having characteristics $\boldsymbol{X} \sim N[5,1]$ as described above. The central image displays the locations of the quadrature points for the 3-point PMI method and the image on the right shows locations of the quadrature points for the 5-point PMI method.

Figure 4.19 Detail of transformation of the linear test function from X-space (left) to standard U-space. The locations of the quadrature points are shown for both the 3-point (center) and 5-point (right) PMI methods.

As shown in Table 4.5, all methods produce nearly the exact same result. The UDR and PMI method both are able to accurately approximate the mean and standard deviation of the performance function with less than 1% error when compared to a Monte Carlo simulation of 10000 samples. The 5-point quadrature PMI method did not demonstrate a discernible increase in accuracy despite more than double the computational cost of the 3-point quadrature method.

Table 4.5 Numerical results of uncertainty quantification for linear test function.

Method	Mean (μ)	% Error	St. Dev. (σ)	% Error	No. of F.E.
Monte Carlo (10000 samples)	115.03		2.25		
UDR	114.99	-0.03	2.24	-0.44	9
PMI (3-point)	115.00	-0.03	2.24	-0.44	51
PMI (5-point)	115.00	-0.03	2.24	-0.44	116

4.5.1.2   Nonlinear Test Function - Mixed Terms

The second performance function used to evaluate the methods for uncertainty quantification is a nonlinear function of two variables based on the test function seen in the works of Lee and Choi [75] [35]

$$h(X) = 5 - \frac{X_1^2\, X_2}{20} \tag{4.18}$$

This function is evaluated in order to demonstrate that nonlinear functions and functions with mixed terms can increase the error seen in the UDR and PMI methods. Figure 4.20 shows a contour of the function in standard X-space and the transformation to standard U-space for random variables having characteristics $X \sim N[5,1]$ as described above.
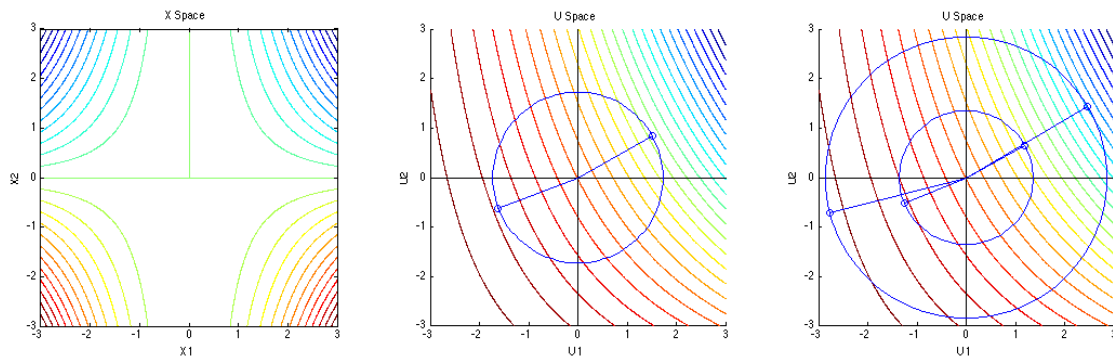
Figure 4.20 Detail of transformation of the non-linear test function from X-space (left) to standard U-space. The locations of the quadrature points are shown for both the 3-point (center) and 5-point (right) PMI methods.

The comparative numerical results, as given in Table 4.6, show some increase in overall error for all methods when compared to the example in 4.5.1.1 for a linear performance function. Similar to what has been demonstrated in the work of Lee [75], the UDR method shows in increased error in approximation of the standard deviation due to the off-diagonal term in the performance function. The PMI method was able to very accurately approximate the standard deviation, demonstrating less than 1% error for both the 3-point and 5-point methods, with reasonable estimation of the mean as well. It should be noted that there was no significant difference in value for the 3-point and 5-point PMI methods despite the large increase in computational cost.

Table 4.6 Numerical results of uncertainty quantification for nonlinear test function with mixed term.

Method	Mean (μ)	% Error	St. Dev. (σ)	% Error	No. of F.E.
Monte Carlo (10000 samples)	-1.54		2.87		
UDR	-1.50	-2.79	2.81	-2.02	9
PMI (3-point)	-1.65	6.95	2.89	0.83	62
PMI (5-point)	-1.65	6.96	2.90	0.97	132

4.5.1.3   Nonlinear Test Function - No Mixed Terms

The last trail performance function is designed to be highly non-linear while having no mixed terms.   In order to investigate the accuracy of the uncertainty quantification methods under those conditions, the trial function is given as

$$h(X) = \exp X_1 + \exp X_2 + X_1^4 + 2X_2^4 + 8X_1^3 + 7X_2^3 + X_1^2 + 3X_2^2 + 50X_1 + 10X_2 + 1 , \quad (4.19)$$

which is the sum of a 4th-order polynomial and two exponential terms. Figure 4.21 shows a contour of the function in standard X-space and the transformation to standard U-space for random variables having characteristics $X \sim N[5,1]$ as described above.
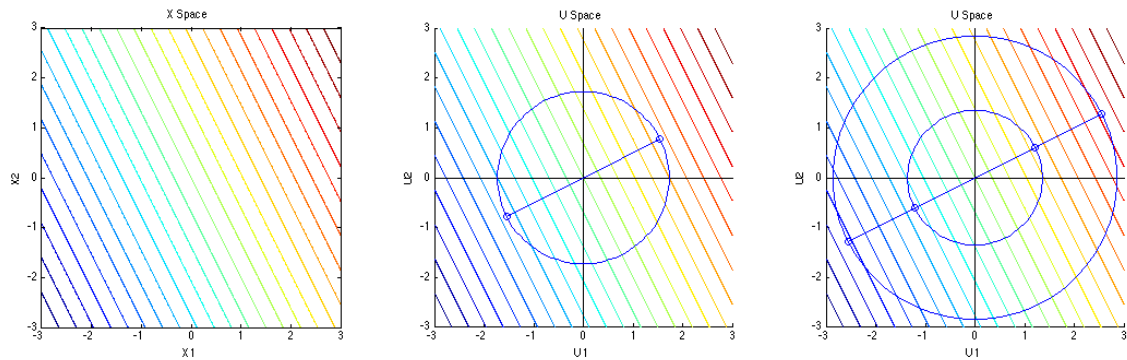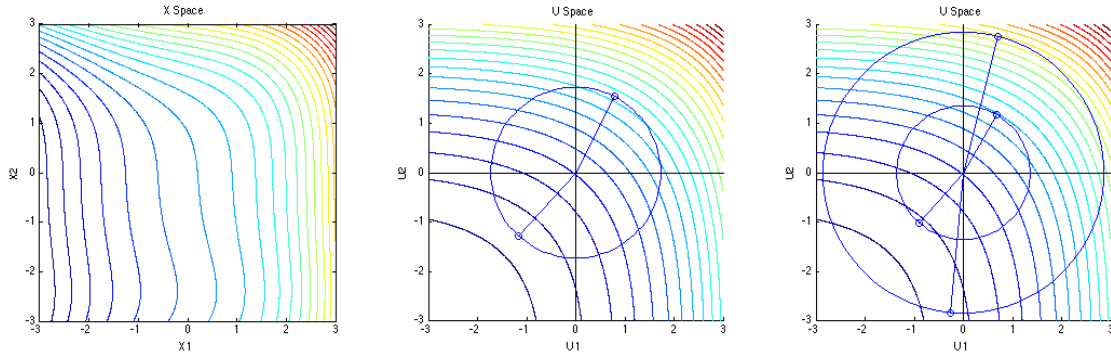
Figure 4.21 Detail of transformation of the non-linear exponential test function from X-space (left) to standard U-space. The locations of the quadrature points are shown for both the 3-point (center) and 5-point (right) PMI methods.

Since there are no mixed terms included in the function, the UDR again provides a good approximation of both the mean and standard deviation, accumulating less than 1% error in both cases and required only the standard nine function evaluations associated with that method. The highly non-linear character of the test function yields an increased error in the PMI method results, however, with both the 3-point and 5-point quadrature methods having an error of over 5%. As shown in Table 4.7, the 5-point quadrature PMI method resulted in a negligible increase in accuracy (less than 1%), while requiring a substantial increase in computational cost. This increase in computational cost can also be thought of as the result of the non-linear nature of the function, since the optimization solver requires the use of more iterations to find the values of the quadrature points via inverse reliability analysis.

Table 4.7 Numerical results of uncertainty quantification for exponential test function with no mixed terms.

Method	Mean (μ)	% Error	St. Dev. (σ)	% Error	No. of F.E.
Monte Carlo (10000 samples)	5296.36		2571.30		
UDR	5323.36	0.51	2575.90	0.18	9
PMI (3-point)	4896.20	-7.56	2380.86	-7.41	58
PMI (5-point)	4910.40	-7.29	2402.49	-6.57	323

In general, we can conclude from these numerical tests that both the UDR and PMI methods can be used to effectively approximate the low-order statistical moments of certain performance functions. The UDR method has the advantage of only requiring nine function evaluations while maintaining a fairly high degree of accuracy in very nonlinear cases. However, it does demonstrate some error when the performance function has mixed terms for which some cross-contamination of the random variables is possible. In contrast, the PMI method can require substantially more function evaluations to solve for the quadrature point values, but is not as susceptible to error caused by functions with mixed terms. In these investigations, the use of 5-point quadrature did not exhibit an increase in accuracy that was worthy of the additional computational cost involved.

4.5.2   Plate Design Applications

In order to apply the methods of uncertainty quantification to the area of plate design, numerical function evaluations are replaced by finite element simulations to calculate the maximum deflection of the plate under uncertain loading conditions. In this way, the statistical moments of the protection response can be approximated for a given design. The amount of deflection below the datum plane, $P_c(\boldsymbol{d})$ as given in the general optimization problem in Chapter 2, is now a function of both the design variables $\boldsymbol{d}$ and the vector of random variables $\boldsymbol{X}$, and can be stated as $P_c(\boldsymbol{d}, \boldsymbol{X})$. This creates a need for the introduction of uncertain quantities into the design.

Staying within the framework of vehicle protection, there are two chief candidates for sources of epistemological uncertainty: blast magnitude and blast location. The deterministic loading cases as investigated in the first half of Chapter 4 assumed a single loading case, that being a charge of 5 kg TNT located at a position of 40 cm above the plate dead center. In order to investigate the uncertainty propagation throughout the system, those deterministic conditions are replaced by random variables, each considered to have standard normal distribution using the deterministic cases as the mean values.
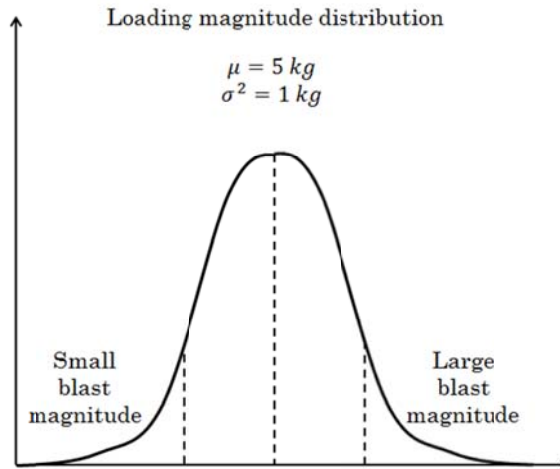
Figure 4.22 Normal distribution of the blast magnitude.

The magnitude of the blast X_M is therefore defined as a normally distributed random variable with a mean of 5 kg TNT a variance of 1 kg TNT, or $X_M \sim N[5,1]$. Considering all the cases which fall under plus/minus three standard deviations, which would account for the majority of the cases, this allows the blast magnitude to vary between a relatively small blast magnitude of 2 kg TNT to a relatively large magnitude of 8 kg TNT, as illustrated in Figure 4.22. Similarly, the x-coordinate of the blast location, X_L, is defined as a standard normal random variable having with a mean value of 0 m and a standard deviation of 0.0625 m, or $X_L \sim N[0,0.0625]$. This allows for the location of the blast to be modeled as occurring to the left or right of the vehicle, while the majority of the points will fall within $\pm$ 0.5 m of dead center, as shown in Figure 4.23.
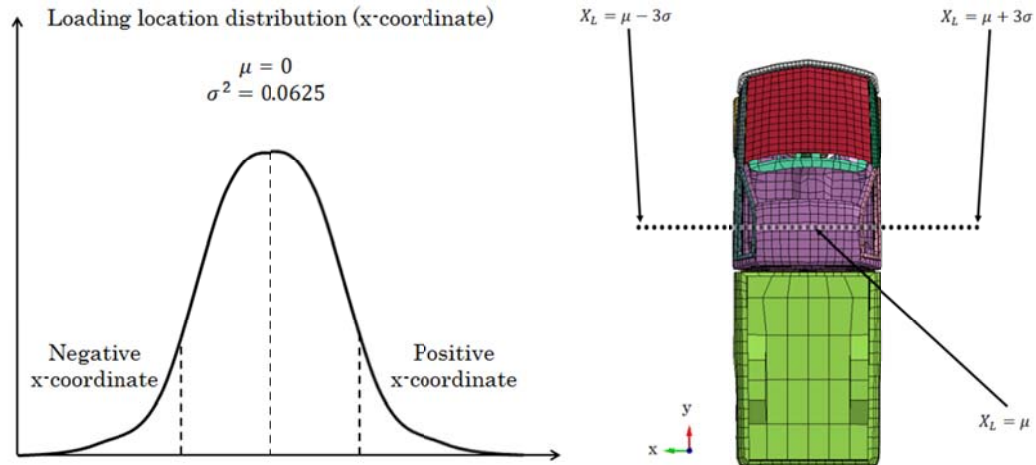
Figure 4.23 Normal distribution of blast location (left) with corresponding schematic to illustrate adaptation from vehicle protection framework (right).

To evaluate the methods for uncertainty quantification, three of the designs generated under deterministic loading cases are chosen and the statistical moments of the protection performance value μ_P and σ_P are calculated. The three deterministic designs chosen are the flat plate design, the pyramid profile design, and the polynomial function design as described in sections 4.2.1, 4.2.2, and 4.3.1, respectively. These deterministic designs represent cases of few design variables (base and pyramid) and a case of an increased number of design variables (polynomial), in order to investigate the application and accuracy of the uncertainty quantification methods across the range of design domains.

4.5.2.1   UDR Application
The UDR method is implemented in plate design by using LS-DYNA finite element simulations to calculate the value for $P_c(\mathbf{d}, \mathbf{X})$ under loading conditions corresponding to the quadrature points utilized by the method described in section 3.2. As was the case with the numerical test problems, the random variables are normally distributed, thus the UDR method requires only nine function evaluations to approximate the mean and standard deviation of the protection response. The values generated by the

UDR method are compared to values generated by a computationally costly Monte Carlo simulation that utilized 5000 finite element simulations to approximate each value.

As shown in Table 4.8, the values found via UDR approximation compare favorably with those generated by the Monte Carlo simulation. For all deterministic design cases, the relative error of the mean calculation with respect to the Monte Carlo results was within 10%, while the mean values for the base and pyramid designs was with 2%. Similar results were found for the standard deviation, with the largest error being observed in the pyramid design, at approximately 8%.

Table 4.8 Numerical results for UDR method in plate design application.

Method	Flat Plate		Pyramid		Polynomial	
	Mean (μ)	St. Dev. (σ)	Mean (μ)	St. Dev. (σ)	Mean (μ)	St. Dev. (σ)
UDR	-0.0252	0.0096	-0.0522	0.0321	-0.0434	0.0254
Monte Carlo	-0.0256	0.0092	-0.0512	0.0297	-0.0459	0.0247
% Error	-1.68	4.47	1.95	8.01	-5.53	3.00

4.5.2.2 PMI Application

As the results presented in Section 4.5.1 clearly demonstrate, the PMI requires a greater number of function calls to approximate the statistical moments of the performance function than the UDR method when implemented via SQP applications. In some cases, hundreds of function evaluations were necessary to apply the PMI method. Due to the large number of function evaluations the PMI method requires relative to the nine function evaluations needed by UDR method, an alternative means was used for application of the PMI method in plate design.

As a means to improve computational efficiency, metamodelling with radial basis function networks is utilized for application of the PMI method to the area of plate design. The RBF network metamodels are used to approximate the output of the

protection performance function such that the inverse reliability problem necessary to determine the quadrature points can be solved efficiently. As is stated in Chapter 2, these networks require some initial training with several sets of input data in order to achieve the desired level of accuracy.
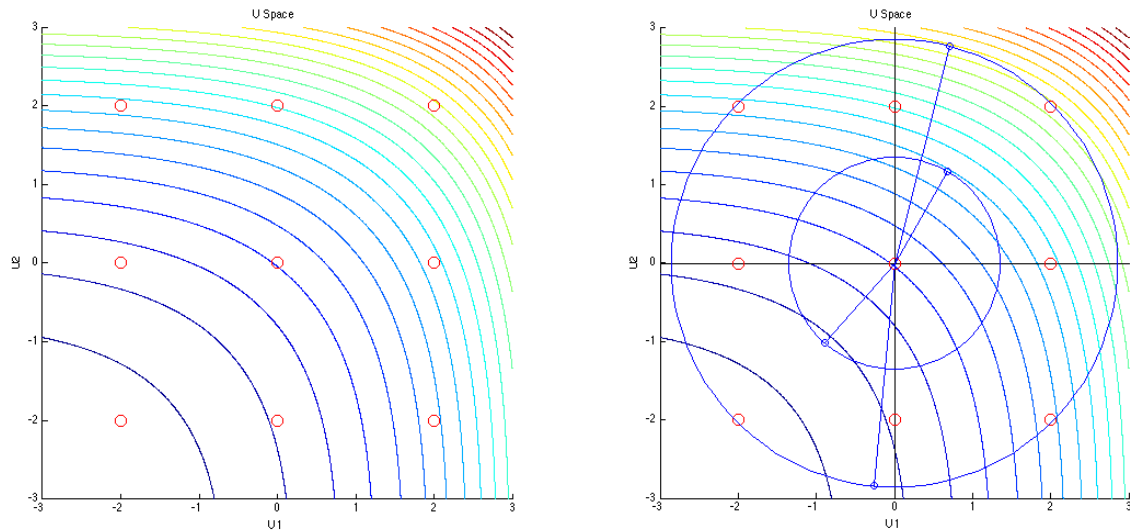
Figure 4.24 Contour of a nonlinear performance function in standard U-space with sample points shown in red (left), and solution of the quadrature points for the PMI method solved via RBF network methods (right).

Consider Figure 4.24 above. The image on the left shows the contour plot of a nonlinear function in standard U-space with nine sample points (shown in red) evenly distributed about the origin (point 0,0). These nine sample points are used to initially train the RBF network which is in turn used to solve for the quadrature points necessary for application of the PMI method. Through the metamodelling procedure, the computational cost of the PMI method for both the 3-point and 5-point applications is nine, which allows for a direct comparison of accuracy with the UDR method at the same computational cost.

The numerical results for the 3-point and 5-point quadrature PMI methods are given in Table 4.9. For all deterministic design cases, the relative error of the mean calculation with respect to the Monte Carlo results was roughly 15-30%. Similar results were found for the standard deviation, with the largest error being observed in the pyramid design, at approximately 25%. The relative error observed in the PMI method is

larger than that observed in the UDR method in all cases, possibly due to the error introduced by the RBF networks and the highly nonlinear performance function. Of note is that the difference in percent error for the 3-point and 5-point quadrature PMI methods is negligible.

Table 4.9 Numerical results for PMI method in plate design application.

Method	Flat Plate		Pyramid		Polynomial	
	Mean (μ)	St. Dev. (σ)	Mean (μ)	St. Dev. (σ)	Mean (μ)	St. Dev. (σ)
PMI (3-point)	-0.0299	0.0088	-0.0356	0.0222	-0.0329	0.0228
Monte Carlo	-0.0256	0.0092	-0.0512	0.0297	-0.0459	0.0247
% Error	16.71	-4.14	-30.47	-25.30	-28.35	-7.51
PMI (5-point)	-0.0301	0.0093	-0.0368	0.0225	-0.0335	0.0227
Monte Carlo	-0.0256	0.0092	-0.0512	0.0297	-0.0459	0.0247
% Error	17.49	1.31	-28.13	-24.29	-27.05	-7.91

4.6   Design Under Uncertainty

This section applies all of the design under uncertainty methods introduced in the uncertainty methodology section of Chapter 3 to area of isotropic plate design for blast mitigation. As was explained, the primary characteristic of all design under uncertainty problems is the probabilistic analysis of the design rooted in the approximation of statistical moment of performance. In the application of these methods, all of the statistical moments are calculated via the univariate dimensional reduction method as it applies to plate design (see Section 4.5.2). This method is chosen for its accuracy and low computational cost.

To investigate the applications in plate design, the deterministic polynomial function design method is adapted to each specific design under uncertainty method. The deterministic design case, thoroughly discussed in 4.3.1, involves the generation of a 3rd order polynomial function where the coefficients are considered the design variables. The polynomial function can then be used to generate a surface by rotating the curve

about the z-axis. In the following sections, 4.6.1 through 4.6.3, the design under uncertainty methods are examined on a case by case basis. Comparisons are drawn between results from the various methods and between results of the deterministic design.

4.6.1   Robust Design

In application to the polynomial function design, the optimization problem for robust design is a restatement of the general robust problem given in Chapter 3, with the same envelope and protection constraints as the deterministic case. The robust problem is expressed as

$$
\begin{aligned}
&\text{find} && c, C_0, C_1, C_2, C_3 \\
&\text{minimize} && \sigma_P^2(c, C_0, C_1, C_2, C_3, \boldsymbol{X}) \\
&\text{subject to} && P_c(c, C_0, C_1, C_2, C_3) - P_{c\,max} \leq 0 \\
& && x_i^2 + y_i^2 = r_i^2 \\
& && \boldsymbol{z} - C_0 + C_1 r + C_2 r^2 + C_3 r^3 = 0 \\
& && h = 120 \; mm \\
& && 7.5 \; \text{mm} \leq c \leq 20 \; \text{mm} \\
& && C_0 - h \leq 0 \\
& && C_0 + RC_1 + R^2 C_2 + R^3 C_3 = 0
\end{aligned}
\tag{4.20}
$$

where c, C_0, C_1, C_2, C_3 is the set of all design variables characterizing the shape and thickness of the plate, consisting of the thickness of the plate and the four polynomial constants. $\boldsymbol{X} \sim N[\mu, \sigma^2]$ represents the normally distributed random variables for blast magnitude and location. The term $\sigma_P^2(c, C_0, C_1, C_2, C_3, \boldsymbol{X})$ is the variance of the protection performance (maximum plate deflection) and is a function of both the design variables and the random variables.

The results of the optimization procedure reveal a fundamental problem with the application of robust optimization to lightweight plate design: if the mass of the structure is not included in the objective function or applied as a constraint, the optimal result to minimize the variance of protection will always be the heaviest structure.   The convergent solution, shown in Figure 4.25, is a thick, cone-shaped structure where thickness is at the upper boundary (20 mm) with a mass of 159.42 kg. The polynomial

coefficient values are: $C_0 = 0.12$, $C_1 = -0.24$, $C_2 = 0$, $C_3 = 0$. These coefficients in effect reduce the polynomial to first order, in other words the topography is described as a straight line from the peak to the edge revolved about the z-axis. In profile, this design is identical to the pyramid profile design given in Section 4.2.2, but because it is generated as a surface of revolution, is conical in shape as opposed to pyramidal.
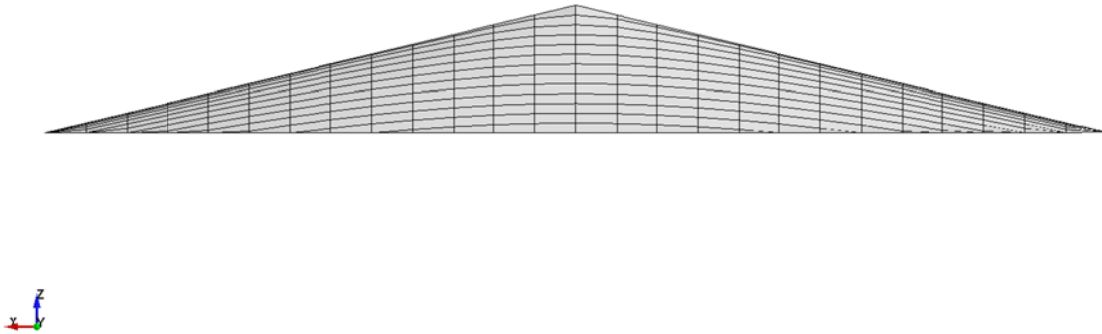
Figure 4.25 Convergent design, robust optimization.

The SQP algorithm required only one iteration to find the optimal shape, as the design variables are at the boundaries of the constraints. In essence this is not optimization, but instead a generation of a topography completely described by the design constraints. Investigation of other design shapes, the flat plate and the pyramid designs, yielded identical results: a single iteration which generates the heaviest structure allowable by the constraints. For these reasons, the robust optimization problem as stated is not considered a valuable optimization tool.

4.6.2   Reliability-Based Design

The application of the reliability-based design optimization problem to the polynomial function design involves the application of a probability of failure constraint to the deterministic design problem. For this test application, and all proceeding problems

that require a probability of failure, an arbitrary small value of 0.05 or 5% is used at the target. The reliability-based problem is expressed as

$$
\begin{aligned}
&\text{find} && c, C_0, C_1, C_2, C_3 \\
&\text{minimize} && M(c, C_0, C_1, C_2, C_3) \\
&\text{subject to} && P[P_c(\boldsymbol{d}, \boldsymbol{X}) > P_{c\,max}] \le 0.05 \\
& && x_i^2 + y_i^2 = r_i^2 \\
& && \boldsymbol{z} - C_0 + C_1 r + C_2 r^2 + C_3 r^3 = 0 \\
& && h = 120\,mm \\
& && 7.5\text{ mm} \le c \le 20\text{ mm} \\
& && C_0 - h \le 0 \\
& && C_0 + RC_1 + R^2 C_2 + R^3 C_3 = 0
\end{aligned}
\tag{4.21}
$$

where c, C_0, C_1, C_2, C_3 is the set of all design variables characterizing the shape and thickness of the plate, consisting of the thickness of the plate and the four polynomial constants. $\boldsymbol{X} \sim N[\mu, \sigma^2]$ represents the normally distributed random variables for blast magnitude and location. The mass of the plate, $M(c, C_0, C_1, C_2, C_3)$, is applied as the objective function. The failure criterion, $P_{c\,max}$, is chosen as a dynamic deflection greater than 30 mm. The probability constraint is expressed as $P[P_c(\boldsymbol{d}, \boldsymbol{X}) > P_{c\,max}] \le 0.05$ to indicate that the probability of failure must be less than 5% under the given uncertain loading conditions.
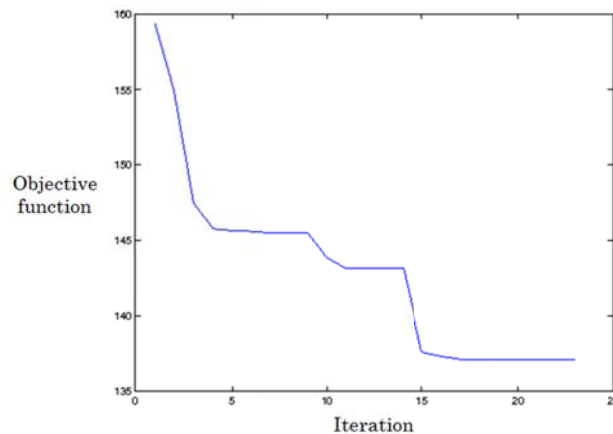
Figure 4.26 Objective function vs. iteration, reliability based design.

Convergence of the optimization is clearly demonstrated by plot of objective function at each iteration shown in Figure 4.26, requiring 23 iterations and a total of 1350 finite element simulations. The convergent structure, shown in Figure 4.27, has a similar

topography to that of the robust design, but it does exhibit a slightly concave topography and a thickness within the bounds at 17.24 mm. The convergent polynomial coefficient values have the characteristics of a third-order polynomial: $C_0 = 0.12$, $C_1 = -0.28064$, $C_2 = 0.05695$, $C_3 = 0.04867$. The mass of the structure is increased from 112 kg, the result of deterministic design method, to 137.06 kg in order to satisfy the probability constraint.
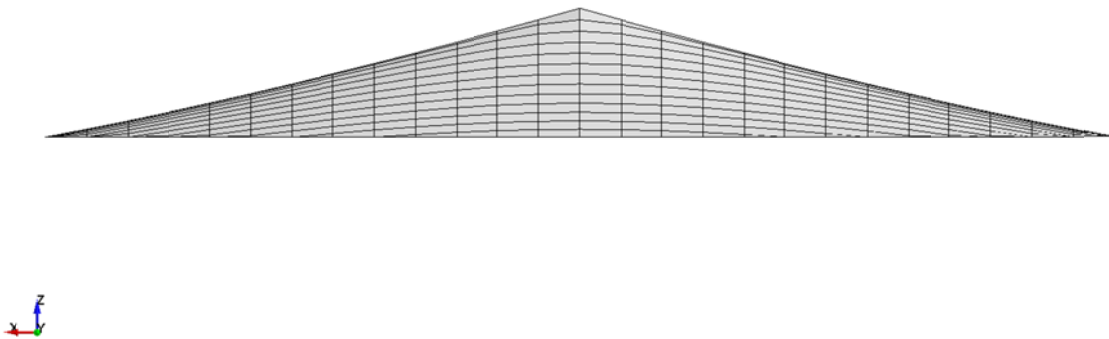
Figure 4.27 Convergent design, reliability-based optimization.

As was stated in Chapter 3, the ultimate goal of this type of optimization is to increase the reliability of the structure through re-characterization of the low order statistical moments. To demonstrate the reliability of the convergent design, the probability density function (PDF) of the reliability-based design is given in Figure 4.28, along with the PDF of the deterministic design. The failure criteria, $P_{c\,max} = -0.03$ m, is shown as the red line. It is clear from the figure that the mean of the protection performance has shifted above the failure criterion and the variance greatly reduced.
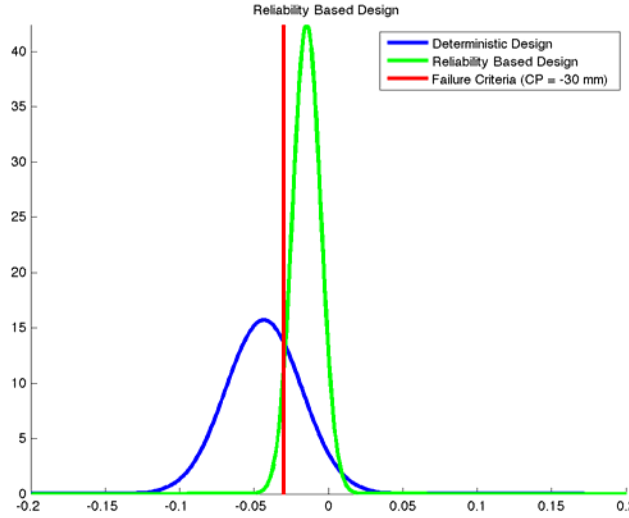
Figure 4.28 Probability density function for convergent design produced by reliability-based design optimization.

4.6.3   Reliability-based Robust Design

Reliability-based robust design optimization (RBRDO) combines variance-minimizing approach utilized by robust design optimization with the probabilistic constraint approach utilized by reliability-based design optimization. The general implementation of RBRDO in the polynomial function plate design can be stated as

$$
\begin{aligned}
&\text{find} && c, C_0, C_1, C_2, C_3 \\
&\text{minimize} && F_C(c, C_0, C_1, C_2, C_3, \mu_P, \sigma_P^2) \\
&\text{subject to} && P[P_c(\boldsymbol{d}, \boldsymbol{X}) > P_{c\,max}] \le 0.05 \\
& && x_i^2 + y_i^2 = r_i^2 \\
& && \boldsymbol{z} - C_0 + C_1 r + C_2 r^2 + C_3 r^3 = 0 \\
& && h = 120\ mm \\
& && 7.5\ \text{mm} \le c \le 30\ \text{mm} \\
& && C_0 - \text{h} \le 0 \\
& && C_0 + RC_1 + R^2 C_2 + R^3 C_3 = 0
\end{aligned}
\tag{4.22}
$$

where c, C_0, C_1, C_2, C_3 is the set of all design variables characterizing the shape and thickness of the plate, consisting of the thickness of the plate and the four polynomial constants. $\boldsymbol{X} \sim N[\mu, \sigma^2]$ represents the normally distributed random variables for blast

magnitude and location. The statistical moments of the protection performance are μ_P and σ_P^2. The failure criterion, $P_{c\,max}$, and the probability constraint, $P[P_c(\boldsymbol{d}, \boldsymbol{X}) > P_{c\,max}] \leq 0.05$, are implemented in exactly the manner as was done for the reliability-based optimization in 4.6.2.

The objective function, $F_C(c, C_0, C_1, C_2, C_3, \mu_P, \sigma_P^2)$, often called the cost function in RBRDO, is a function of all of the design variables as well as the statistical moments of performance. Characterization of the cost function can have a substantial impact on the outcome of the optimization. In order to investigate the effect the cost function on the optimization results, two different formulations are used in the optimization problem given by equation (4.22): a mean-based cost function and a mass-based cost function. Detailed descriptions of the mean-based and mass-based formulation can be found in Chapter 3, Section 3.6.

4.6.3.1 <u>Mean-based Cost Function</u>
The expression for the mean-based cost function used in RBRDO optimization is

$$F_C(c, C_0, C_1, C_2, C_3, \mu_P, \sigma_P^2) = w_1 \left(\frac{\mu_P - (-0.03)}{(-0.05) - (-0.03)} \right)^2 + w_2 \left(\frac{\sigma_P}{0.02} \right)^2 \qquad (4.23)$$

where w_1 and w_2 are the weights for this bi-objective problem as chosen by the designer. The value -0.03 represents a target vale for the mean of the performance function of 30 mm. The values -0.05 and 0.02 represent initial values for the mean and variance of the performance function, which are included to reduce the dimensionality of the two terms. In this example, the weights are chosen as $w_1 = w_2 = 0.5$ as both of the terms in the cost function are considered to be of equal value.
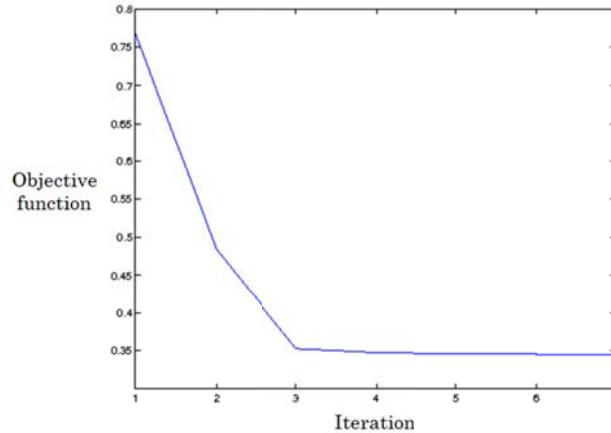
Figure 4.29 Objective function vs. iteration, RBRDO with mean-based cost function.

The optimization converged after 7 iterations and a total of 936 finite element simulations, as is shown in the plot of the objective function value at each iteration, given in Figure 4.29. The convergent structure, shown in Figure 4.30, has a similar topography to that of the reliability-based design, but it is smaller, having a maximum height of ~85 mm and exhibits a comparatively very concave topography. The thickness of the design demonstrates an increase over the RBDO design as well, at 22.34 mm. The convergent polynomial coefficient values have the characteristics of a third-order polynomial: $C_0 = 0.08447$, $C_1 = -0.30164$, $C_2 = 0.24950$, $C_3 = 0.03181$. The mass of the structure is increased from 112 kg, the result of deterministic design method, to 175.62 kg due to the increase in the thickness of the structure.
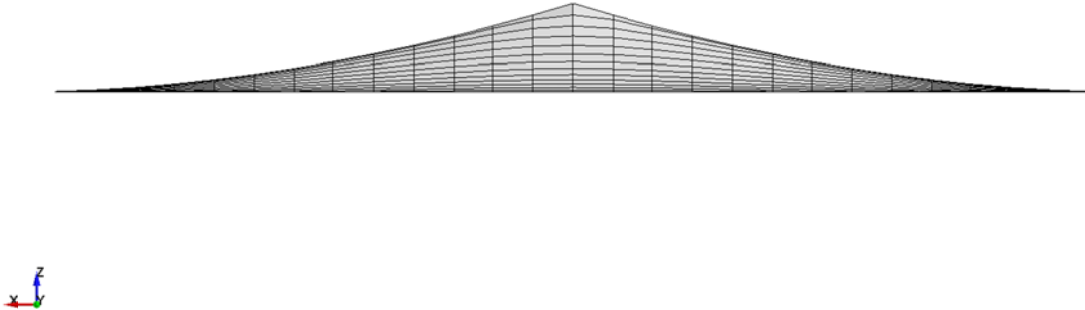
Figure 4.30 Convergent design, RBRDO with mean-based cost function.

In terms of reliability, the structure is very similar to the structure produced by the RBDO optimization. Both of the structures exhibit a probability of failure of ~5% due to the imposition of identical probability constraints. The PDF of the RBRDO mean-based design is given in Figure 4.31, along with the PDF of the deterministic design.
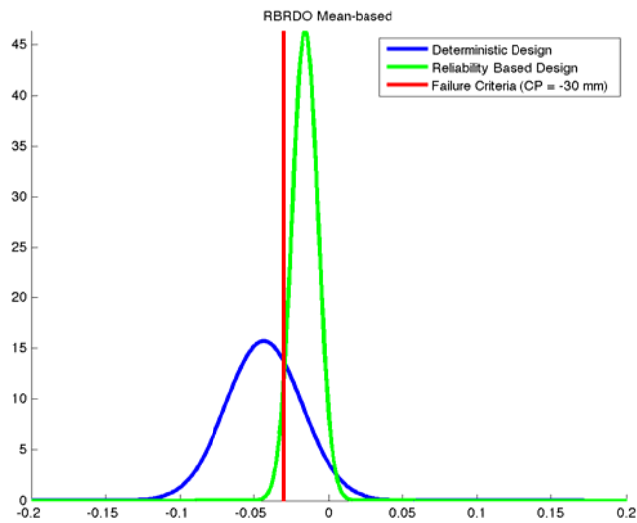
Figure 4.31 Probability density function for convergent design produced by RBRDO with mean-based cost function

4.6.3.2   Mass-based Cost Function

The expression for the mean-based cost function used in RBRDO optimization is

$$F_C(c, C_0, C_1, C_2, C_3, \mu_P, \sigma_P^2) = w_1 \left(\frac{M(c, C_0, C_1, C_2, C_3)}{160} \right) + w_2 \left(\frac{\sigma_P}{0.02} \right)^2 \qquad (4.24)$$

where w_1 and w_2 are the weights for this bi-objective problem as chosen by the designer. $M(c, C_0, C_1, C_2, C_3)$ is the mass of the structure as a function of the design variables. This formulation of the cost function emphasizes the mass of the plate as opposed to the mean of the protection performance function. In the first set of optimized results, the weights are chosen as $w_1 = w_2 = 0.5$. A proceeding example will examine the use of unequal weights.
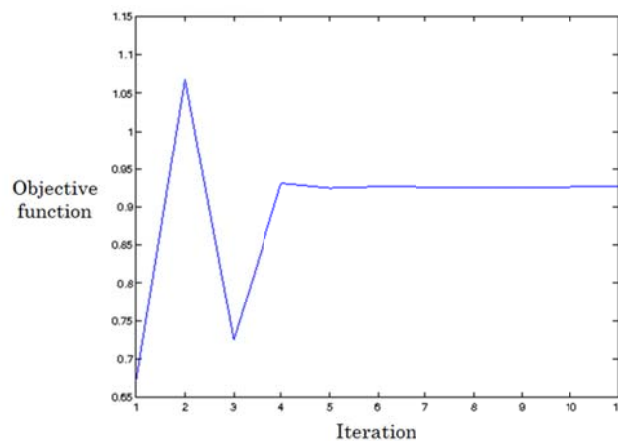
Figure 4.32 Objective function vs. iteration, RBRDO with mass-based cost function and even weights.

The converged optimization results for the evenly-weighted coast function required 10 iterations and 837 finite element simulations, as shown in Figure 4.32. The resulting structure has a mass of 146.43 kg, less than the optimal structure generated by the mean-based RBRDO cost function. Unlike all previous optimization results, this structure exhibits a convex topography, as can be seen in Figure 4.33. The convergent values for the polynomial coefficients reflect this convexity: $C_0 = 0.11560$, $C_1 = -0.15178$, $C_2 = -0.12655$, $C_3 = -0.06455$.
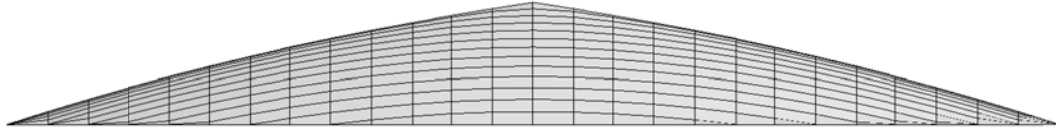
Figure 4.33 Convergent design, RBRDO with mass-based cost function and even weights.

This design exhibits excellent reliability characteristics as well, having a probability of failure of less than 1%. As illustrated in Figure 4.34, the mean of the performance function is well above the failure criterion and the variance is very small. It can be concluded that the change to a mass-based cost function formulation resulted in the generation of a lighter and more dependable structure that was found using the mean-based formulation.
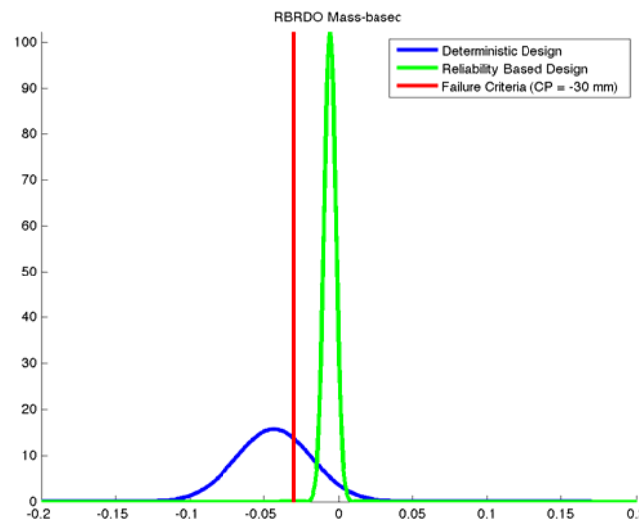
Figure 4.34 Probability density function for convergent design produced by RBRDO with mass-based cost function and even weights.

In order to further investigate a change in cost function formulation, the mass-based formulation given by (4.24) is again implanted in the optimization problem, but with the weight values chosen as unequal values, where $w_1 = 0.8$ and $w_2 = 0.2$. This formulation will emphasize the reduction of mass as opposed to considering minimization of the mass and variance as equal objectives. When compared to the evenly-weighted mass-based formulation, the design required more iteration and finite element simulation to optimize, as given in Figure 4.35. The total computational cost is 12 iterations and 1386 FEA simulations, an increase of over 60% above the evenly weighted optimization.
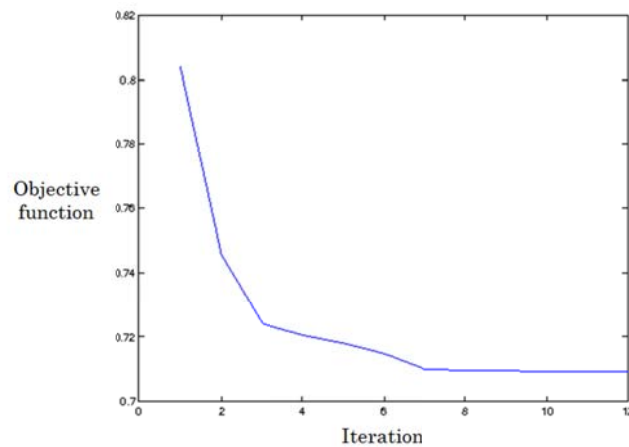
Figure 4.35 Objective function vs. iteration, RBRDO with mass-based cost function and unequal weights

The resulting structure exhibits good performance characteristics, however. The topography has a convex shape very similar to that of the evenly-weighted design, although the curvature slightly differs, as demonstrated by different polynomial coefficients: $C_0 = 0.11560$, $C_1 = -0.11953$, $C_2 = -0.21643$, $C_3 = 0.02100$.
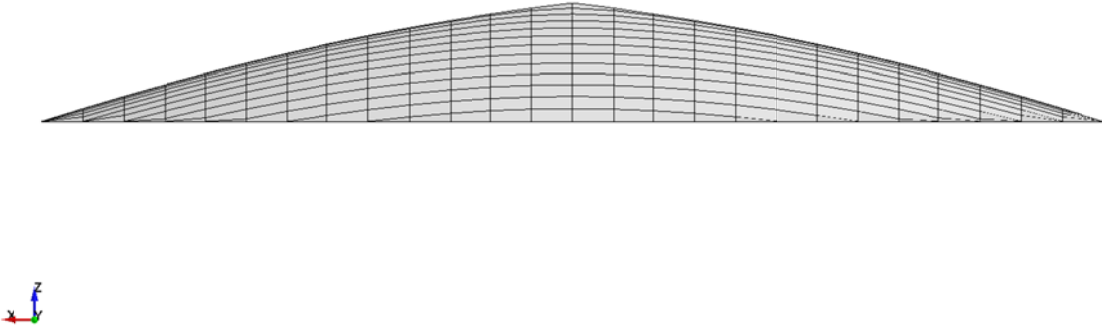
Figure 4.36 Convergent design, RBRDO with mass-based cost function and unequal weights.

The greatest benefit of this unevenly-weighted formulation is seen in the optimized mass value of 131.29 kg. This value is less than the optimized result found in the evenly-weighted RBRDO formulation and even exceeds the performance of the RBDO optimization result, which had been the lightest observed in this investigation. Despite this decrease in mass, the structure still maintains a probability of failure of just under 5% under uncertain loading conditions, as given by Figure 4.37.
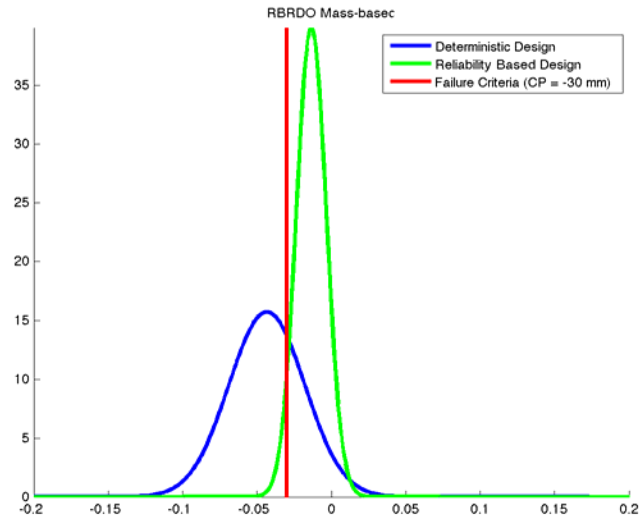
Figure 4.37 Probability density function for convergent design produced by RBRDO with mass-based cost function and unequal weights.

4.7 Comparison of Design Under Uncertainty Results

In the interest of comparing numerical results, all of the design under uncertainty optimization procedures demonstrated for the polynomial function design in the proceeding sections are also performed for two additional design methods: the flat plate design and the pyramid design. The flat plate design is chosen as a baseline for comparison and an example of a design with a minimal amount of design variables. The pyramid design is chosen in order to compare a design, which has relatively few design variables (in this case, two), to a design such as the polynomial which has a relatively large number of design variables (five). The results for each design method are presented individually in tabular form.

Table 4.10 gives the results of all optimization methods for the flat plate design. The deterministic design has an approximately 30% probability of failure when uncertain loading conditions are considered. Interestingly, the remaining optimization methodologies each produce nearly identical results. The mass of the optimized structure is approximately 262 kg with a 5% probability of failure in all cases, except in robust

design optimization where the mass is higher at the benefit of a reduced variance. These results are indicative of a lack of robustness in the design methodology itself. In order to satisfy the failure constraint present in RBDO and RBRDO, the thickness of the plate must be increased. Since there are no other design variables, as soon as the thickness is such that is satisfies the constraint the design is considered converged. Put simply, the only way to increase the reliability of the structure under uncertain conditions is to increase the plate thickness.

Table 4.10 Numerical results for optimization of flat plate design.

Flat Plate Optimization	Mass	No. of iterations	No. of F.E.	Mean (μ)	St. Dev. (σ)	Prob. Of Failure
Deterministic Design	226.32	18	71	-0.0252	0.0096	0.3085
Reliability Based Design	262.30	14	446	-0.0164	0.0083	0.0506
Robust Design	273.00	2	36	-0.0142	0.0077	0.0506
RBRDO (Mean-based cost function)	262.30	10	621	-0.0164	0.0083	0.0506
RBRDO (Mass-based cost function), Weights Even	262.40	10	207	-0.0164	0.0083	0.0506
RBRDO (Mass-based cost function), Weights Skewed	262.33	10	306	-0.0164	0.0083	0.0506

The numerical results for the pyramid design, given by Table 4.11, demonstrate a similar lack of robustness. The structures produced by the various optimization methods again produced nearly identical in terms of mass and reliability. The exceptions to this trend are the RBO method and the even-weighted mass-based RBRDO method, both of which privilege minimization of the variance of minimization of the mass and thus produce heavier structures. As was the case in optimization of the flat plate, the convergent structures are nearly identical with only the thickness varying from design to design. An interesting note is that the RBDO and skewed-weights mass-based RBRDO method produced exactly identical structures, although the RBRDO method required 30 fewer iteration and 126 fewer function evaluations to do so.

Table 4.11 Numerical results for optimization of pyramid design.

Pyramid Optimization	Mass	No. of iterations	No. of F.E.	Mean (μ)	St. Dev. (σ)	Prob. Of Failure
Deterministic Design	99.31	17	121	-0.0522	0.0321	0.7554
Reliability Based Design	135.37	40	576	-0.0106	0.0118	0.0500
Robust Design	145.00	2	54	-0.0096	0.0105	0.0260
RBRDO (Mean-based cost function)	135.39	10	306	-0.0106	0.0118	0.0500
RBRDO (Mass-based cost function), Weights Even	144.39	5	135	-0.0080	0.0088	0.0062
RBRDO (Mass-based cost function), Weights Skewed	135.37	10	450	-0.0106	0.0118	0.0501

In the case of the polynomial function design method, however, some real variation in the convergent structures produced is demonstrated. As given in Table 4.12, the results for the optimization procedures show distinct structures generated by the design under uncertainty procedures. The reliability-based design produces a heavier structure than the deterministic case, but reduces the probability of failure from ~70% to ~5%. The robust design procedure yields a structure with even larger mass, but with an even lower probability of failure. The RBRDO optimization results clearly demonstrate structures that vary as function of the optimization method. The mean-based RBRDO procedure, which defines a target value for the mean, produces the structure with the largest mass value at ~175 kg. The mass-based RBRDO procedure, which in turn privileges reduction of mass, produces lighter structures. Of particular interest is the result for the skewed-weights mass-based RBRDO procedure, which yielded a structure of ~131 kg and probability of failure of only ~5%. This result exceeds the performance of the pyramid design produced by the same optimization procedure, in contrast to the deterministic results in which the pyramid out performs the polynomial function.

Table 4.12 Numerical results for optimization of polynomial design.

Polynomial Optimization	Mass	No. of iterations	No. of F.E.	Mean (μ)	St. Dev. (σ)	Prob. Of Failure
Deterministic Design	112.38	173	1398	-0.0434	0.0254	0.7011
Reliability Based Design	137.06	23	1350	-0.0146	0.0094	0.0507
Robust Design	160.00	1	54	-0.0127	0.0091	0.0286
RBRDO (Mean-based cost function)	175.62	7	936	-0.0158	0.0086	0.0494
RBRDO (Mass-based cost function), Weights Even	146.43	10	837	-0.0058	0.0039	0.0001
RBRDO (Mass-based cost function), Weights Skewed	131.29	12	1386	-0.0135	0.0100	0.0495

The reason for this variation of results stems from the additional design variables present in the polynomial design which allow for the generation of more complicated topography. Consider Figure 4.38, which shows a side by side comparison of the pyramid structure produced via deterministic optimization (left) and the structure produced via RBRDO optimization (right). The structures have identical topographies with a height of 120 mm, but have different thickness and thus different mass.

Figure 4.38 Finite element models of the pyramid structures produced by deterministic optimization (left) and RBRDO optimization (right).

In contrast, consider the polynomial design structures produced via deterministic optimization (left) and the structure produced via RBRDO optimization (right), as shown by Figure 4.39. In this case, we see two distinct topographies, as the shape was able to conform to the optimization constraints in terms of shape and thickness.
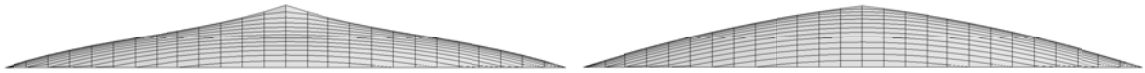
Figure 4.39 Finite element models of the polynomial function structures produced by deterministic optimization (left) and RBRDO optimization (right).

There are two primary conclusions to be made from these comparative results. The first: for the design of lightweight structures where mass is considered to be the key performance metric, unless there are enough design variables such that the structure can adapt to uncertain conditions under various constraint criteria, all methods for design under uncertainty will produce similar or identical results. The second: the more complex design method, that is the polynomial function design with more design variables, is able to produce structures that out-perform simpler designs.

5   CONCLUSION

This chapter contains all concluding remarks related to this thesis in regard to the deterministic design, uncertainty quantification, and stochastic design methods incorporated in this work. The following sections deal with each major facet of the work and provide salient details including: objectives reached, contributions, and recommendations for future work.

5.1   Deterministic Design

A substantially-realized computational framework for shape optimization of plate structures under deterministic blast loading conditions has been developed. This framework represents a general computational tool for the generation of lightweight plate structures under blast loading, not only for deterministic loading cases, but for the design of plate structures under uncertain loading conditions as well. This framework should be considered as the primary tangible contribution of this research. A graphical summary of this computational framework is given by Figure 5.1. These designs are optimized by gradient-based, sequential quadratic programming methods, and the measures of performance are mass and dynamic plate deflection. Through an integration of LS-DYNA finite element software and the Matlab optimization toolbox, convergent designs for progressively more complex geometrically constrained designs are generated for investigation, and the results are understood.
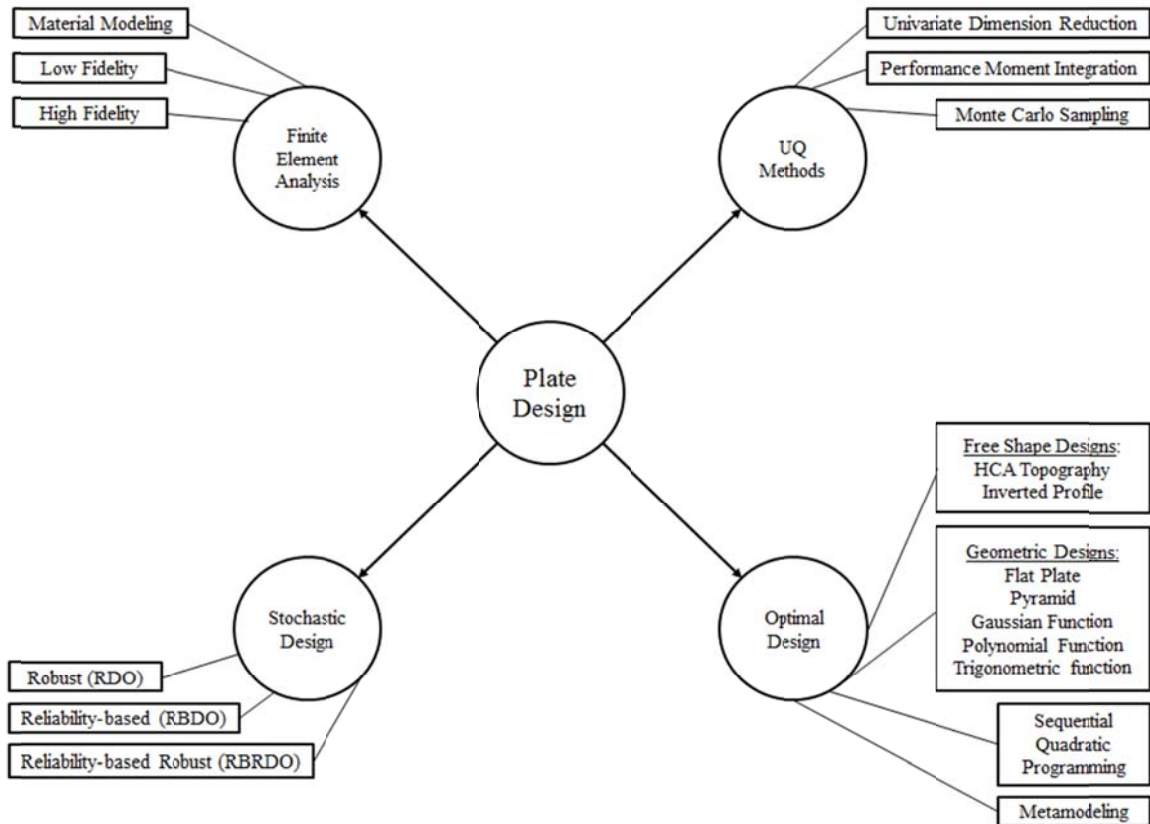
Figure 5.1 Graphical summary of computational framework for plate design

While some previous work exists related to the generation of geometrically constrained structures [23, 20], this work represents a comprehensive effort to objectively compare optimal designs within the same design space and subject to identical constraints.The complexity of the design increases rapidly as the problem is relaxed and the design domain is expanded to include additional design variables. The results demonstrate a clear increase in performance as the complexity of the basis function increases. The design based on the most complex basis function, the trigonometric function design, exhibits by far the best performance over baseline. This design is unique in the research field and shows great promise as a design method moving forward.

Two additional free shape designs, the HCA topography and inverted profile designs, which are not constrained geometrically to basis functions, are also investigated.

These methods represent heuristic approaches, which do not rely on gradient-based optimization techniques, and this work represents an objective comparison between these methods and the geometrically constrained designs. The HCA topography approach builds upon the use of HCA in topology optimization [22], and is a thorough test of previous attempts to apply HCA to topography optimization [23]. This research finds that the HCA topography method functions well and exhibits a number of advantages over geometrically constrained designs, including the ease of application to irregular design spaces and the ability to produce non-symmetric convergent designs. Despite these benefits, the HCA topography method does find sub-optimal solutions when compared with the best geometrically constrained methods. The inverted profile method does not produce structures which compare favorably with either the HCA topography method or the geometrically constrained designs. Additional secondary contributions include: a mesh refinement study, and development of computer code for the automated generation of deterministic designs. The mesh refinement study demonstrates that the HCA topography is for the most part insensitive to the mesh size. The computer code developed in this research is open source and is available at the Engineering Design Research Laboratory[2] repository.

There are additional efforts that can be made based on the investigations and conclusions made here. Future work in the area of deterministic design should address the following subjects:

- The primary disadvantage of this type of empirical model for blast loading is the absence of reflective waves from surrounding surfaces, i.e., the ground, buildings, etc. Future studies should include MM-ALE or similar solver to account for fluid-material interactions and include those effects. Similarly, future FEA implementations could monitor strain values and account for fracture of the material.

- Much attention has been paid recently to the development of sandwich structures as a multi-material approach to blast mitigation problems and some have

---

[2] http://www.engr.iupui.edu/engr/me/edrl/

demonstrated significant reduction of stress amplitude, especially through the use of honeycomb structures. Future work will incorporate concurrent material and shape optimization, and if possible will include the application of the design candidates examined here to multiple-material design.

- The trigonometric function based geometrically constrained design shows great promise, but additional development is needed in terms a more robust finite element model which can allow for accurate rendering of the complex curvature and a more accurate material model.

- There is still great potential for the HCA topography to overcome the limitations in performance caused by its current displacement-based formulation. There is a distinct need for future work to investigate alternative formulations, possibly rooted in nodal acceleration or structural internal energy.

5.2   Uncertainty Quantification

This work represents a concentrated effort to examine recently developed methods uncertainty quantification (UQ): the univariate dimensional reduction method (UDR) and the performance moment integration method (PMI). These methods are generally employed in the context of analytical, computationally inexpensive test functions. This research represents one of the first attempts to extend these methods to finite element–based design. Furthermore, this research adapts such methods to the generation of reliable plate structures for blast mitigation. In this thesis, the UQ methods are first applied to various analytical test cases, and then to finite element simulation cases, in order to compare the results to well-understood but computationally expensive methods for uncertainty quantification such as Monte Carlo simulation. The adaptation of these methods to FEA simulation created a need to keep computation costs down. This in turn led to the development of a metamodelling technique based in radial basis function (RBF) neural networks; the integration of RBF networks in performance moment integration is unique to this research. It is demonstrated by this thesis that in the uncertainty quantification of uncertain loading conditions in the performance of plate

structures under blast loading, the univariate dimensional reduction technique applied here has a very high level of accuracy. Through the employment of metamodelling, the performance moment integration method is also successful at a low computational cost in estimation of uncertainty with an acceptable level of error.

Future research can be conducted to improve upon the methods developed and applied in this work, including:

- As the number of random inputs to the design increases, the computational cost of implementing the RBF network also increases. There is additional work that can be done in the implementation of a RBF network at a low computational cost and with improved accuracy.

- The use of metamodels requires the consideration of trust region management methods that support the accuracy of the approximations at a reasonable computational cost. These methods provide acceptance/rejection criteria and a metric to scale and/or update the metamodels.

5.3   Stochastic Design

Through the application of uncertainty quantification methods described above, the development and evaluation of design under uncertainty methodology for blast-resistant component design has been accomplished. The investigation of those methods has allowed objective assessment of the benefit of each stochastic optimization strategy. The simple robust design optimization formulation has limited practical value in application to lightweight structure design. However, the application of the hybrid reliability-based robust design optimization method results in the generation of lightweight, robust structures which are reliable and demonstrate little sensitivity to uncertain loading conditions. It is demonstrated that structures with a high degree of adaptability, structures generated by basis functions with a large number of design variables (i.e., a relaxed design domain), show an increase in performance.

Literature on design optimization methods for blast mitigation under uncertainty is scarce. This work represents one of the few contributions that includes an exhaustive, objective evaluation of these methods. Future work should include:

- There is an interest to perform more encompassing study by expanding the amount of uncertainty in the design. This can be achieved through the introduction of additional stochastic variables. Possible additions should include: material properties, manufacturing and control variables, and blast type (surface and air).

- An exhaustive effort should be made to determine the reliability of the trigonometric function based design to determine the reliability of the structure under uncertain loading conditions.

LIST OF REFERENCES

LIST OF REFERENCES

[1]   L. Shaughnessy, "IEDs top cause of US Afghanistan casualties," ed: CNN, 2012.

[2]   S. G. Chesser, "Afghanistan Casualties: Military Forces and Civilians," Congressional Research Service, CRS Report for CongressDecember 6 2012.

[3]   S. Wei, J. Bowers, and W. Andrews. (2013). *Fallen: causes of death*. Available:http://www.wlwt.com/news/national/IEDs-top-cause-of-US-Afghanistan-casualties/-/9837944/17768196/-/13damgbz/-/index.html

[4]   Associated Press. (2007, March 10). Available:http://usatoday30.usatoday.com/news/military/2007-07-15-ied-cover_N.htm

[5]   M. Grujicic, G. Arakere, W. C. Bell, and I. Haque, "Computational investigation of the effect of up-armouring on the reduction in occupant injury or fatality in a prototypical high-mobility multi-purpose wheeled vehicle subjected to mine blast," *Journal of Automobile Engineering,* vol. 223, 2009.

[6]   B. McAndrew, "Shock isolation parameters based on a damped harmonic oscillator model for mine blast protected seating," Army Research Laboratory, Tech. Rep.2007.

[7]   H. Wang, Y. Cui, Z.-D. Ma, and D. Rose, "Function-Oriented design of innovative composite materials for high speed impact," in *Materials Science and Technology Conference and Exhibition, MS and T'07 - "Exploring Structure, Processing, and Applications Across Multiple Materials Systems", September 16, 2007 - September 20, 2007*, Detroit, MI, United states, 2007, pp. 275-286.

[8]   D. Jiang, Y. Liu, C. Qi, Z.-D. Ma, B. Raju, and W. Bryzik, "Innovative composite structure design for blast protection," presented at the SAE World Congress, 6501 E 11 Mile Rd Warren MI 48397-5000, 2007.

[9]   P. J. Tan, S. R. Reid, J. J. Harrigan, Z. Zou, and S. Li, "Dynamic compressive strength properties of aluminium foams. Part II - 'shock' theory and comparison with experimental data and numerical models," *Journal of the Mechanics and Physics of Solids,* vol. 53, pp. 2206-2230, 2005.

[10]   A. G. Hanssen, L. Olovsson, T. Brvik, and M. Langseth, "Close-range blast loading of aluminium foam panels: A numerical study," in *IUTAM Symposium on Mechanical Properties of Cellular Materials, September 17, 2007 - September 20, 2007*, Cachan, France, 2009, pp. 169-180.

[11]   K. P. Dharmasena, H. N. G. Wadley, Z. Xue, and J. W. Hutchinson, "Mechanical response of metallic honeycomb sandwich panel structures to high-intensity dynamic loading," *International Journal of Impact Engineering,* vol. 35, pp. 1063-1074, 2008.

[12]   B. Schimizze, S. F. Son, R. Goel, A. P. Vechart, and L. Young, "An experimental and numerical study of blast induced shock wave mitigation in sandwich structures," *Applied Acoustics,* vol. 74, pp. 1-9, 2013.

[13]   D. K. Lee and B. J. O'Toole, "Energy Absorbing Sandwich Structures Under Blast Loading," presented at the Proc. of 8th International LS-DYNA Users Conference, Dearborn, MI, 2004.

[14]   B. A. Gama, T. A. Bogetti, B. K. Fink, C.-J. Yu, T. Dennis Claar, H. H. Eifert, and J. W. Gillespie Jr, "Aluminum foam integral armor: A new dimension in armor design," *Composite Structures,* vol. 52, pp. 381-395, 2001.

[15]   A. Tasdemirci and I. W. Hall, "Development of novel multilayer materials for impact applications: A combined numerical and experimental approach," *Materials and Design,* vol. 30, pp. 1533-1541, 2009.

[16]   M. P. Sheyka, B. Colak-Altunc, M. M. R. Taha, G. Cruz, T. Connolly, and D. Tortorelli, "Multi-objective blast resistant composite plate design optimization," in *51st AIAA/ASME/ASCE/AHS/ASC Structures, Structural Dynamics and Materials Conference, April 12, 2010 - April 15, 2010*, Orlando, FL, United states, 2010.

[17]   W. W. Chen, A. M. Rajendran, B. Song, and X. Nie, "Dynamic fracture of ceramics in armor applications," *Journal of the American Ceramic Society,* vol. 90, pp. 1005-1018, 2007.

[18]   Altair. (Mar 13). *Altair Enlighten Knowledge Center*. Available: http://altairenlighten.com/2012/07/sandwich-structures/ - Honeycomb

[19]   M. V. Dharaneepathy and K. G. Sudhesh, "Optimal stiffening of square plates subjected to air-blast loading," *Computers and Structures,* vol. 36, pp. 891-899, 1990.

[20]   V. Argod, S. K. Nayak, A. K. Singh, and A. D. Belegundu, "Shape optimization of solid isotropic plates to mitigate the effects of air blast loading," *Mechanics Based Design of Structures and Machines,* vol. 38, pp. 362-371, 2010.

[21]   V. Argod, A. D. Belegundu, A. Aziz, V. Agrawala, R. Jain, and D. Rajan, "MPI-enabled Shape Optimization of Panels Subjected to Air Blast Loading," *Int. J. Simul. Multidisci. Des. Optim.,* vol. 2, pp. 273-282, 2008.

[22]   J. Goetz, H. Tan, J. Renaud, and A. Tovar, "Two-material optimization of plate armour for blast mitigation using hybrid cellular automata," *Engineering Optimization,* vol. 44, pp. 985-1005, 2012.

[23]   J. C. Medina and A. Tovar, "Topography Optimization of Shell Structures Under Transient Loading; A Comparative Approach," presented at the Proceedings of the ASME 2012 International Design Engineering Technical Conference & Computers and Information Engineering Conference Chicago, IL, 2012.

[24]   S. Gano, H. Agarwal, J. Renaud, and A. Tovar, "Reliabilty Based Design Using Variable Fidelity Optimization," presented at the 1st AIAA Multidisciplinary Design Optimization Conference Austin, Texas, USA, 2005.

[25]   G. Randers-Pehrson and K. A. Bannister, "Airblast loading model for DYNA2D and DYNA3D," Army Research Laboratory, 1997.

[26]   A. L. Kuhl, "Dynamics of detonations and explosions - explosion phenomena," American Institute of Aeronautics and Astronautics, Washington, D.C., 1991.

[27]   C. W. Hirt, A. A. Amsden, and J. L. Cook, "An arbitrary lagrangian-eulerian computing method for all flow speeds," *Journal of Computational Physics,* vol. 14, pp. 227-253, 1974.

[28]   S. H. Lee and W. Chen, "A Comparative Study of Uncertainty Propagation Methods for Black-Box Type Functions," presented at the ASME 2007 International Design Engineering Technical Conferences & Computers and Information in Engineering Conference, Las Vegas, Nevada, USA, 2007.

[29]   P. Thoft-Christiansen and M. J. Baker, *Structural reliability theory and its applications*: Springer, 1982.

[30]   H. O. Madsen, S. Krenk, and S. C. Lind, *Methods of Structural Safety*. Mineola, NY: Dove Publications, 2006.

[31]   C. G. Bucher, ""Adaptive Sampling - an iterative fast Monte Carlo procedure"," *Structural Safety,* vol. 5, 1988.

[32]   A. M. Hasofer and N. C. Lind, "Exact and invariant second order code format," *Journal of the Engineering Mechanics Division - ASCE,* vol. 100, 1974.

[33]   M. S. Eldred, C. G. Webster, and P. G. Constantine, "Design under uncertainty employing stochastic expansion methods," in *12th AIAA/ISSMO Multidisciplinary Analysis and Optimization Conference, MAO, September 10, 2008 - September 12, 2008*, Victoria, BC, Canada, 2008.

[34]   R. G. Ghanem and P. D. Spanos, *Stochastic finite elements: a spectral approach.* New York, NY: Springer-Verlag NewYork Inc., 1991.

[35]   B. D. Youn, K. K. Choi, and K. Yi, "Performance Moment Integration (PMI) method for quality assessment in reliability-based robust design optimization," *Mechanics Based Design of Structures and Machines,* vol. 33, pp. 185-213, 2005.

[36]   S. Rahman and H. Xu, "A univariate dimension-reduction method for multi-dimensional integration in stochastic mechanics," *Probabilistic Engineering Mechanics,* vol. 19, pp. 393-408, 2004.

[37]   H. Xu and S. Rahman, "A generalized dimension-reduction method for multidimensional integration in stochastic mechanics," *International Journal for Numerical Methods in Engineering,* vol. 61, pp. 1992-2019, 2004.

[38]   I. Lee, K. K. Choi, L. Du, and D. Gorsich, "Dimension reduction method for reliability-based robust design optimization," *Computers and Structures,* vol. 86, pp. 1550-1562, 2008.

[39]   V. P. Joynt, "Mine Resistant Armored Vehicle," United Sates Patent, 2008.

[40]   H. Tan, "Vehicle Hull Shape Optimization for Minimum Deformation Under Blast Loading " Disseration, University of Notre Dame, 2010.

[41]   L. F. Troyano, *Bridge Engineering: A Global Perspective.* Thomas Teflord, 2003.

[42]   R. Osserman, "How the Gateway Arch Got its Shape," *NEXUS NETWORK JOURNAL,* vol. 12, pp. 167-189, 2010.

[43]   S. Krenk, *Non-linear modeling and analysis of solids and structures*. New York, NY: Cambridge University Press, 2009.

[44]   L. S. T. Corporation, "LS-DYNA Theory manual Version 971," ed, 2007.

[45]   O. J. Centeno, "Finite Element modeling of Rubber Bushing for Crash Simulation," Doctoral, Division of Structural Mechanics, Lund University, Lund, Sweden, 2009.

[46]   T. Erhart, "An Overview of User Defined Interfaces in LS-DYNA," ed. Stuttgart, Germany: Dynamore GmbH.

[47] J. O. Hallguist, "LS-DYNA theoretical manual, 1998," ed: Livermore Software Technology Corporation, 1998.

[48] C. N. Kingery and G. Bulmash, "Air Blast Parameters from TNT Spherical Air Burst and Hemispherical Surface Burst," U.S. Army Ballistic Research Laboratory1984.

[49] K. Williams, S. McClennan, R. Durocher, B. St-Jean, and J. Tremblay, "Validation of a Loading Model for Simulating Blast Mine Effects on Armoured Vehicles," presented at the 7th International LS-DYNA Users Conference, Dearborn, MI, 2002.

[50] S. McClennan and K. Williams, "A numerical analysis of mine blast effects on simplified target geometries: Validation of loading models," Defence Research and Development Canada - Valcatartier Tech. Rep., 2003.

[51] A. Tovar, N. Patel, A. K. Kaushik, G. A. Letona, J. E. Renaud, and B. Sanders, "Hybrid cellular automata: A biologically-inspired structural optimization technique," in *Collection of Technical Papers - 10th AIAA/ISSMO Multidisciplinary Analysis and Optimization Conference, August 30, 2004 - September 1, 2004*, Albany, NY, United states, 2004, pp. 2844-2858.

[52] Mathworks, "Global Optimization Toolbox: User's Guide (r2011b)," ed, 2011.

[53] A. D. Belegunda and T. R. Chandrupatla, *Optimization Concepts and Applications in Engineering*. New York, NY: Cambridge University Press, 2011.

[54] M. C. Biggs, "Constrained Minimization Using Recursive Quadratic Programming," in *Towards Global Optimization* L. C. W. Dixon and G. P. Szergo, Eds., ed: North-Holland, 1975.

[55] S. P. Han, "A Globally Convergent Method for Nonlinear Programming," *Journal of Optimization Theory and Applications,* vol. 22, 1977.

[56] M. J. D. Powell, "A Fast Algorithm for Nonlinearly Constrained Optimization Calculations," *Numerical Analysis,* vol. Vol. 630, 1978.

[57] M. J. D. Powell, "The Convergence of Variable Metric Methods for Nonlinearly Constrained Optimization Calculations," in *Nonlinear Programming 3*, O. L. Mangasarian, R. R. Meyer, and S. M. Robinson, Eds., ed: Academic Press, 1978.

[58] A. Tovar, N. M. Patel, A. K. Kaushik, and J. E. Renaud, "Optimality conditions of the hybrid cellular automata for structural optimization," *AIAA journal,* vol. 45, pp. 673-683, 2007.

[59]   A. Tovar, N. M. Patel, G. L. Niebur, M. Sen, and J. E. Renaud, "Topology optimization using a hybrid cellular automaton method with local control rules," *Journal of Mechanical Design,* vol. 128, pp. 1205-1216, 2006.

[60]   A. Tovar, N. M. Patel, G. L. Niebur, M. Sen, and J. E. Renaud, "Topology optimization using a hybrid cellular automaton method with local control rules," *Journal of Mechanical Design,* vol. 128, pp. 1205-1216, Nov 2006.

[61]   K. Khandelwal and A. Tovar, "Control-based topology optimization for structural systems," presented at the Engineering Mechanics Institute (EMI 2010), Los Angeles, California, 2010.

[62]   A. Tovar, "Optimización topológica con la técnica de los autómatas celulares híbridos," *Revista internacional de métodos numéricos para cálculo y diseño en ingeniería,* vol. 21, pp. 365-383, 2005.

[63]   D. Karagiannis and P. Hofferer, "Metamodels in action: An overview," in *1st International Conference on Software and Data Technologies, ICSOFT 2006, September 11, 2006 - September 14, 2006*, Setubal, Portugal, 2006, pp. IS27-IS36.

[64]   L. Abbott and T. J. Sejnowski, *Neural Codes and Distributed Representations: Foundations of Neural Computation*: MIT Press, 1999.

[65]   T. Poggio and F. Girosi, "Networks for approximation and learning," *Proceedings of the IEEE,* vol. 78, pp. 1481-1497, 1990.

[66]   W. Chen, J. K. Allen, K.-L. Tsui, and F. Mistree, "Procedure for robust design: Minimizing variations caused by noise factors and control factors," *Journal of Mechanical Design, Transactions of the ASME,* vol. 118, pp. 478-485, 1996.

[67]   S. H. Lee and W. Chen, "A comparative study of uncertainty propagation methods for black-box type functions," in *33rd Design Automation Conference, presented at - 2007 ASME International Design Engineering Technical Conferences and Computers and Information in Engineering Conference, IDETC/CIE2007, September 4, 2007 - September 7, 2007*, Las Vegas, NV, United states, 2008, pp. 1275-1284.

[68]   R. Y. Rubinstein, *Simulation and Monte Carlo Method*. New York, NY: John Wiley & Sons, 1981.

[69]   H. O. Madsen and P. F. Hansen, "A Comparison of Some Algorithms for Reliability Based Structural Optimization and Sensitivity Analysis," in *Reliability and Optimization of Structural Systems '91*. vol. 76, R. Rackwitz and P. Thoft-Christensen, Eds., ed: Springer Berlin Heidelberg, 1992, pp. 443-451.

[70]   M. Kalsi, K. Hacker, and K. Lewis, "A comprehensive robust design approach for decision trade-offs in complex systems design," *ASME Journal of Mechanical Design,* vol. 123, 2001.

[71]   Y. Noh, K. K. Choi, and I. Lee, "MPP-based dimension reduction method for RBDO problems with correlated input variables," in *12th AIAA/ISSMO Multidisciplinary Analysis and Optimization Conference, MAO, September 10, 2008 - September 12, 2008*, Victoria, BC, Canada, 2008.

[72]   X. Du and W. Chen, "A Most Probable Point Based Method for Uncertainty Analysis " in *ASME 2000 Design Engineering Technical Conference and Computers and Information in Engineering Conference*, Baltimore, MD, 2000.

[73]   K. E. Atkinson, *An Introduction to Numerical Analysis*. New York, NY: John Wiley & Sons, 1989.

[74]   M. Rosenblatt, *Remarks on a Multivariate Transformation* vol. 23: The Institute of Mathematical Sciences, 1952.

[75]   I. Lee, "Reliability-based design optimization and robust design optimization using univariate dimension reduction method," Dissertation, Mechanical Engineering, University of Iowa, 2008.

[76]   G. Jiang, M. Zhu, and Z. Wu, "Reliability Allocation Using Probabilistic Analytical Target Cascading with Efficient Uncertainty Propagation," *Maintenance and Reliability,* vol. 14, pp. 270-277, 2012.

[77]   W. Chen, J. K. Allen, K.-L. Tsui, and F. Mistree, "A Procedure for Robust Design: Minimizing Variations Caused by Noise Factors and Control Factors," *Journal of Mechanical Design,* vol. Vol. 188, pp. 478-485, 1996.

[78]   T. C. Palle and J. B. Michael, *Structural Reliabilty Theory and its Applications*. Heidelberg: Springer-Verlag, 1982.

[79]   M. J. Chandra, *Statistical Quality Control*. Boca Raton, FL: CRC Press, 2001.

[80]   T. Ngo, P. Mendis, A. Gupta, and J. Ramsay, "Blast loading and blast effects on structures - An overview," *Electronic Journal of Structural Engineering,* vol. 7, pp. 76-91, 2007.

[81]   S. Wolfram, *A New Kind of Science*. Champaign, IL: Wolfram Media, 2002.

[82]   L. A. Schmit, "Some approximation concepts for structural synthesis," *AIAA Journal,* vol. 12, pp. 692-699, 1974.

[83]   A. Tovar, N. M. Patel, G. L. Niebur, M. Sen, and J. E. Renaud, "Topology Optimization Using a Hybrid Cellular Automaton Method with Local Control Rules," *ASME Journal of Mechanical Design,* vol. 128, pp. 1205-1216, 2006.

APPENDIX

APPENDIX: SAMPLE CODE

RBRDO – Polynomial Design

Main script:

"runOpt.m"

```matlab
%%% Main script to call optimization
clc;clear;

[history,searchdir] = runfmincon

figure(1)
plot(history.fval);
xlabel('Iteration');
ylabel('Mass')
print(figure(1),'-dpng','FvalPlot.png');
```

Sub function: "runfmincon.m"

```matlab
% Set up shared variables with OUTFUN
history.x = [];
history.fval = [];
searchdir = [];

% call optimization
R = 0.5; h = 0.12;
x0 = [h; -h/R; 0; 0; 0.02]; % This is x = [c0 ... c3, t]
%x0 = [0;0;0;0;0.02];
A = [1 0.1 0.1^2 0.1^3 0
     1 0.2 0.2^2 0.2^3 0
     1 0.3 0.3^2 0.3^3 0
     1 0.4 0.4^2 0.4^3 0
     1 0.5 0.5^2 0.5^3 0];
b = [0.12;0.12;0.12;0.12;0.12];
Aeq = [1 R R^2 R^3 0];
beq = 0;
lb = [0; -1e6; -1e6; -1e6; 0.005];
ub = [h; 1e6; 1e6; 1e6; 1e6];
options =
optimset('outputfcn',@outfun,'MaxIter',40,'display','iter',...
'Algorithm','active-set','DiffMinChange',0.0001);
```

```matlab
[X,Fval,exitflag,output] =
fmincon(@VarFuncRBRDO,x0,A,b,Aeq,beq,lb,ub,@ProbFunc,options);
 function stop = outfun(x,optimValues,state)
     stop = false;

     switch state
         case 'init'
             hold on
         case 'iter'
         % Concatenate current point and objective function
         % value with history. x must be a row vector.
           history.fval = [history.fval; optimValues.fval];
           history.x = [history.x; x];
         % Concatenate current search direction with
         % searchdir.
           searchdir = [searchdir;...
                        optimValues.searchdirection'];
         % plot(x(1),x(2),'o');
         % Label points with iteration number and add title.
         % Add .15 to x(1) to separate label from plotted 'o'
           text(x(1)+.15,x(2),...
                num2str(optimValues.iteration));
           title('Sequence of Points Computed by fmincon');
         case 'done'
             hold off
         otherwise
     end
 end


IT = getfield(output, 'iterations');
FC = getfield(output, 'funcCount');

Mfinal = PolyMassFunc2(X);

results='resultsFmincon.txt';
fileR = fopen(results, 'wt');
fprintf(fileR,'Results from fmincon \n\n');
fprintf(fileR,'Starting point: c0 = %1.3f  c1 = %1.  c2 = %1.3f
c3 = %1.3f  T = %1.3f \n\n',x0(1),x0(2),x0(3),x0(4),x0(5));
fprintf(fileR,'  c0         c1         c2         c3        Thick
Mass\n');
fprintf(fileR,' %2.5f      %2.5f      %2.5f      %2.5f      %2.
5f      %2.5f \n',X(1),X(2),X(3),X(4),X(5),Mfinal);
fprintf(fileR,'Iterations =  %4.0f  Function Calls =  %4.0f
\n',IT,FC);


end
```

Sub function: "VarFuncRBRDO.m"

```matlab
function [F] = VarFuncRBRDO(x)
%ProbFunc Summary of this function goes here
CP_max = -0.03;

% constants for cost function
w1 = 0.8;
```

```matlab
w2 = 0.2;
Mu0 = -0.05;
Sig0 = 0.02;
M0 = 159.4;
MuTarget = -0.03;

%plate characteristics
a0 = x(1);
a1 = x(2);
a2 = x(3);
a3 = x(4);
t = x(5);
fprintf('\n\n **************** \n\n')
fprintf('a0 = %2.5f \n',a0)
fprintf('a1 = %2.5f \n',a1)
fprintf('a2 = %2.5f \n',a2)
fprintf('a3 = %2.5f \n',a3)
fprintf('t = %2.5f \n',t)
fprintf('\n *************** \n\n')

%create .k file for x values
PolyFileWrite2(a0,a1,a2,a3,t)

%% random variable data
n=2; % number of random variables
mean_x1 = 5; sig_x1 = 1;    %blast magnitude
mean_x2 = 0; sig_x2 = 0.25; %blast location (x-coordinate)

% ok ok

%% UDR - Statistical Moments
% Weights and double approximation for UDR
w = [0.011257 0.222076 0.533333 0.222076 0.011257];
P1 = mean_x1 + sig_x1*[-2.856970 -1.355626 0 1.355626 2.856970];
P2 = mean_x2 + sig_x2*[-2.856970 -1.355626 0 1.355626 2.856970];

N = 5; %5 integration points
% Moment approximations UDR
G_mean_UDR=0;
G_Var_UDR=0;
MeanFun = CFuncPoly(mean_x1,mean_x2);   % function call at both
means
for i=1:N
    Point1 = CFuncPoly(P1(i),mean_x2);
    Point2 = CFuncPoly(mean_x1,P2(i));
    G_mean_UDR = G_mean_UDR + (w(i)*(Point1 + Point2 - (n-
1)*MeanFun));
    G_Var_UDR = G_Var_UDR + (w(i)*(Point1^2 + Point2^2 - (n-
1)*MeanFun^2));
end
G_Var_UDR = G_Var_UDR - G_mean_UDR^2;

Mu = G_mean_UDR
Sig = sqrt(G_Var_UDR)

% Probability calculation
if Sig == 0
    P = 0;
else
    fun = @(X) 1/(Sig*sqrt(2*pi)) * exp(-((X-Mu).^2/(2*Sig^2)));
    P = integral(fun,-Inf,CP_max);
```

```matlab
        end

    M = PolyMassFunc2(x);

    % cost function
    F = w1*(M/M0) + w2*(Sig/Sig0)^2;


    end
```

Sub function: "ProbFunc.m"

```matlab
function [P dP] = ProbFunc(x)
%ProbFunc Summary of this function goes here
CP_max = -0.03;

%plate characteristics
a0 = x(1);
a1 = x(2);
a2 = x(3);
a3 = x(4);
t = x(5);
fprintf('\n\n **************** \n\n')
fprintf('a0 = %2.5f \n',a0)
fprintf('a1 = %2.5f \n',a1)
fprintf('a2 = %2.5f \n',a2)
fprintf('a3 = %2.5f \n',a3)
fprintf('t = %2.5f \n',t)
fprintf('\n *************** \n\n')

%create .k file for x values
PolyFileWrite2(a0,a1,a2,a3,t)

%% random variable data
n=2; % number of random variables
mean_x1 = 5; sig_x1 = 1;    %blast magnitude
mean_x2 = 0; sig_x2 = 0.25; %blast location (x-coordinate)

% ok ok

%% UDR - Statistical Moments
% Weights and double approximation for UDR
w = [0.011257 0.222076 0.533333 0.222076 0.011257];
P1 = mean_x1 + sig_x1*[-2.856970 -1.355626 0 1.355626 2.856970];
P2 = mean_x2 + sig_x2*[-2.856970 -1.355626 0 1.355626 2.856970];

N = 5; %5 integration points
% Moment approximations UDR
G_mean_UDR=0;
G_Var_UDR=0;
MeanFun = CFuncPoly(mean_x1,mean_x2);   % function call at both
means
for i=1:N
    Point1 = CFuncPoly(P1(i),mean_x2);
    Point2 = CFuncPoly(mean_x1,P2(i));
    G_mean_UDR = G_mean_UDR + (w(i)*(Point1 + Point2 - (n-
1)*MeanFun));
```

```
      G_Var_UDR = G_Var_UDR + (w(i)*(Point1^2 + Point2^2 - (n-
1)*MeanFun^2));
end
G_Var_UDR = G_Var_UDR - G_mean_UDR^2;

Mu = G_mean_UDR
Sig = sqrt(G_Var_UDR)

% Probability calculation
if Sig == 0
    P = 0;
else
    fun = @(X) 1/(Sig*sqrt(2*pi)) * exp(-((X-Mu).^2/(2*Sig^2)));
    P = integral(fun,-Inf,CP_max);
end


P = P - 0.05;
dP = [];
end
```

Sub function: PolyFileWrite2.m"

```
function [fileout] = PolyFileWrite2(a0,a1,a2,a3,t)
%PolyFileWrite2 writes a .k file for a plate with Polynomial
profile
%   It takes alpha and delta as inputs
%   opens a new .k file and writes the info from the old .k fie
%   the only changes are the nodal coordinates, which are replaced
%   with the new coordinates for the Gaussian surface
%
%   returns the name of the file as a string

%these constants are only valid for a 26x26 plate
Y=linspace(-0.5,0.5,27);
X=linspace(-0.5,0.5,27);
n=length(X);
m=length(Y);

t_p=t;

nn=n*m;


filename_in = '26x26_test2.k';
fid_in = fopen(filename_in, 'rt');

filename_out = 'Poly_1.k';
fileID = fopen(filename_out, 'wt');

Col=0:27:nn;
tline = fgetl(fid_in);
while feof(fid_in) == 0
    matches = strfind(tline,'*NODE');
    flagN = length(matches);
    if flagN == 0

        fprintf(fileID,tline);
```

```matlab
            fprintf(fileID,'\n');
            tline = fgetl(fid_in);

    else
            fprintf(fileID,tline);
            fprintf(fileID,'\n');
            tline = fgetl(fid_in);
            fprintf(fileID,tline);
            fprintf(fileID,'\n');
            tline = fgetl(fid_in);

                %this generates the nodal coordinates
                G=zeros(n,m);
                for i=1:n
                    for j=1:m
                        r=sqrt(X(i)^2 + Y(j)^2);
                        if r>=0.5
                            G(i,j)=0;
                        else
                            G(i,j) = (a0 + a1.*r + a2.*r.*r +
a3.*r.*r.*r);
                        end


fprintf(fileID,'    %4.0f        %2.5f        %2.5f        %2.5f
0        0\n'...
                            ,j+Col(i),X(i),Y(j),G(i,j));
                        tline = fgetl(fid_in);

                    end
                end

    end

end

%add the file end
fprintf(fileID,'*END\n');

%close the file
fclose(fileID);

filename_in2 = 'Poly_1.k';
fid_in2 = fopen(filename_in2, 'rt');

filename_out2 = 'Poly_2.k';
newfile = fopen(filename_out2, 'wt');

tline = fgetl(fid_in2);
while feof(fid_in2) == 0
    matches = strfind(tline,'*SECTION_SHELL');
    flagN = length(matches);
    if flagN == 0
        % if the flag is not found, copy the line and check the
next line
        fprintf(newfile,tline);
        fprintf(newfile,'\n');
        tline = fgetl(fid_in2);
    else
        % when a flag is found, copy the next four lines
```

```matlab
            fprintf(newfile,tline);
            fprintf(newfile,'\n');
            tline = fgetl(fid_in2);
            fprintf(newfile,tline);
            fprintf(newfile,'\n');
            tline = fgetl(fid_in2);
            fprintf(newfile,tline);
            fprintf(newfile,'\n');
            tline = fgetl(fid_in2);
            fprintf(newfile,tline);
            fprintf(newfile,'\n');
            tline = fgetl(fid_in2);
            %insert thickness values for integration points
            fprintf(newfile,'  %1.6f  %1.6f  %1.6f  %1.6f     0.000
0.000     0.000          0\n',t_p,t_p,t_p,t_p);
            tline = fgetl(fid_in2);

        end

    end

    %close the file
    fclose(newfile);
    fclose('all');

    fileout=filename_out2;

end
```

Sub function: "RandomFileWrite.m"

```matlab
function [fileout] = RandomFileWrite(B_mag,B_loc)

%these constants are only valid for a 26x26 element plate
y=linspace(-0.5,0.5,27);
x=linspace(-0.5,0.5,27);
n=length(x);
m=length(y);
nn=n*m;

filename_in2 = 'Poly_2.k';
fid_in2 = fopen(filename_in2, 'rt');

filename_out2 = 'Poly_3.k';
newfile = fopen(filename_out2, 'wt');

tline = fgetl(fid_in2);
while feof(fid_in2) == 0
    matches = strfind(tline,'*LOAD_BLAST_ENHANCED');
    flagN = length(matches);
    if flagN == 0
        % if the flag is not found, copy the line and check the
next line
        fprintf(newfile,tline);
        fprintf(newfile,'\n');
        tline = fgetl(fid_in2);
    else
```

```matlab
        % when a flag is found, copy the next two lines
        fprintf(newfile,tline);
        fprintf(newfile,'\n');
        tline = fgetl(fid_in2);
        fprintf(newfile,tline);
        fprintf(newfile,'\n');
        tline = fgetl(fid_in2);
        %insert load case
        fprintf(newfile,'          1  %1.5f  %1.5f      0.000
0.400000      0.000           2         2\n',B_mag,B_loc);
        tline = fgetl(fid_in2);

    end
end

%close the file
fclose('all');

fileout=filename_out2;

end
```